

# POLITECNICO DI TORINO

Collegio di Ingegneria Chimica e dei Materiali

**Master of Science Course  
in Materials Engineering**

Master of Science Thesis

## **Synthesis of photocurable hydrogels**



**Tutor**

prof. Sangermano Marco

.....

**Candidate**

Noè Camilla

.....

October 2018



*To my parents, Dario and Franca,  
my sister Carlotta and to my grandmother Carla*

*In memory of my grandparents Lucia, Mario and Enrico*



## Abstract

Hydrogels are three-dimensional cross-linked polymeric networks that have been widely explored in the biomedical field for both *in vitro* and *in vivo* applications. They can absorb a large quantity of water or aqueous solution without dissolving and their tunable chemical and physical structures make them suitable for tissue engineering (TE) scaffolds and drug delivery systems. However, conventional hydrogels for TE applications adapt incompletely to defect sites and often require surgical implantation, which enhance risk of infections. By overcoming these issues, injectable multicomponent hydrogels are gaining an increasing interest in the last decades. Indeed, through the integration of heterogeneous building blocks, enhanced bioactivity can be achieved and physical properties can be easily manipulated.

In this study, a novel photo-curable hydrogel based on the generation of an amphiphilic network has been developed. Two kinds of biocompatible macromers, namely polyethylene glycol dimethacrylate (PEGDMA) and polycaprolactone dimethacrylate (PCLDMA), were synthesized with different molecular weights. The synthesis relied on the esterification reaction of polyethylene glycol (PEG) and polycaprolactone (PCL) oligomers, by using methacryloyl chloride in the presence of triethylamine. The success of the methacrylation was confirmed by attenuated total reflectance - Fourier transform infrared spectroscopy (ATR-FTIR), proton - nuclear magnetic resonance (H-NMR), size-exclusion chromatography (SEC) and differential scanning calorimetry (DSC) measurements. Bio-based nanographene oxide (nGO) type carbon dots were also synthesized in this work *via* a green microwave assisted carbonization process and then methacrylated using methacryloyl chloride (MA-nGO). The functionalization was confirmed by means of ATR-FTIR and thermogravimetric (TGA) analysis. Then, photocurable hydrogels were obtained *via* free radical photopolymerization in the presence of bis(acyl)phosphane oxide (BAPO), an UV-visible light photoinitiator. The effectiveness of cross-linking was evaluated by means of ATR-FTIR, whereas the thermomechanical and swelling behaviours of the hydrogels were investigated varying both the molecular weight of the oligomers and their relative concentrations in the photocurable formulations.

In summary, we successfully prepared hydrogels with promising potential for biomedical applications. In the future, MAnGO incorporation, biocompatibility, cell viability assays and cells adhesion tests will be conducted in order to verify expected improvements over standard hydrogels.



# Table of Contents

<b>1. Introduction</b> .....	1
1.1 <i>Hydrogels</i> .....	2
1.1.1 Structure parameters.....	2
1.1.2 Swelling mechanism.....	4
1.1.3 Classification.....	6
1.1.4 Mechanism of network formation.....	7
1.1.4.1 Physical gels.....	7
1.1.4.2 Chemical cross-linking.....	8
1.1.6 Biomedical applications.....	9
1.2 <i>Aim of the study</i> .....	11
<b>2 Materials</b> .....	13
2.1 <i>Hydrogel precursors</i> .....	13
2.1.1 Oligomers functionalization.....	13
2.1.1.1 Polycaprolactone diacrylation.....	14
2.1.1.2 Polycaprolactone dimethacrylation.....	15
2.1.1.3 Polyethylene glycol dimethacrylation.....	17
2.2 <i>Nanographene oxide synthesis and functionalization</i> .....	19
2.3 <i>Hydrogel preparation</i> .....	24
<b>3 Methods</b> .....	29
3.1 <i>Proton nuclear magnetic resonance (H-NMR)</i> .....	29
3.2 <i>Attenuated Total Reflectance - Fourier transform infrared (ATR-FTIR) spectroscopy</i> .....	31
3.3 <i>Differential scanning calorimetry (DSC)</i> .....	32
3.4 <i>Size-exclusion chromatography (SEC)</i> .....	33
3.5 <i>Thermogravimetric analysis (TGA)</i> .....	35
3.6 <i>Zeta potential analyzer</i> .....	36
3.7 <i>Swelling degree</i> .....	38
3.8 <i>Dynamic mechanical thermal analysis (DMTA)</i> .....	38
<b>4 Results and discussion</b> .....	41
4.1 <i>Evaluation of functionalization of PCL and PEG</i> .....	41
4.1.1 Characterization of the oligomers by means of ATR-FTIR.....	41
4.1.1.1 PCL diacrylation and dimethacrylation.....	41
4.1.1.2 PEG dimethacrylation.....	43
4.1.2 H-NMR.....	46

4.1.3	Comparison between the thermal behaviours of both virgin and functionalized oligomers by means of DSC.....	52
4.1.4	Evaluation of the oligomers molecular weights .....	55
4.2	<i>Methacrylation of nanographene oxide evaluation</i> .....	57
4.2.1	Confirmation of nGO methacrylation by means of ATR-FTIR spectroscopy.....	57
4.2.2	Thermal behaviours of nGO and MA-nGO .....	58
4.2.3	Evaluation of the nGO and MAnGO stability in water .....	59
4.3	<i>Hydrogels characterization</i> .....	59
4.3.1	Spectroscopic characterization.....	60
4.3.2	DMTA .....	63
4.3.3	DSC .....	64
4.3.4	Swelling behaviour .....	65
<b>5</b>	<b>Conclusion and future works</b> .....	<b>67</b>
	<b>References</b> .....	<b>69</b>
	<b>Acknowledgements</b> .....	<b>73</b>

## List of figures

<b>Figure 1.1:</b> Hydrogels applications.....	1
<b>Figure 1.2:</b> Physical and chemical external stimuli.....	2
<b>Figure 1.3:</b> Schematic representation of a hydrogel network.....	3
<b>Figure 1.4:</b> Main chain defects.....	3
<b>Figure 1.5:</b> Steps of swelling mechanism.....	5
<b>Figure 2.1:</b> Schematic representation of PCLDA synthesis procedure and PCLDA final product.....	15
<b>Figure 2.2:</b> Experimental set-up of PCL dimethacrylation: PCL-diol weighted with a precision balance, dissolution in toluene, triethylamine salt stacked in the filter.....	16
<b>Figure 2.3:</b> Schematic representation of PCLDMA synthesis procedure and PCLDMA final product.....	17
<b>Figure 2.4:</b> From the left: addition of methacryloyl chloride in ice-bath environment; filtration performed to remove triethylamine salt, precipitation in ice-cold diethyl ether, final product after freeze-drying process.....	18
<b>Figure 2.5:</b> Experimental procedure followed for the synthesis of nGO.....	20
<b>Figure 2.6:</b> First synthesis route of MA-nGO.....	21
<b>Figure 2.7:</b> Second synthesis route of MA-nGO.....	21
<b>Figure 2.8:</b> Schematic illustration of the third route procedure.....	22
<b>Figure 2.9:</b> From left batch with nGO and reagents, cellulose dialysis bag and MA-nGO after dialysis.....	22
<b>Figure 2.10:</b> Schematic illustration of the fourth route procedure.....	23
<b>Figure 2.11:</b> From the left: vacuum system, dialysis, final product.....	23
<b>Figure 2.12:</b> Schematic illustration of the fifth route procedure.....	23
<b>Figure 2.13:</b> BAPO photobleaching mechanism under UV irradiation.....	24
<b>Figure 2.14:</b> Experimental protocol followed for the preparation of the photocurable hydrogels.....	25
<b>Figure 2.15:</b> Examples of photocuring failures induced by the evaporation of the solvent.....	26
<b>Figure 2.16:</b> Hydrogels prepared via photocrosslinking.....	27
<b>Figure 3.1:</b> Correlation between the spin states and the magnetic field.....	29
<b>Figure 3.2:</b> H-NMR apparatus [19], sample tubes required for this analysis and scheme of the process [20].....	30
<b>Figure 3.3:</b> Schematic representation of ATR-FTIR working principle.....	31
<b>Figure 3.4:</b> ATR-FTIR instrumental apparatus.....	32
<b>Figure 3.5:</b> Scheme of a DSC measurement chamber [21].....	33
<b>Figure 3.6:</b> DSC Mettler Toledo 820 and crucibles used in DSC analysis.....	33
<b>Figure 3.7:</b> GPC column principle of work [23].....	34
<b>Figure 3.8:</b> SEC apparatus and sample tubes used in this technique.....	35
<b>Figure 3.9:</b> Schematic representation of TGA measurement chamber [24].....	35
<b>Figure 3.10:</b> TGA apparatus and alumina crucible.....	36
<b>Figure 3.11:</b> $\zeta$ -potential [25].....	36
<b>Figure 3.12:</b> Sample holder [26].....	37
<b>Figure 3.13:</b> Z potential instrument [27].....	37
<b>Figure 3.14:</b> Complex modulus.....	39
<b>Figure 4.1:</b> ATR-FTIR spectra of PCL-diol and PCLDA 2k.....	42
<b>Figure 4.2:</b> ATR-FTIR spectra of PCL-diol and PCLDMA 2k.....	42
<b>Figure 4.3:</b> ATR-FTIR spectra of PCL-diol 14k and PCLDMA14k.....	43
<b>Figure 4.4:</b> ATR-FTIR spectra of PEG and PEGDMA 3k.....	44
<b>Figure 4.5:</b> ATR-FTIR spectra of PEG 4k and PEGDMA 4k.....	45

<b>Figure 4.6:</b> ATR-FTIR spectra of PEG and PEGDMA 6k.....	46
<b>Figure 4.7:</b> H-NMR spectrum of PCL-diol 2k.....	47
<b>Figure 4.8:</b> H-NMR spectrum of PCLDMA 2k.....	48
<b>Figure 4.9:</b> H-NMR spectrum of PCL-diol 14k.....	49
<b>Figure 4.10:</b> H-NMR spectrum of PCLDMA 14k.....	50
<b>Figure 4.11:</b> H-NMR spectra of PEG and PEGDMA 3k.....	51
<b>Figure 4.12:</b> H-NMR spectra of PEG and PEGDMA 4k.....	51
<b>Figure 4.13:</b> H-NMR spectra of PEG and PEGDMA 6k.....	52
<b>Figure 4.14:</b> DSC thermograms of PCL-diol, PCLDA and PCLDMA.....	53
<b>Figure 4.15:</b> DSC thermograms of PCL-diol and PCLDMA 14k.....	53
<b>Figure 4.16:</b> DSC thermograms of PEG and PEGDMA 3k.....	54
<b>Figure 4.17:</b> DSC thermograms of PEG and PEGDMA 6k.....	55
<b>Figure 4.18:</b> SEC plots of PCL-diol 2k, PCLDA 2k, PCLDMA 2k, PCL-diol 14k and PCLDMA 14k.....	56
<b>Figure 4.19:</b> ATR-FTIR spectra of nGO spheres.....	57
<b>Figure 4.20:</b> FTIR spectra comparison of MA-nGO spheres.....	58
<b>Figure 4.21:</b> TGA thermograms of nGO, MA-nGO black, MA-nGO dialyzed and MA-nGO not dialyzed.....	59
<b>Figure 4.22:</b> ATR-FTIR spectra of the PCLDMA 2k + PEGDMA 750 [30:70] formulation before and after the UV-irradiation.....	60
<b>Figure 4.23:</b> ATR-FTIR spectra of the PCLDMA 2k + PEGDMA 750 [50:50] formulation before and after the UV-irradiation.....	61
<b>Figure 4.24:</b> ATR-FTIR spectra of the PCLDMA 2k + PEGDMA 750 [70:30] formulation before and after the UV-irradiation.....	61
<b>Figure 4.25:</b> ATR-FTIR spectra of the PCLDMA 14k + PEGDMA 750 [30:70] formulation before and after the UV-irradiation.....	62
<b>Figure 4.26:</b> ATR-FTIR spectra of the PCLDMA 14k + PEGDMA 750 [50:50] formulation before and after the UV-irradiation.....	63
<b>Figure 4.27:</b> Thermomechanical behaviour of the PCLDMA 2k + PEGDMA 750 (50:50) and PCLDMA 14k + PEGDMA 750 (50:50) hydrogels.....	64
<b>Figure 4.28:</b> DSC graph comparison between PCLDMA 2k + PEGDMA 750 and PCLDMA 14k + PEGDMA 750.....	64
<b>Figure 4.29:</b> Pictures taken on the samples before and after the swelling measurement.....	66

## List of Tables

<b>Table 1.1:</b> Correlation between diffusional exponent and type of transport in a hydrogel slab. ....	5
<b>Table 1.2:</b> Relation between porosity and swelling kinetics [6]. ....	6
<b>Table 1.3:</b> Hydrogel classifications. ....	7
<b>Table 1.4:</b> Important parameters of hydrogels used in tissue engineering [4]. ....	10
<b>Table 1.5:</b> List of advantages and disadvantages in the use of hydrogel in tissue engineering. ....	11
<b>Table 2.1:</b> Chemicals used for PCL diacrylation. ....	14
<b>Table 2.2:</b> Chemicals used for PCL 2k dimethacrylation. ....	16
<b>Table 2.3:</b> Chemicals used for PCL 14k dimethacrylation. ....	16
<b>Table 2.4:</b> Chemicals used for PEG 3k dimethacrylation. ....	18
<b>Table 2.5:</b> Chemicals used for PEG 4k dimethacrylation. ....	19
<b>Table 2.6:</b> Chemicals used for PEG 6k dimethacrylation. ....	19
<b>Table 2.7:</b> Chemicals used for the synthesis of nGO following the first route. ....	20
<b>Table 2.8:</b> Chemicals used for the synthesis of nGO following the third route. ....	22
<b>Table 2.9:</b> Solution prepared with different molecular weights, weight ratios and solvents. ....	25
<b>Table 2.10:</b> Formulation prepared with PEGDMA 750. ....	26
<b>Table 3.1:</b> Geometrical parameters of the samples used for DTMA. ....	39
<b>Table 4.1:</b> DSC data. ....	54
<b>Table 4.2:</b> DSC data. ....	55
<b>Table 4.3:</b> Highlights results from SEC graphs. ....	56
<b>Table 4.4:</b> nGO and MAnGO data. ....	59
<b>Table 4.5:</b> Equilibrium water content and swelling degree. ....	65



## Sommario

Questo lavoro di tesi è incentrato sulla preparazione di idrogeli in policaprolattone (PCL) e polietilene glicole (PEG). I due precursori, con diversi pesi molecolari, sono stati metacrilati al fine di poter ottenere un reticolo chimico tridimensionale tramite fotopolimerizzazione.

Il primo capitolo è rivolto ad introdurre il tema trattato facendo riferimento allo stato dell'arte. Dopo un breve richiamo all'origine del termine "Idrogelo", vengono analizzate le caratteristiche e le proprietà principali degli idrogeli, con un interesse particolare per quelli fotoreticolabili utilizzati in ambito biomedicale.

Il termine "Idrogelo" è stato introdotto nella letteratura scientifica nel 1900 per descrivere un gel colloidale ottenuto a partire da sali inorganici. Sessant'anni dopo Wichterle e Lim usarono per primi questo termine riferendosi ad un reticolo di macromolecole cross-linkate in grado di rigonfiarsi in acqua, attribuendogli pertanto il significato che conserva tutt'ora. Il loro studio, considerato pionieristico, era basato sulla realizzazione di gel a base di poli(2-idrossietil methacrilato) (pHEMA) utilizzabili in oftalmologia.

Teoricamente gli idrogeli possono essere ottenuti a partire da qualunque polimero solubile in acqua. Tuttavia, è possibile aggiungere catene polimeriche idrofobiche per ottenere speciali proprietà richieste in specifiche applicazioni. La loro abilità di rigonfiarsi una volta immersi in soluzioni acquose, comunemente nota come *swelling*, deriva dalla presenza di gruppi funzionali idrofili (acidi o basici) connessi allo scheletro del polimero che favoriscono la ritenzione delle molecole d'acqua nelle regioni interne, mentre la capacità di non dissolversi è dovuta alla presenza di nodi chimici tra le catene. L'elevato contenuto d'acqua, che in un idrogelo rigonfiato può anche superare il peso del polimero stesso, e le analogie meccanico-composizionali con la matrice extracellulare (metaplasma), conferiscono a queste strutture reticolari un elevato grado di biocompatibilità. Di conseguenza, gli idrogeli hanno riscontrato un notevole interesse per applicazioni in campo biomedico e soprattutto nell'ingegneria tissutale e nel *drug-delivery*.

La loro struttura reticolare è caratterizzata da nodi, permanenti o reversibili, che si formano tra le catene. I primi sono costituiti da legami chimici covalenti, mentre i secondi sono il risultato di legami di tipo fisico, come ad esempio interazioni ioniche o legami a idrogeno. La reticolazione per via chimica si può ottenere mediante un processo a singolo *step*, quando la reazione di reticolazione è contemporanea a quella di polimerizzazione, o a *step* multiplo, nel caso in cui i monomeri reagiscano a formare catene che solo in un secondo momento vengono fatte reticolare.

Tra i diversi fattori che possono dare inizio ad un processo di reticolazione chimica, ha riscontrato un particolare interesse l'utilizzo della radiazione luminosa, sia essa luce visibile [400-800 nm] o ultravioletta [200-400 nm]. La reticolazione foto-indotta possiede numerosi vantaggi rispetto ad altri processi volti alla generazione di reticoli chimici, in quanto necessita di una bassa quantità di energia, è relativamente economica, è veloce e si esegue a temperatura ambiente. Essa si ottiene irraggiando con luce UV/vis un'opportuna formulazione contenente un fotoiniziatore, ossia una specie reattiva che, se colpita da una determinata

radiazione luminosa, è soggetta a fotolisi (Norrish I) o induce astrazione di idrogeno (Norrish II). In entrambi i casi il risultato è la generazione di specie radicaliche che, interagendo con i monomeri presenti nella formulazione, iniziano il processo di reticolazione.

In generale l'efficienza di tale processo è valutata sulla base del tipo di polimero, delle proprietà del fotoinziatore e dalle caratteristiche del fascio di luce incidente. Sono stati svolti studi approfonditi sugli idrogeli fotoreticolati poiché essi possono essere funzionalizzati con molecole biologiche e prodotti in forme complesse in tempi brevi. Fattori, questi, che ne hanno consentito l'impiego nei sistemi di trasporto farmacologico, di incapsulamento cellulare e di stampaggio 3D. Tuttavia, nonostante i potenziali vantaggi in questi campi applicativi, il loro utilizzo è limitato da alcune problematiche ancora irrisolte, quali la tipologia delle radiazioni luminose utilizzate (la componente UVB dello spettro ultravioletto può danneggiare il DNA nel caso di stampaggio di formulazioni contenenti cellule) e la pericolosità delle specie radicaliche non reagite che possono essere dannose sia per le cellule che per i tessuti. Per queste ragioni, negli ultimi anni, le ricerche si sono orientate su fotoiniziatori sensibili alla luce visibile che, sebbene presentino una minore reattività, sono tollerati maggiormente dalle cellule.

Il secondo capitolo di questo elaborato introduce i materiali utilizzati nel lavoro sperimentale. Dopo un breve cenno alle caratteristiche ed alle proprietà di PCL e PEG, sono presentati i protocolli seguiti per sintetizzare gli oligomeri a diverso peso molecolare, la strategia di funzionalizzazione adottata per ottenere la metacrilazione degli oligomeri, la sintesi e successiva metacrilazione delle nanosfere di grafene ossido ed infine il metodo seguito per la preparazione degli idrogeli.

Il PCL è un poliestere semicristallino idrofobo ottenuto mediante polimerizzazione per apertura di anello dell' $\epsilon$ -caprolattone. È caratterizzato da una temperatura di transizione vetrosa ( $T_g$ ) di  $-60^\circ\text{C}$ , una temperatura di fusione ( $T_m$ ) compresa tra  $58$  e  $65^\circ\text{C}$  ed una resistenza a trazione di  $0,4$  GPa. È un materiale che gode dell'approvazione della Food and Drug Administration statunitense (FDA) per le applicazioni biomediche in quanto degrada lentamente per idrolisi e viene espulso dai reni o incorporato nel ciclo dell'acido tricarbossilico. Il PEG invece è uno dei polimeri più utilizzati nella sintesi di idrogeli, soprattutto nell'ingegneria dei tessuti cartilaginei. In ambiente biologico non provoca alcuna risposta immunologica e degrada facilmente. Viene sintetizzato mediante una reazione ad alta pressione tra ossido di etilene e acqua in presenza di un catalizzatore. È idrofilo e possiede una  $T_g$  di  $-65^\circ\text{C}$  ed una  $T_m$  che varia tra  $61$  e  $65^\circ\text{C}$ .

In questo lavoro sono stati selezionati oligomeri a diversi pesi molecolari:  $2000$  e  $14000$  g/mol per quanto riguarda il PCL;  $3000$ ,  $4000$  e  $6000$  g/mol relativamente al PEG. Come accennato in precedenza, gli oligomeri sono stati funzionalizzati così da avere, come terminazione di catena, dei gruppi metacrilici che possano essere reattivi durante la fotoreticolazione. Si è scelto di funzionalizzare le catene con gruppi metacrilici e non acrilici perché, sebbene meno reattivi, presentano dei vantaggi in termini di biocompatibilità.

In Figura 1 è riportato lo schema di sintesi del policaprolattone dimetacrilato. Inizialmente l'oligomero è stato solubilizzato in toluene, poi sono stati aggiunti metacriloil cloruro come co-reagente e trietilammina come catalizzatore. La soluzione è stata prima riscaldata per  $3$  h a  $60^\circ$  sotto agitazione magnetica ed in seguito filtrata in condizioni di vuoto utilizzando un filtro avente dimensione dei pori di  $0,45\mu\text{m}$ , al fine di eliminare il sale di trietilammina

idrocloridrica. Il PCLDMA, ottenuto infine per precipitazione in eptano, è stato lasciato ad essiccare in un forno a vuoto per 48 ore a temperatura ambiente.

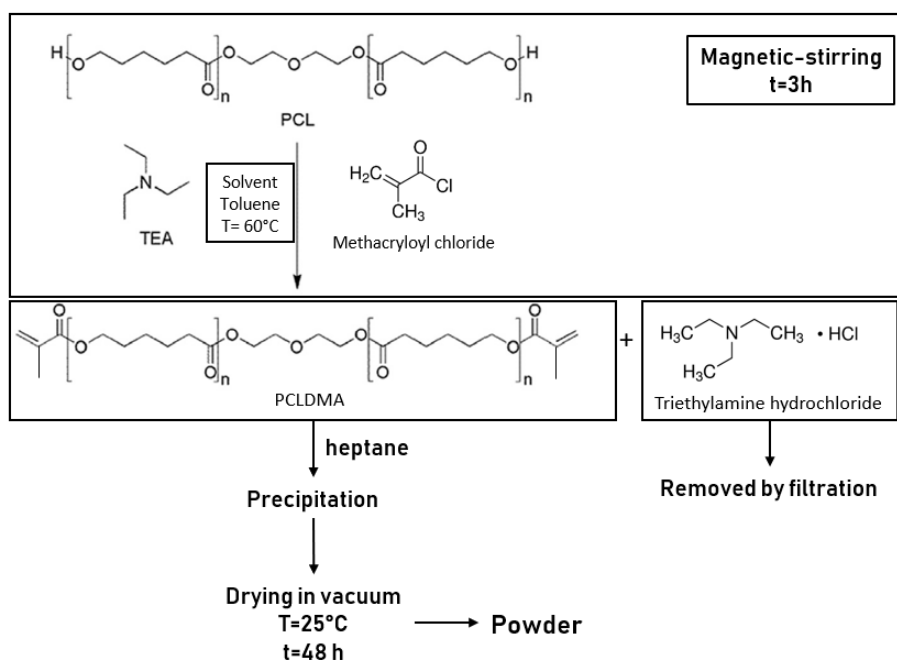


**Figura 1:** Rappresentazione schematica della sintesi del PCLDMA.

A fine comparativo è stato anche sintetizzato un campione di policaprolattone diacrilato (PCLDA).

La funzionalizzazione del PEG, schematizzata in Figura 2, è stata più complessa. La prima fase, riguardante la solubilizzazione in diclorometano e la lenta aggiunta di metacrilato di cloro e trietilammina, è simile a quella del processo seguito per la funzionalizzazione del PCL. Tuttavia in questo caso la reazione è stata condotta sotto flusso costante di azoto a temperatura ambiente per un'intera notte. La fase di filtrazione è analoga a quella precedentemente descritta, mentre, a differenza del PCLDMA, il PEGDMA è stato fatto precipitare per tre volte in dietil-etero a zero gradi. Una volta precipitato, il prodotto è stato ridissolto in acqua deionizzata e sottoposto ad un processo di dialisi per la durata di tre giorni, passati i quali è stato congelato e liofilizzato.

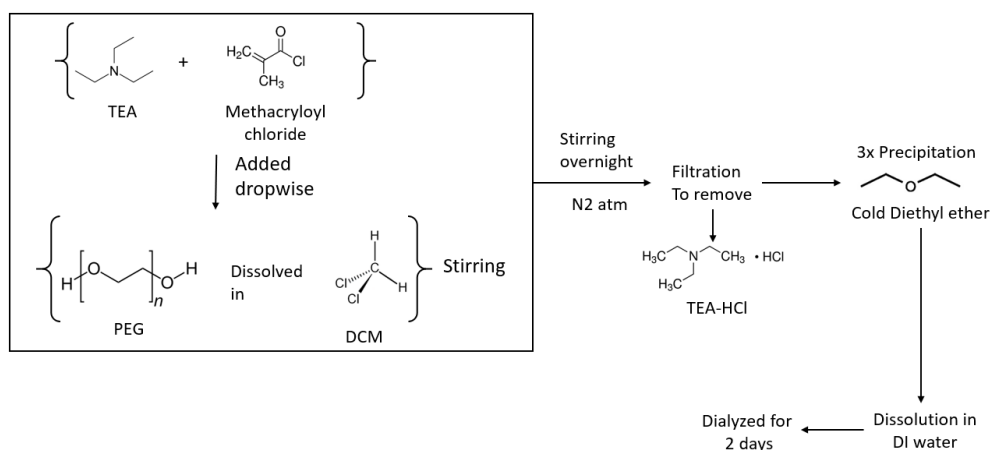


**Figura 2:** Rappresentazione schematica della sintesi del PEGDMA.

In questo lavoro di tesi sono anche state sintetizzate nanoparticelle di grafene ossido (nGO) mediante un processo di *green synthesis*, a partire da  $\alpha$ -cellulosa trattata in soluzione acquosa con acido solforico in concentrazione pari a 0.1 g/mL. Si tratta di un processo termico condotto in un microonde flexiWave settato in modo tale da ottenere un incremento di 20°C al minuto fino al raggiungimento della temperatura di processo di 220°C, che è stata in seguito mantenuta costante per due ore sotto continuo flussaggio di azoto. Questo passaggio ha portato all'ottenimento di nanoparticelle di grafene che sono state filtrate, lavate con acqua deionizzata ed infine lasciate asciugare in forno a vuoto per 12 ore a 25°C. Le nano-sfere sono state ossidate in una soluzione 70% HNO<sub>3</sub>, opportunamente sonicata per 50 minuti a 45°C e riscaldata a 90°C per ulteriori 50 minuti sotto costante agitazione magnetica. In seguito l'acidità della soluzione è stata ridotta aggiungendo dell'acqua deionizzata e le nanoparticelle di grafene-ossido sono state separate dal mezzo acido mediante evaporazione assistita da vuoto, liofilizzate e poste in forno in vuoto a temperatura ambiente per una settimana. La figura 2.5 riporta i passaggi principali di questa sintesi.

Le nanoparticelle sono state successivamente funzionalizzate seguendo cinque diversi processi, dei quali solo 3 hanno permesso di ottenere del grafene ossido metacrilato (MA-nGO) analizzabile. Tali processi hanno in comune l'iniziale dispersione delle nanoparticelle in etanolo cui è stato aggiunto il metacrilato cloruro goccia a goccia, ma differiscono per gli *steps* successivi.

Nel primo caso, dopo due ore di agitazione ed un'ulteriore aggiunta di acqua deionizzata, la temperatura è stata aumentata fino a 120°C in modo tale da eliminare l'acido cloridrico e il solvente rimasto. Terminato questo passaggio, è stata aggiunta nuovamente dell'acqua deionizzata e la soluzione è stata sottoposta ad un processo di liofilizzazione.

Nel secondo caso si è scelto di eliminare l'acido cloridrico scaldando la soluzione fino ad 80°C utilizzando un sistema a vuoto. In seguito la soluzione è stata sottoposta a dialisi, aggiungendo dell'acqua deionizzata, ed a liofilizzazione.

Nel terzo processo, (Figura 3) le fasi sono del tutto analoghe a quelle del secondo caso sopra descritto, ad eccezione dello *step* di dialisi, che in questo caso non è stata effettuato.

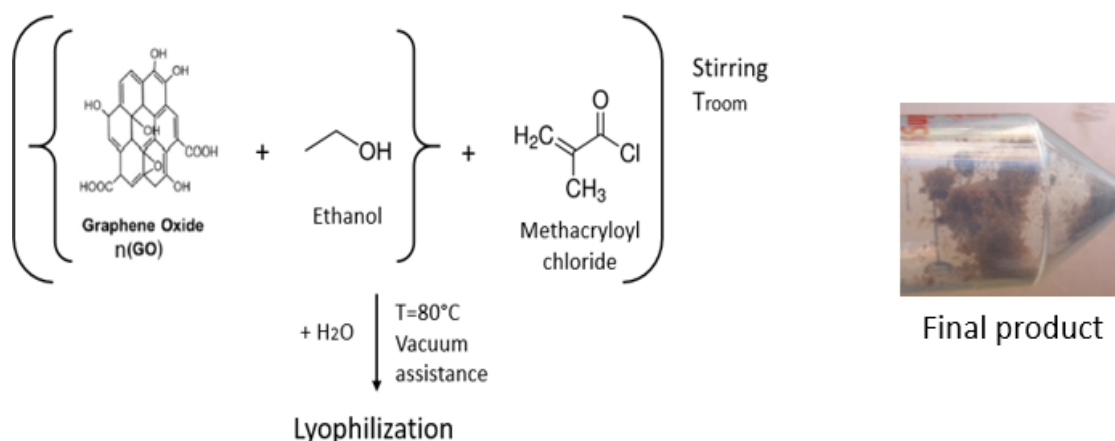


**Figura 3:** Schema del processo di sintesi del PEGDMA.

Per quanto riguarda la preparazione degli idrogeli, i primi tentativi di fotoreticolazione effettuati sulle formulazioni hanno evidenziato problemi di instabilità dimensionale dovuti sia all'eccessiva velocità di evaporazione dei solventi inizialmente scelti (acetone/etanolo), sia all'elevata lunghezza delle catene e dalla bassa reattività del polietilene glicole precedentemente funzionalizzato. Per ovviare a tali problematiche si è deciso di utilizzare come solvente il propilencarbonato ed il PEGDMA sintetizzato è stato sostituito con un PEGDMA commerciale a minor peso molecolare (750 g/mol).

Le formulazioni finali utilizzate sono riportate in Tabella 1 ed alcune fotografie degli idrogeli reticolati con lampada UV sono riportate nella Figura 4. Nel caso del PCLDMA 14k [70:30] il network non si è formato a causa dell'eccessiva lunghezza delle catene.

**Tabella 1:** Formulazioni ottenute con il PEGDMA 750.

1° Oligomero	2° Oligomero	Solvente	Rapporto tra i materiali
PCLDMA 2k	PEGDMA 750	PC (70%wt)	30:70
			50:50
			70:30
PCLDMA 14k	PEGDMA 750	PC (70%wt)	30:70
			50:50

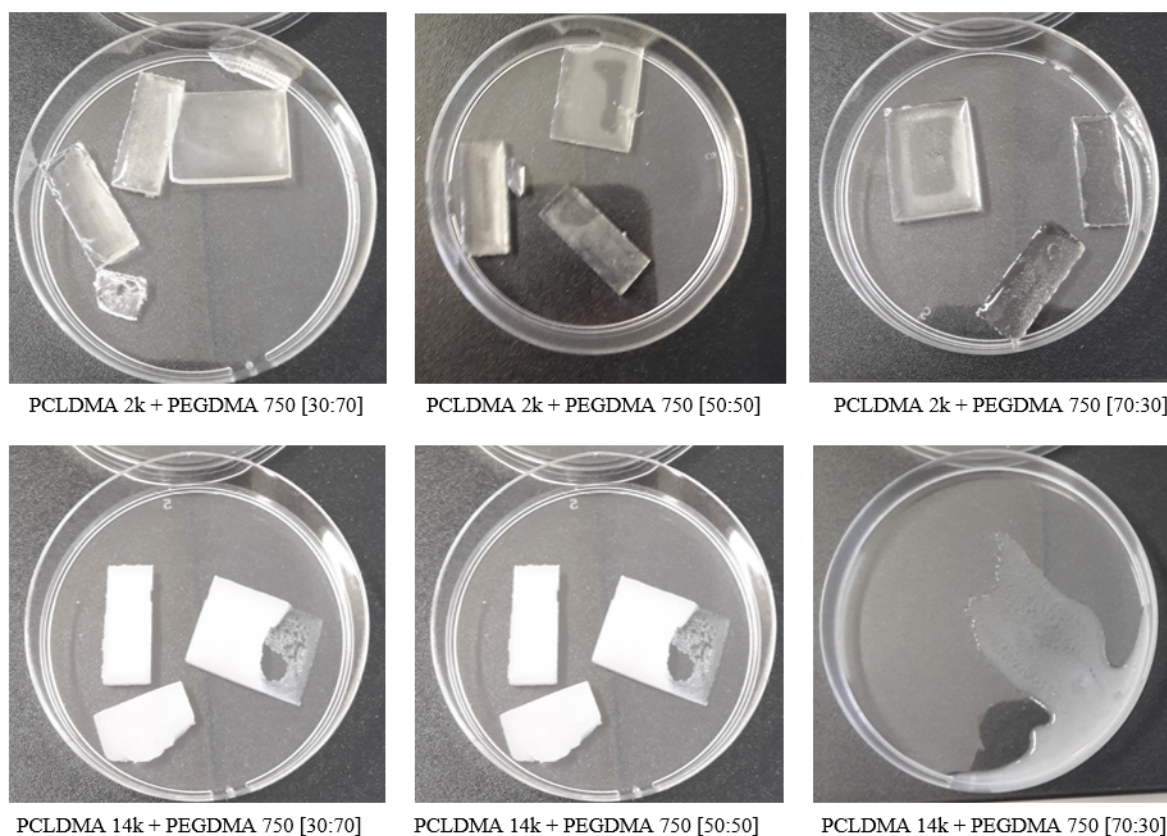


**Figura 4:** Fotografie delle varie formulazioni post trattamento con lampada UV.

Il terzo capitolo di questo lavoro è incentrato sulla descrizione delle tecniche di caratterizzazione che sono state utilizzate per: 1) confermare l'avvenuta funzionalizzazione degli oligomeri e delle nanoparticelle di grafene ossido, 2) valutare il peso molecolare degli oligomeri di PCL, 3) analizzare la stabilità delle nanoparticelle di grafene ossido ed infine 4) valutare la reticolazione, il comportamento termomeccanico e lo swelling degli idrogeli.

La risonanza magnetica protonica (H-NMR), eseguita con lo strumento Avance 400 (400.13 MHz-Bruker USA) su campioni disciolti in cloroformio deuterato (10 mg/mL), ha consentito di confermare la presenza di nuovi  $\delta$ -shift nello spettro degli oligomeri funzionalizzati, dovuti alla variazione dell'intorno chimico degli atomi di idrogeno delle unità terminali.

La spettroscopia infrarossa in riflettanza totale attenuata (ATR-FTIR) è stata eseguita utilizzando lo spettrometro Perkin-Elmer Spectrum 2000 (risoluzione  $2\text{ cm}^{-1}$ ) con l'intenzione di verificare la presenza di gruppi metacrilici negli oligomeri funzionalizzati. Questa tecnica è stata inoltre sfruttata per confermare la scomparsa di tali gruppi dalle formulazioni post reticolazione. In questa seconda analisi è stato utilizzato uno spettrometro Nicolet iS50 FT-IR, (risoluzione  $4\text{ cm}^{-1}$ ). Per entrambe le analisi è stato eseguito un background prima di testare ogni campione e gli spettri sono stati registrati eseguendo 16 scansioni in un range di lunghezze d'onda compreso tra  $4000$  e  $650\text{ cm}^{-1}$ .

La calorimetria differenziale a scansione (DSC) ha consentito di valutare sia le variazioni della temperatura di fusione ( $T_m$ ) e dell'entalpia di fusione ( $\Delta H_{\text{fus}}$ ) degli oligomeri prima e dopo la funzionalizzazione, sia l'eventuale presenza di domini cristallini nei seguenti idrogeli: PCLDMA 2k + PEGDMA 750 e PCLDMA 14k + PEGDMA 750 entrambi con rapporto 50:50 in peso realizzati. Queste analisi sono state eseguite sotto flusso costante di azoto e su

campioni di 10-12 mg utilizzando una DSC/TGA (Mettler Toledo) ed impostando una rampa termica da 20 a 100 °C per i test sugli oligomeri e da -80 a 100 °C per quelli sugli idrogeli.

La cromatografia ad esclusione dimensionale (SEC), eseguita sui soli oligomeri di policaprolattone e policaprolattone dimetacrilato è servita ad avere un'indicazione dei pesi molecolari medi di queste catene.

L'analisi termogravimetrica (TGA) è stata invece utilizzata per confrontare la stabilità termica delle nanoparticelle di grafene ossido pre e post funzionalizzazione. Per eseguire tali misure, effettuate da 0 a 800°C sotto flussaggio costante di azoto, è stata utilizzata una TGA Mettler Toledo.

L'analizzatore di potenziale zeta Zetasizer Malvern è servito a valutare la stabilità a temperatura ambiente della delle nanoparticelle, tal quali e metacrilate, in soluzione acquosa (0,1 mg/mL).

Il grado di rigonfiamento degli idrogeli è stato valutato mediante ripetute misure gravimetriche. I campioni sono stati pre-trattati in stufa a vuoto a 50°C per 2 giorni e successivamente immersi in acqua deionizzata ed il loro peso è stato monitorato ad intervalli regolari. Una volta raggiunta la condizione di equilibrio, sono state calcolate la capacità di rigonfiamento e il contenuto d'acqua

L'analisi dinamo-meccanica termica infine, è stata utilizzata per lo studio delle proprietà termomeccaniche degli idrogeli. Le prove sono state eseguite utilizzando un Tritec 2000 DMA, impostando una frequenza di 1 Hz ed una rampa di temperatura di 3°C/min.

Nel quarto capitolo sono riportati e discussi i risultati delle prove di caratterizzazione. Esso è strutturato in 3 sezioni: 1) conferma della metacrilazione degli oligomeri, 2) conferma della metacrilazione del nanografene ossido e 3) caratterizzazione degli idrogeli.

L'avvenuta metacrilazione degli oligomeri è stata confermata dai risultati dell'analisi spettroscopica. Confrontando lo spettro del PCL con quello relativo al PCLDMA, è stato possibile constatare la scomparsa del picco diffuso del legame OH a 3500  $\text{cm}^{-1}$  e la comparsa di due nuovi picchi a 830 e 1630  $\text{cm}^{-1}$  corrispondenti alla vibrazione del C=C. Per quanto riguarda la metacrilazione del PEG, oltre che alla scomparsa della vibrazione appartenente al gruppo OH intorno ai 3500  $\text{cm}^{-1}$ , si è potuta notare la presenza di tre nuovi segnali, rispettivamente a 1700, 1640 e 1323  $\text{cm}^{-1}$ , appartenenti alle vibrazioni del legame -COO-, C=C e CH<sub>3</sub>. Inoltre, confrontando tali spettri, si è notato che la conversione dei gruppi ossidrilici terminali del PEGDMA è stata completa solo nei pesi molecolari 4k e 6k, mentre per il 3k è stata solo parziale.

La risonanza magnetica nucleare (H-NMR) ha permesso di confermare la presenza di gruppi metacrilici negli oligomeri funzionalizzati grazie alla comparsa di  $\delta$ -shift attribuibili a tali gruppi a  $\delta$  6.11, 5.56 e 1.95.

Negli spettri dei PCL è stato possibile, integrando opportunamente l'area dei picchi, avere una stima del peso molecolare. Mentre nel caso del PEG questi spettri sono stati valutati solo a scopo comparativo.

Gli spettri del PCL-diol 2k e PCLDMA 2k sono riportati in Figura 4 e Figura 5. Due esempi di calcoli eseguiti su tali spettri al fine di valutare il peso molecolare degli oligomeri sono riportati nelle equazioni 1,2,3,4,5 e 6.

$$\delta_i = 1 = 4H \rightarrow 1H = 0,25 \quad (1)$$

$$\delta_d = 8,06 \sim 8 \rightarrow 32H \rightarrow 16C_d \rightarrow 16\_unit\grave{a}\_ripetitive \rightarrow 16 * 114 = 1824 \frac{g}{mol} \quad (2)$$

$$M_{w\_PCL\_2k} = 1824 + 104 + (2 * 115) = \mathbf{2158} \frac{g}{mol} \quad (3)$$

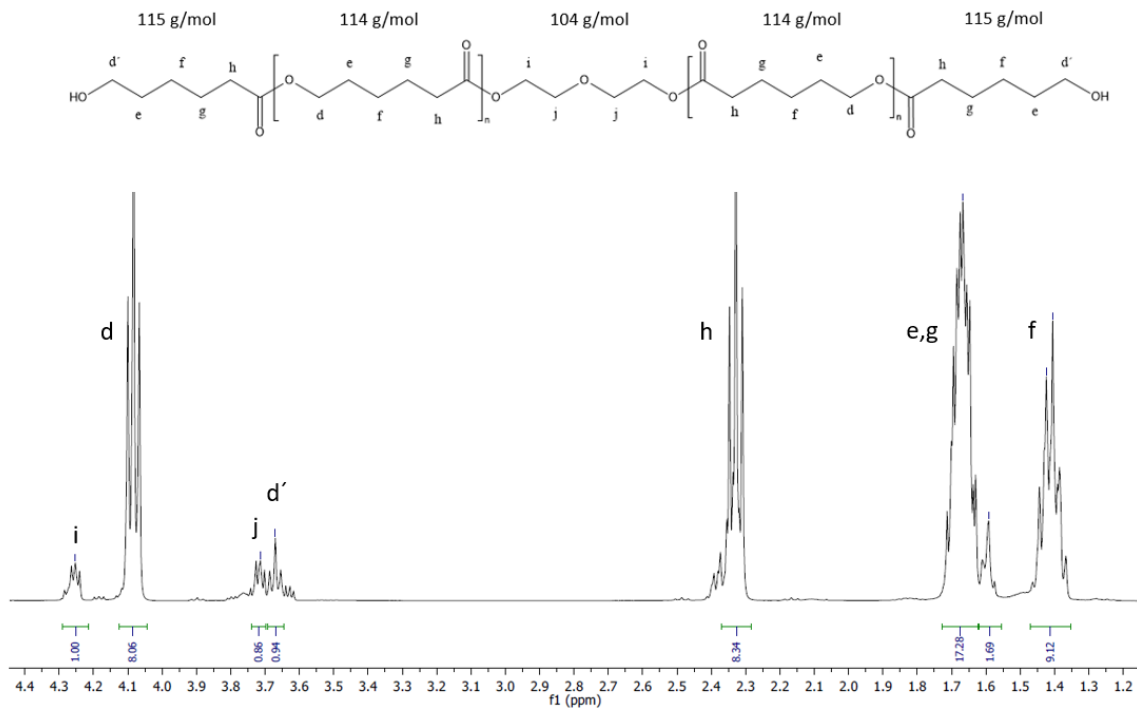


**Figura 4:** Spettro H-NMR del PCL-diol 2k.

$$\delta_i = 2,39 \sim 2 = 4H \rightarrow 1H = 0,5 \quad (4)$$

$$\delta_d = 26,32 \sim 26 \rightarrow 52H \rightarrow 26C_d \rightarrow 26\_unit\grave{a}\_ripetitive \rightarrow 26 * 114 = 2964 \frac{g}{mol} \quad (5)$$

$$M_{w\_PCLDMA\_2k} = 2964 + 104 + (2 * 159) = \mathbf{3386} \frac{g}{mol} \quad (6)$$

Il valore ottenuto, maggiore del previsto, può essere spiegato con il verificarsi di reazioni parassite durante il processo di funzionalizzazione.

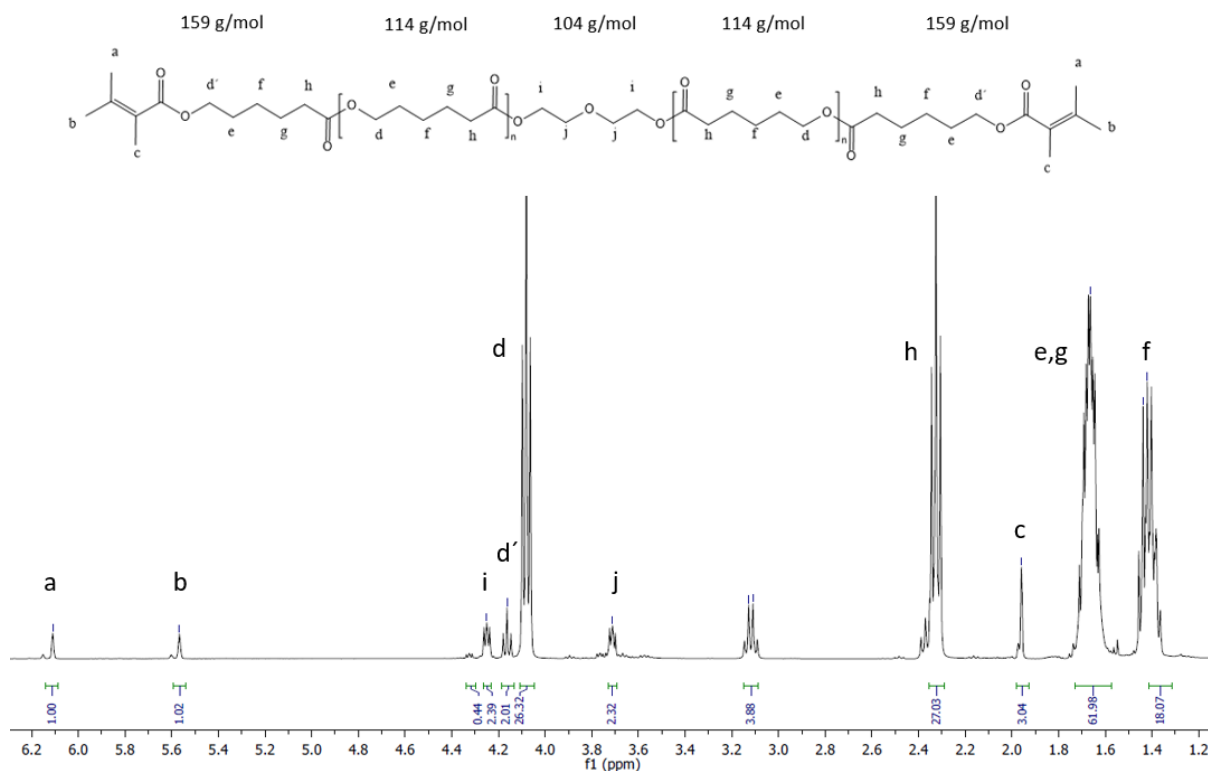


**Figura 5:** Spettro H-NMR del PCLDMA 2k.

È stato inoltre possibile calcolare la percentuale di conversione basandosi sulla comparazione del rapporto dell'integrale teorico (ossia corrispondente ad una conversione totale) dei picchi a, b, c, i e j e sperimentale (Equazione 7).

$$\delta_a : \delta_b : \delta_c : \delta_i : \delta_j = 1 : 1 : 3 : 2 : 2 \quad (7)$$

Questo rapporto corrisponde ad una conversione del 100%.

Per quanto riguarda invece il PCL 14, il peso molecolare dell'oligomero iniziale è stato stimato pari a 9950 g/mol mentre quello del PCLDMA è 10262, con una percentuale di conversione del 33%.

Sia negli spettri del PCL, sia in quelli del PEG, sono presenti dei picchi estranei alla struttura principale. In particolare il doppio picco a  $\delta$  3.13 e 3.11 prova che si siano verificate alcune reazioni parassite. In Figura 6 sono riportati gli spettri del PEG e PEGDMA 6k, nei quali è evidente la presenza dei gruppi metacrilici.

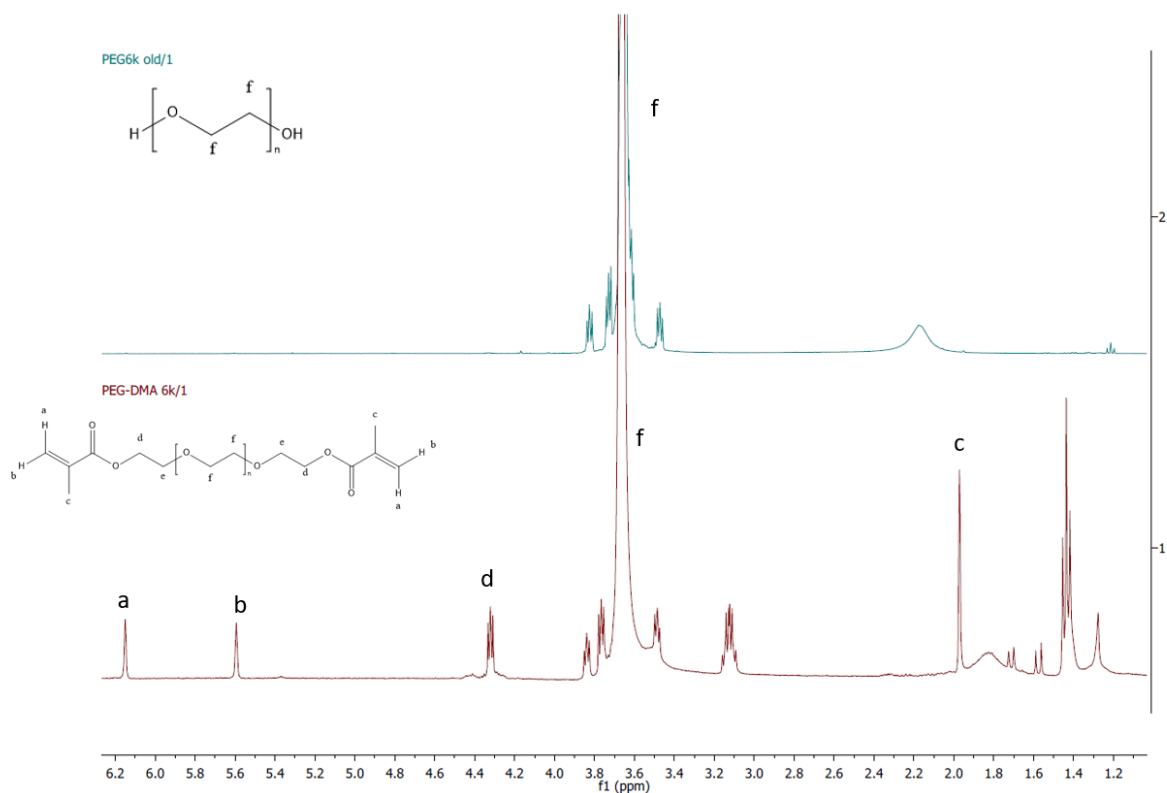


**Figura 6:** Spettro H-NMR del PEG e del PEGDMA 6k.

I risultati dell'analisi calorimetrica hanno evidenziato una diminuzione della temperatura di fusione del campione funzionalizzato rispetto a quello non modificato, che può essere spiegata considerando la presenza di gruppi metacrilici che sono responsabili di una variazione nel grado di cristallinità del polimero. Analizzando i termogrammi, è stata inoltre calcolata l'entalpia di fusione prendendo come riferimento l'entalpia di fusione del policaprolattone 100% cristallino ( $\Delta H=135.44$  J/mol).

Tutti i risultati dell'analisi DSC sono riportati in Tabella 2.

**Tabella 2:** Dati ricavati dall'analisi calorimetrica differenziale a scansione.

Materiale	$T_m$ (°C)	$\Delta H_m$ (J/g)	Crystallinity (%)
PCL-diol 2k	62.57	96.38	71.16
PCLDA 2k	54.78	66.36	49.00
PCLDMA 2k	53.23	56.89	41.01
PCL-diol 14k	66.09	85.34	63.01
PCLDMA 14k	59.75	76.46	56.45
PEG 3k	60.15	202.16	/
PEGDMA 3k	48.65	88.27	/
PEG 6k	62.15	228.33	/
PEGDMA 6k	57.82	180.29	/

La cromatografia ad esclusione dimensionale (SEC) ha consentito di valutare le variazioni di peso molecolare a seguito della metacrilazione del PCL. Dall'analisi dei volumi idrodinamici si è notato che nel caso del PCL 2k le variazioni non sono rilevanti, mentre nel caso del PCL 14 k la variazione riscontrata è del 5%. In tutti i casi, l'indice di polidispersità è stato valutato pari a 1,5 che è il valore atteso per una polimerizzazione radicalica e quindi risulta compatibile con il meccanismo di reazione che ha portato all'ottenimento degli oligomeri di partenza.

La seconda parte del capitolo è invece dedicata ai risultati delle prove di caratterizzazione eseguite sulle nanoparticelle di grafene ossido.

I risultati della spettroscopia infrarossa effettuata sui campioni metacrilati e confrontati con quelli relativi all'analisi di un campione non metacrilato usato come riferimento, hanno confermato la presenza di due nuovi picchi a 2929 e 2851  $\text{cm}^{-1}$  che possono essere attribuiti alla vibrazione di stiramento del gruppo C-H appartenente al gruppo metile.

Nel grafico riportato in Figura 6, la curva in rosso si riferisce allo spettro relativo al MA-nGO ottenuto effettuando prima il riscaldamento a 120°C ed in seguito la dialisi, mentre gli altri due campioni di MA-nGO sono stati riscaldati ad 80°C in condizioni di vuoto e successivamente sottoposti ad un trattamento di liofilizzazione.

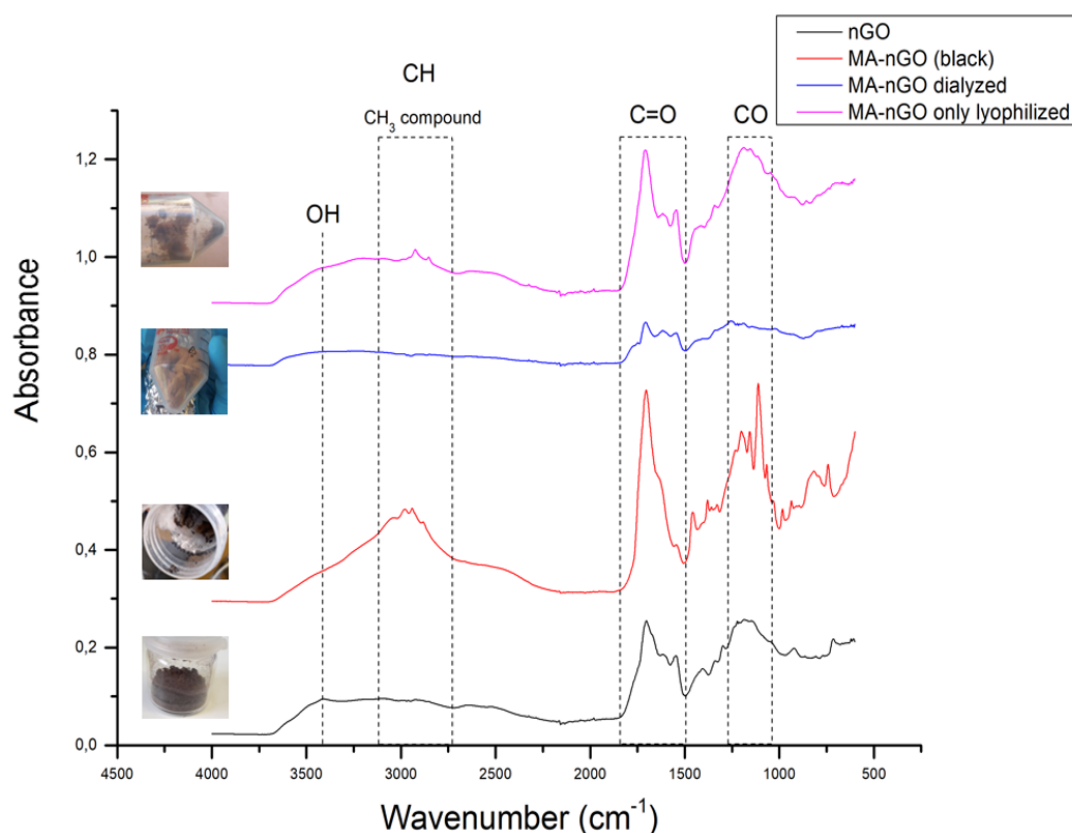


**Figura 6:** Spettro ATR-FTIR comparativo tra le varie nanoparticelle di MA-nGO.

L'avvenuta metacrilazione può essere ulteriormente confermata dalla diminuzione dell'intensità del picco OH in due casi (spettro rosso e viola già citate in precedenza) mentre nel terzo caso (spettro blu), rimane pressoché costante.

L'analisi termogravimetrica ha permesso di valutare la stabilità termica delle nanoparticelle. I risultati ottenuti hanno evidenziato una parziale degradazione termica del nanografene ossido non metacrilato già a 100°C, pertanto è stata ritenuta plausibile l'ipotesi che la funzionalizzazione dello stesso ad una temperatura superiore ne avesse causato una parziale degradazione.

Una ulteriore conferma dell'avvenuta metacrilazione è stata ottenuta con i risultati dell'analisi del potenziale zeta che hanno evidenziato una diminuzione di stabilità delle nanoparticelle in soluzione acquosa a seguito della funzionalizzazione. Complessivamente, grazie ai risultati ottenuti con queste tre prove, è stato possibile selezionare una tecnica definitiva per la funzionalizzazione delle nGO.

La terza parte di questo capitolo è incentrata sull'analisi dei risultati delle prove di caratterizzazione effettuate sugli idrogeli. La spettroscopia ATR-FTIR è stata utilizzata per verificare l'effettiva scomparsa del doppio legame a seguito della reticolazione. In tutti gli spettri relativi a formulazioni con PCLDMA 2k è stata confermata questa assunzione, e, in particolare, è stata osservata la scomparsa dei picchi dei legami C=C e CH<sub>3</sub> a 810 e 1320 cm<sup>-1</sup> rispettivamente.

L'analisi termo-dinamo meccanica è stata eseguita sui due idrogeli (PCLDMA 2k + PEGDMA 750 e PCLDMA 14k + PEGDMA 750) aventi percentuali in peso 50:50. Entrambi gli spettri riportati in Figura 7 mostrano la presenza di due temperature di transizione vetrosa, risultato questo compatibile con l'ipotesi di una parziale separazione di fase. Il grafico del PCLDMA 2k + PEGDMA 750 mostra una prima Tg più alta rispetto all'idrogelo con PCLDMA 14k, poiché nel primo caso le catene più corte hanno portato alla formazione di un network avente densità di reticolazione maggiore.

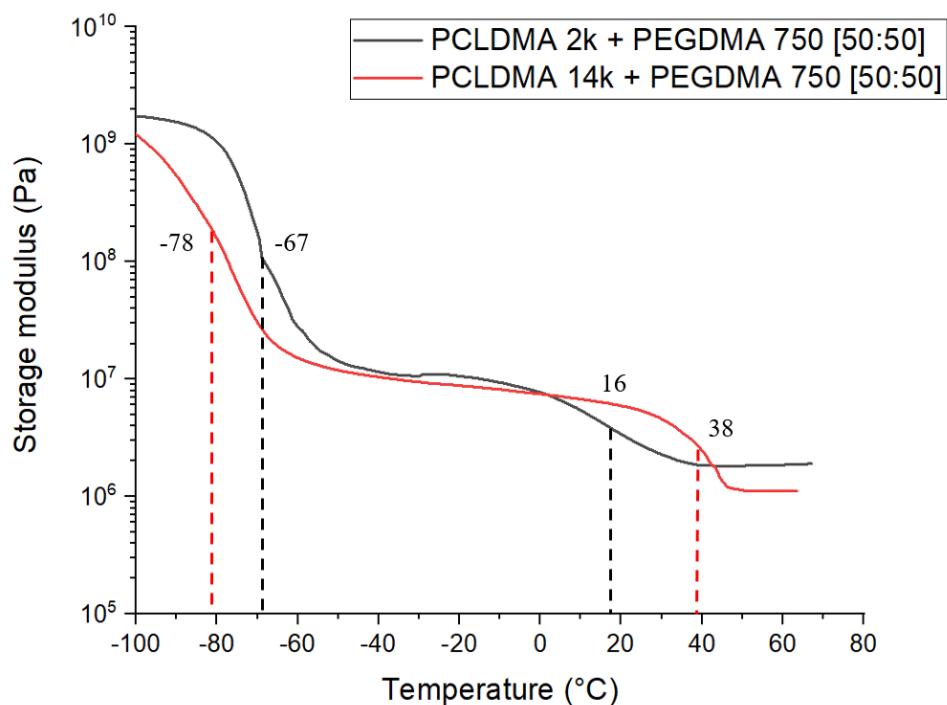


**Figura 7:** Comportamento termomeccanico degli idrogeli PCLDMA 2k + PEGDMA 750 e PCLDMA 14k + PEGDMA 750 aventi percentuali in peso 50:50

Per quanto riguarda i risultati delle prove calorimetriche eseguite sui due campioni PCLDMA 2k + PEGDMA 750 e PCLDMA 14k + PEGDMA 750 (entrambi 50:50), si può notare che nel primo caso la lunghezza delle catene è risultata insufficiente a creare un dominio cristallino nella struttura reticolata, mentre nel secondo è stata constatata la presenza di un picco di fusione a 38°C che ha confermato la presenza di domini cristallini nel campione.

Il grado di rigonfiamento e il contenuto d'acqua all'equilibrio sono riportati in Tabella 2. Da questi dati si può notare come il contenuto di PCLDMA influenzi negativamente questi due fattori, in quanto comporta un aumento di idrofobicità. Mentre, a parità di percentuale in peso, l'idrogel con catene più lunghe rigonfia in maniera maggiore poiché possiede una densità di reticolazione minore. In Figura 8 sono riportate alcune fotografie dei campioni ottenuti, prima e dopo lo swelling.

**Tabella 2:** Contenuto d'acqua all'equilibrio e grado di rigonfiamento dei vari idrogeli.

Idrogelo	Contenuto d'acqua all'equilibrio	Grado di rigonfiamento
PCLDMA 2k + PEGDMA [30:70]	34.08%	51.7%
PCLDMA 2k + PEGDMA [50:50]	28.98%	40.87%
PCLDMA 2k + PEGDMA [70:30]	5.15%	5.4%
PCLDMA 14k + PEGDMA [30:70]	44.96%	81.7%
PCLDMA 14k + PEGDMA [50:50]	36.54%	57.59%
PEGDMA 750	68.36%	216.13%

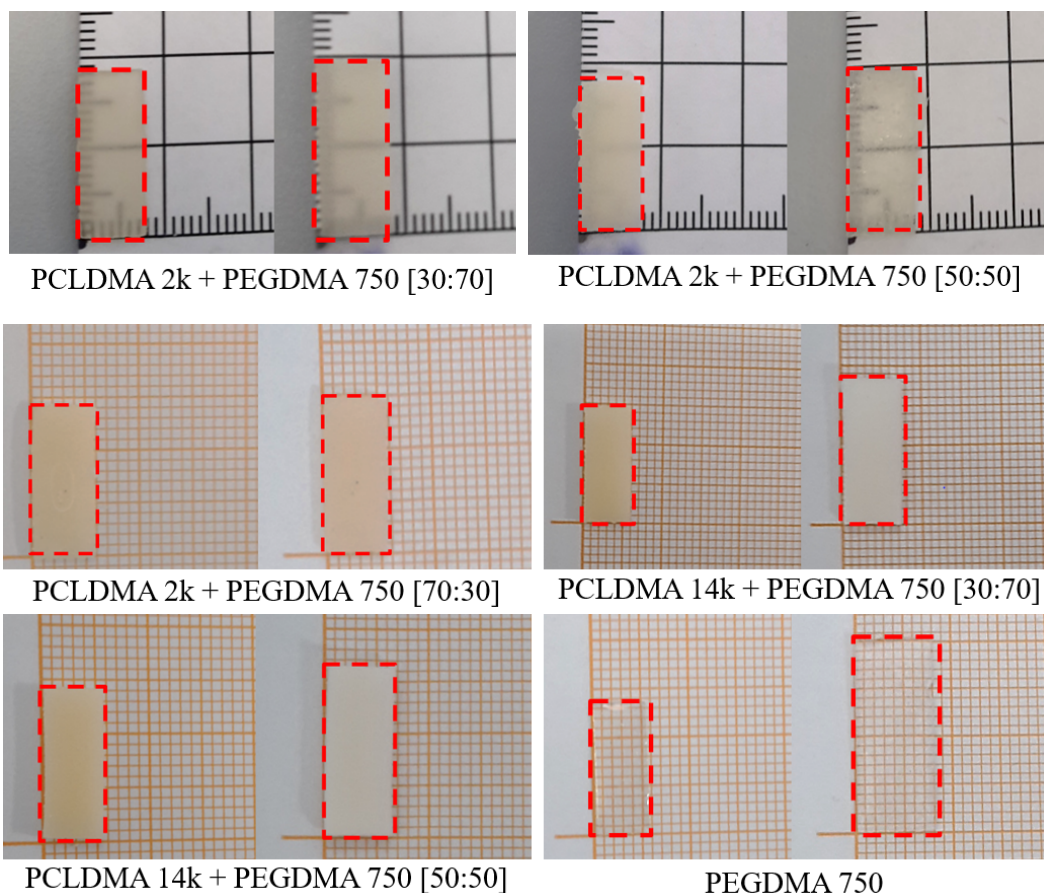


**Figura 7:** Fotografie dei differenti network analizzati.

In conclusione sono stati ottenuti cinque differenti idrogeli a partire dalla funzionalizzazione dei singoli oligomeri (PCL e PEG) tramite una reazione di metacrilazione. Le analisi ATR-FTIR, H-NMR, DSC e SEC hanno confermato l'avvenuta metacrilazione.

Sono state inoltre funzionalizzate delle nanoparticelle di grafene ossido precedentemente sintetizzate a partire da cellulosa. Anche in questo caso la metacrilazione è stata confermata dai risultati delle analisi ATR-FTIR, TGA e dalle misure del potenziale zeta.

Cinque differenti formulazioni sono state reticolate con irraggiamento UV utilizzando l'IRGACURE 819 come fotoiniziatore. Le proprietà degli idrogeli ottenuti combinando il PCLDMA sintetizzato con un PEGDMA commerciale sono state valutate mediante analisi ATR-FTIR, DMTA, DSC e misure di rigonfiamento.

I lavori futuri si incentreranno su studi di biocompatibilità legati all'incorporazione delle MA-nGO nel reticolo.

# 1. Introduction

The term “hydrogel” was used in the scientific literature for the first time in 1894 to describe a colloidal gel obtained from an inorganic salt. Almost sixty years later, the scientific journal Nature reported the first research work on synthetic hydrogels. Throughout this study, whose aim was to develop a material usable in permanent contact with the human tissue, the term was used referring to a macromolecular network obtained from polyhydroxyethylmethacrylate (pHEMA). From that moment on, the number of publications on hydrogel started to increase exponentially.

Today, many progresses have been made concerning both hydrogels formulations and applications fields (Figure 1.1) [1].

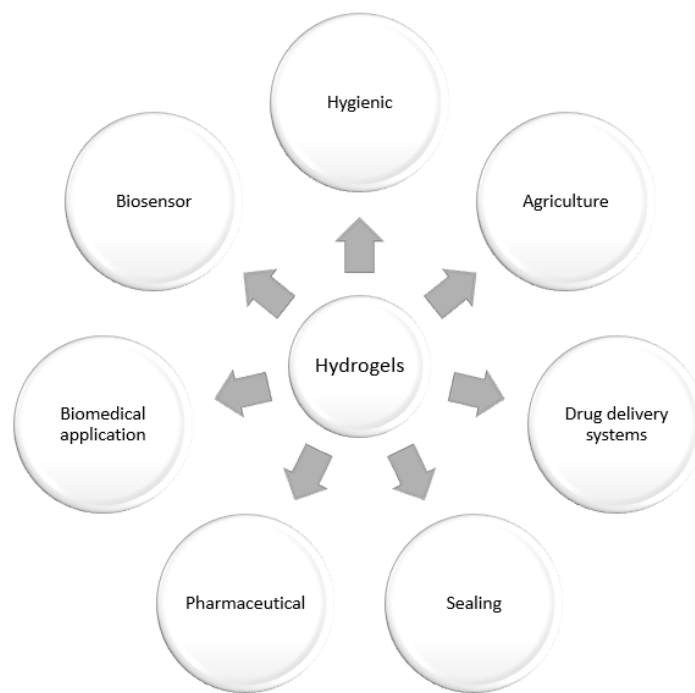


**Figure 1.1:** Hydrogels applications fields.

In the following chapters, hydrogels are first investigated in terms of structure and properties. The swelling mechanism is discussed in detail, introducing general formula commonly used to evaluate the phenomenon. Later, classification methods and mechanisms of network generation are presented, focusing the attention on photocrosslinking.

To conclude, a brief overview of the application fields is given, with a particular stress to biomedical applications because the hydrogels synthesized in this work, since both the oligomers being used are biocompatible, could find a potential application in this area.

## 1.1 Hydrogels

Hydrogels are commonly defined as three-dimensional polymeric network, which could retain a great amount of water or biological fluid within the cross-linked structure, ones immersed in aqueous media. The capability of showing high swelling degrees is due to the combined effect of the hydrophilic part, which tends to absorb water, and the crosslinked network that prevents the dissolution of the structure. Moreover, this unique physical property is completely reversible. This is the reason why hydrogels are considered to own both the cohesive properties of a solid and the diffusion mechanism of transport typical of fluids.

Hydrogels can be also described as multicomponent systems, where two or more polymers generate the network. In these systems, according to their properties, nature and crosslinking density, the total water uptake in the swollen state can be higher than the polymer fraction [2]. In the last sixty years, the list of features required to hydrogels become longer and longer, including low content of residual monomer, high and controlled absorption, re-wetting capability, which is the ability of returning the retained solution or maintaining it, and pH-neutrality in water. Furthermore, according to their application, hydrogels have to satisfy also other special needs. With a closer look to the biomedical field, they have to be also nontoxic, stable in biological environment and their degradation products must not be poisoning.

Hydrogels can be also tailored to perform the swollen-non-swollen state transition in response to an external stimulus either chemical or physical. Examples of chemical variations can be: pH, molecular species and solvent composition changes; while the physical ones could be temperature, light, pressure and magnetic or electric field variations (Figure 1.2).

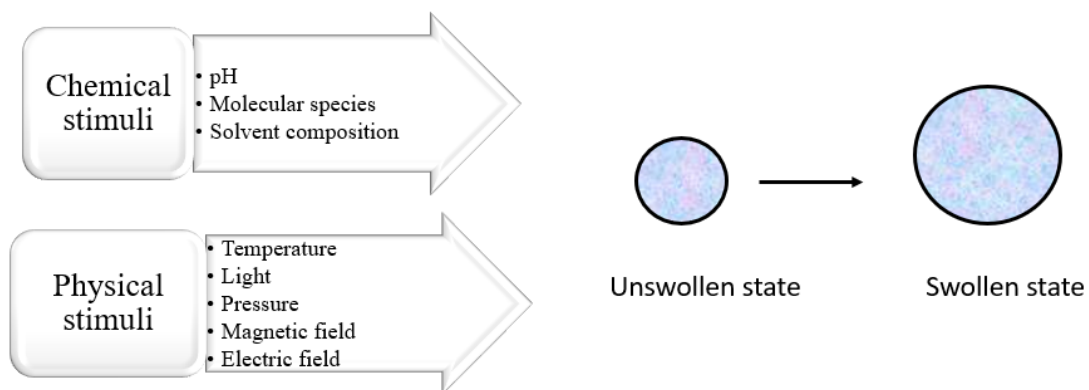


**Figure 1.2:** Physical and chemical external stimuli.

### 1.1.1 Structure parameters

Hydrogels are typically described starting from the analysis of their structure. Accordingly, there are some structural parameters commonly used to investigate the nature of their network: 1) polymeric volume fraction, 2) effective molecular weight and 3) cross-linking distance.

The polymeric volume fraction in the swollen state ( $V_s$ ), which represents the amount of solvent that can be stored inside the gel, can be determined using equation 1.1.

$$V_s = \frac{V_p}{V_g} \quad (1.1)$$

where  $V_p$  is the volume of the polymer and  $V_g$  is the swollen gel volume.

The effective molecular weight of the polymer between two cross-linked points ( $\bar{M}_C$ ) (Figure 1.3) can be calculated as follows (equation 1.2):

$$\bar{M}_C = \frac{M_0}{2X} \quad (1.2)$$

where  $X$  is the degree of cross-links and  $M_0$  is the molecular weight of the repeating unit.

The distance between two cross-links ( $\xi$ ) can be obtained using equation 1.3.

$$\xi = \frac{l}{\sqrt[3]{V_s}} \sqrt{\frac{C_n 2 \bar{M}_C}{M_0}} \quad (1.3)$$

where  $C_n$  is the Flory constant ratio, which depends on the solvent-polymer system, and  $l$  is the carbon-carbon bond length.

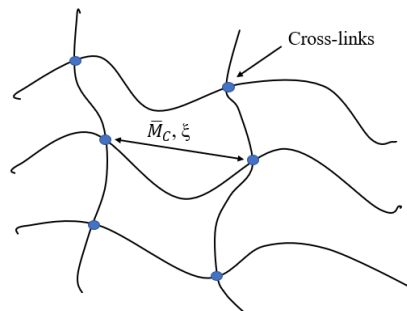


**Figure 1.3:** Schematic representation of a hydrogel network.

The crosslinked structure can be obtained *via* physical or chemical processes. Physical crosslinking regards ionic and hydrophobic interaction, while chemical crosslinking involves real chemical reactions, such as Michael's addition and Michaelis-Arbuzov reactions, which can be started by ultraviolet radiation, heat or by means of cross-linker agents.

Generally, the hydrogels structure doesn't reach the perfection of an ideal network, but is commonly characterized by several defects (Figure 1.4).

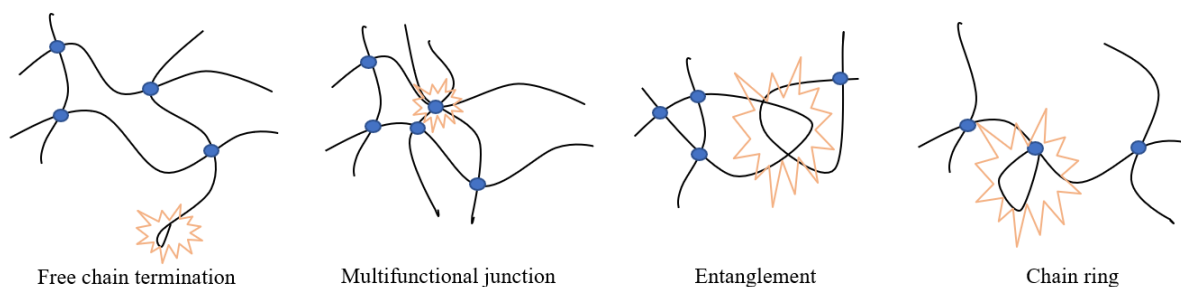


**Figure 1.4:** Main chain defects.

### 1.1.2 Swelling mechanism

When a dried hydrogel is immersed in aqueous media, water molecules start to penetrate its network, and, as a result, the meshes of the net start to expand. This phenomenon, which is reversible, is commonly known as “swelling”. However, the process is limited in time, since the elastic force of the cross-links (either physical or chemical) acts as counter-balance, avoiding further water absorption. The combination of these two forces defines the swelling pressure  $P_{sw}$ , which is equal to zero once the equilibrium state has been reached.  $P_{sw}$  is directly proportional to the polymer concentration according to equation 1.4.

$$P_{sw} = KC^n \quad (1.4)$$

where  $C$  is the polymer concentration, whereas  $K$  and  $n$  are constants.

The total amount of water up-take can be determined using equation 1.5.

$$m_{water} = \frac{m_{hydrogel,wet} - m_{hydrogel,dry}}{m_{hydrogel,wet}} \quad (1.5)$$

The degree of swelling and the swelling ratio are given by equation 1.6 and 1.7 respectively:

$$D_{sw} = \frac{m_{hydrogel,wet}}{m_{hydrogel,dry}} \quad (1.6)$$

$$R_{sw} = D_{sw} \frac{\rho_0}{\rho_{sw}} \quad (1.7)$$

Where  $\rho_0$  and  $\rho_{sw}$  are the density of the dried and swollen hydrogel respectively [3].

Swelling mechanisms can be described in many different ways. Commonly they are investigated according to either the typology of water-hydrogel bond or making consideration on kinetics.

In the first case, the swollen state is reached due to the formation of three consecutive bound-water layers.

Once a dried hydrogel is immersed in an aqueous media, the first water molecules enter the network hydrating the most hydrophilic/polar segments. This primary interaction is called “primary bound water”. When these segments are hydrated, the net swells and the hydrophobic/non-polar groups start to interact, leading to the formation of the so-called “secondary bound water”. The combination of both primary and secondary bounds is defined as “total bound water”.

Once these bounds were formed, the swelling process goes on as a result of the osmotic driving force that tends to push the network towards infinite dilution. The imbibition of water ends when the equilibrium state between the elastic force of the cross-links and the thermodynamic force of dilution is reached. This last volume increase is caused by the so-called “free water” or “bulk water”, which fills completely the free-space inside the hydrogel network [4].

As regards kinetic considerations, the swelling phenomenon can also be described as a transition from a partial glass state to a rubbery state. In most cases, the classical theory of

diffusion cannot define completely the sorption processes. According to Bajpai [5], diffusion can be evaluated in terms of both Case I or Fickian and non-Fickian transport mechanisms. The first can be used when the glass transition temperature ( $T_g$ ) of the polymer matrix is lower than the medium temperature. In this situation, the polymer relaxation rate ( $R_{relax}$ ) is higher than the diffusion one ( $R_{diff}$ ). Whereas, the non-Fickian diffusion arises when the experimental temperature is lower than the  $T_g$ . Moreover, this second transport mechanism can be divided in two others sub-classes: Case II and anomalous transport. In Case II the rate of diffusion is higher than the relaxation one, while in the anomalous transport the two rates are comparable [6].

Generally, the swelling kinetic can be described combining these mechanisms. Indeed, in the time scale, three swelling steps can be distinguished (Figure 1.5). At the beginning, the hydrogel matrix is rigid; therefore the relaxation rate is lower than the diffusion one and the mechanism can be correctly described by the second Fick's law. Whereas, after a while, three separation surfaces can be observed: 1) rubbery zone, 2) solvent front and 3) glassy core; to which correspond different diffusion kinetic that don't follow the Fick's law. Finally, when the system is thermodynamically stable, the whole hydrogel reaches the rubbery state.

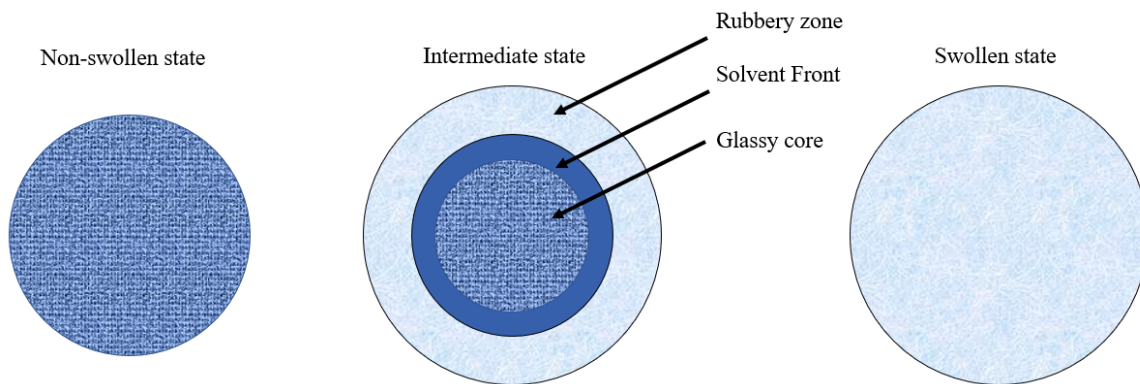


**Figure 1.5:** Swelling mechanism.

The whole kinetic of swelling can be described using an empirical equation known as Power Law (equation 1.8):

$$\frac{M_t}{M_\infty} = kt^n \quad (1.8)$$

where  $M_t$  is the mass of the hydrogel at time  $t$  and  $M_\infty$  is the mass at equilibrium. The diffusional exponent  $n$  is strongly dependent on the solvent uptake mechanism and on the geometry (Table 1.1);  $k$  is a constant based on the polymer-solvent system.

**Table 1.1:** Correlation between diffusional exponent and type of transport in a hydrogel slab.

Type of transport	n	Time dependence
Fickian diffusion	0.5	$t^{1/2}$
Anomalous transport	$0.5 < n < 1$	$t^{n-1}$

Case II transport	1	Time independent
-------------------	---	------------------

The main limitation of this equation is that it can be used only when  $M_t/M_\infty < 0.6$ . Otherwise, if the ratio is higher, the power law fails to predict the proper kinetic of swelling and another equation, which was proposed by Berens-Hopfenberg [7], may be used instead (equation 1.9):

$$\frac{dM_t}{dt} = k_2(M_\infty - M_t) \quad (1.9)$$

where  $k_2$  is the relaxation rate constant.

This equation can be integrated to obtain the following expression (equation 1.10):

$$\frac{M_t}{M_\infty} = (1 - Ae^{-k_2t}) \quad (1.10)$$

where A is a constant.

In the swelling mechanism, also structure parameters play an important role. In the table below (table 1.2) are reported the variation of kinetics according to the porosity of the hydrogel.

**Table 1.2:** Relation between porosity and swelling kinetics [6].

Hydrogel porosity	Morphology	Major type of absorbed water	Major swelling mechanism	Examples of applications
Non-porous	Zero network porosity	Bound water	Very slow Size-dependent	Contact lens, and artificial muscles
Micro-porous	Close cell structure (10-100 nm)	Bound water	Slow Size-dependent	Biomedical application and controlled drug release
Macro-porous	Close cell structure (0.1-1 $\mu$ m)	Bound water	Fast Size-dependent	Superabsorbent in baby diaper
Super-porous	High porosity with interconnected open cell structure	Free water	Very fast Size-independent	Drug Delivery Systems and tissue engineering

### 1.1.3 Classification

Hydrogels can be classified according to different criteria (Table 1.3), namely: 1) origin, 2) composition, 3) network charge, 4) configuration, 5) type of crosslinking, 6) chemical stability and 7) porosity

As regards their origin, in the last three decades, synthetic networks have progressively replaced the natural ones because of their higher gel strength, higher capacity of water

absorption and longer service life. Moreover, their defined structure can be easily tailored to control their degradability and application.

**Table 1.3:** Hydrogel classifications.

<b>Origin</b>	<ul style="list-style-type: none"> <li>• Natural</li> <li>• Synthetic</li> </ul>
<b>Composition</b>	<ul style="list-style-type: none"> <li>• Homopolymeric</li> <li>• Copolymeric</li> <li>• Interpenetrating Polymer Network (IPN)</li> </ul>
<b>Network charge</b>	<ul style="list-style-type: none"> <li>• Nonionic</li> <li>• Ionic</li> <li>• Amphoteric*</li> <li>• Zwitterionic**</li> </ul>
<b>Configuration</b>	<ul style="list-style-type: none"> <li>• Amorphous</li> <li>• Semicrystalline</li> <li>• Crystalline</li> </ul>
<b>Type of crosslinking</b>	<ul style="list-style-type: none"> <li>• Chemical</li> <li>• Physical</li> </ul>
<b>Chemical stability</b>	<ul style="list-style-type: none"> <li>• Biodegradable</li> <li>• Non-biodegradable</li> </ul>
<b>Porosity</b>	<ul style="list-style-type: none"> <li>• Non-porous</li> <li>• Micro-porous</li> <li>• Macro-porous</li> <li>• Super porous</li> </ul>

\*Amphoteric: containing both basic and acidic groups

\*\*Zwitterionic: containing both cationic and anionic groups

Looking at their composition, interpenetrating polymer network (IPNs), which can be seen as alloy of two or more cross-linked polymer without any chemical bonds in between, gained an increasing attention in the last years. IPNs can be further classified into simultaneous and sequential networks. The first category includes those systems in which all the polymers are synthesized simultaneously *via* independent routes. While the second class, incorporates those other systems where one network is already formed and swollen in a solution containing monomers, initiator, activator and sometimes a crosslinker of the second polymer. If the crosslinker is not present, the reaction will produce linear chains, leading to the generation of a semi-IPN. Alternatively, if the cross-linker is present, a fully-IPN network is obtained.

#### 1.1.4 Mechanism of network formation

As previously introduced, the network can be generated by means of many different methods, either physical or chemical.

##### 1.1.4.1 Physical gels

Nowadays physical gels, also known as reversible networks, have gained an increased attention since they don't need any cross-linkers. There exist several examples of physical process that can generate hydrogel networks:

- Physical gels generated by means of hydrogen bonds, e.g. between carboxylic acid and oxygen in polyethylene glycol and polyacrylic acid mixture. In this case, the protonation of the carboxylic acid gives the hydrogel a pH-dependant swelling behaviour.
- Self-assembly formulations made by either block or amphiphilic graft polymers. These tend to form micelles in water, which are able to self-assemble taking advantages from the hydrophobic parts.
- Physical crosslinking can also be reached by crystallization, e.g. polyvinyl alcohol water solution, which gives rise to a gel with low mechanical strength at room temperature.
- Ionic-interaction crosslinking can be observed for example in alginate, which is able to form a network with the aid of calcium ions [8].

#### 1.1.4.2 Chemical cross-linking

Classical chemical methods include both one-step and multiple steps procedures. The first one consists on the contemporary occurrence of the multifunctional monomers polymerization and cross-linking; while the second is a two-steps procedure. The polymer's chain is first synthesized and then left to react with the proper crosslinking agents. Both of these procedures lead to a strong permanent network.

With regard to one step polymerization, five different techniques can be distinguished:

##### 1. Bulk polymerization

Bulk polymerization is the simplest route. It includes one or more type of monomers, an initiator (which has to be soluble in the monomer) and a small amount of crosslinking agent. The reaction can be started by ultraviolet or high-energy radiation or by chemical catalyst. The main disadvantage of this method is that the viscosity of the monomers is inversely proportional to the conversion degree. However, a high amount of heat can be generated if the reaction is not properly controlled. The hydrogel thus obtained has a hard and homogeneous but also a weak structure. The products can be easily shaped in many different forms like membranes or particles.

##### 2. Solution polymerization

In this case, the starting solution is similar to the bulk one but here the crosslinking agent is used in larger amount and, more important, there is a solvent. Common solvents are: water, ethanol or a mixture of them. The solvent total amount has to be calculated carefully in order to avoid phase separation. The major advantage of this polymerization technique is that the solvent removes heat. However, the final product need to be washed.

##### 3. Suspension and inverse-suspension polymerization

The term suspension is usually referred to a mixture of oil in water, while the term inverse-suspension refers to the inverse mixture water. In both of the cases the system is thermodynamically unstable, which means that it tends to separate in two phases. According to that, some hydrophilic-lipophilic-balance must be added, keeping the stirring for the whole process. Generally, both the shape and the size of the products can be tailored regulating the

stirring intensity, the amount of dispersant, the viscosity of monomers and the rotor parameters.

#### 4. Radiation polymerization

The technique consists on irradiating an unsaturated monomer-water solution by means of high-energy radiation (Energy~100KeV). This leads to the creation of radicals in both the monomers and in the aqueous media. Subsequently, macro-radicals are generated and through their combination the covalent network is formed. Gamma ( $\gamma$ ) rays and electron beams ( $e^-$ ) are the typical ionization sources.

#### 5. Grafting to a support polymerization

This technique is merely the reaction of monomers *via* free radical polymerization on the surface of a previously prepared strong substrate. The purpose is to enhance the mechanical properties of the hydrogels [2].

### 1.1.5 Photocurable hydrogels

Photocurable hydrogels can be obtained irradiating proper formulations containing low amount of a photoinitiator under visible [400-800 nm] or ultraviolet [200-400nm] light. The photopolymerization can be induced by photocleavage or hydrogen abstraction, depending on the typology of the photoinitiator, which starts the reaction generating the radical species. This technique takes many advantages over the other methods. Actually, the photo-curing is relatively low cost, it requires low amount of energy, it is fast (only few minutes) and doesn't need high temperature. The overall efficiency depends on the beam wavelength, the type of polymers and the properties of the photoinitiator.

Photocurable hydrogels have been deeply studied for cell encapsulation, drug delivery systems and 3D printing, thanks to their fast production in complex shape and flexible bio-functionalization. Among them, hybrid formulations composed by a mixture of natural and synthetic polymers are preferred, since the biodegradability and the mechanical properties are carefully controlled. Nevertheless, there are some issues that must be taken into account. In particular, as regards UV-light photoinitiator, the ultraviolet spectrum has to be further evaluated. The UV spectrum can be divided in three regions depending on the wavelength: UVA ( $320 < \lambda < 400$  nm), UVB ( $280 < \lambda < 320$  nm) and UVC ( $\lambda < 280$  nm). The solar radiation, which reaches our body, is mainly composed by UVA (95%) and UVB (5%) and, among them, UVB rays can actually provoke a direct DNA damage. Moreover, also the radicals produced in the photobleaching process can be poisoning for both cells and tissues.

The most used UV-photoinitiators in biomedical field are: (2-hidroxy-1-[4-(2-hidroxyethoxy)phenyl]-2-methyl-1- propanone (IRGACURE 2959), 1-hidroxicyclohexyl-1-phenyl ketone (IRGACURE 184) and 2,2- dimethoxy-2-phenylacetophenone (IRGACURE 651). All of them are Norrish type I photoinitiator, which means that they display cleavage if impinged by a photon, thus generating alkyl and benzoyl active radicals. Literature reports researches investigating cells behaviour in many formulations concluding that cells react differently if the photoinitiator changes [9].

Nowadays, researchers have chosen to focus on visible light photoinitiators, because, even if they possess lower efficiency [10], they are more biocompatible.

### 1.1.6 Biomedical applications

The biomedical field is definitely the most important application area of hydrogels. Actually, their porous and hydrophilic structure makes them suitable for tissue scaffolding, wound dressing and drug delivery systems. Some hydrogels exhibit properties, very similar to those of the extracellular matrix (ECM), allowing them to encourage both tissue re-growth and cell proliferation. Furthermore, hydrogels can be both used as supports for the penetration and proliferation of living cells or as delivery systems by simply controlling their degradation kinetic.

With regard to drug delivery, hydrogels are often loaded with drugs and subsequently inserted into the desired *situ via* an implantation procedure. In order to create the network, all the common cross-link methods can be followed. The only requirement is that the final product must be pure, without any non-reacted monomers or toxic initiators. In those cases where the macro-structure of the hydrogel is too bulky to be injected with a needle, it is possible to generate hydrogels with the shape of micro or nanoparticles. To prevent surgical implantations, there can be used either a formulation able to create a hydrogel *in situ* or a non-cross-linked polymer made by linear chains. In the first case, all the risks associated to both chemicals used to start the reaction and their exposure of ultraviolet radiation must be taken into account. In the second case, since the viscosity is proportional to the drug diffusion, it is very hard to control the release kinetic. The most promising solution is to use formulations easily injectable with tuneable release profiles.

In the Table 1.4 are reported the main properties required tissue engineering.

**Table 1.4:** Important parameters of hydrogels used in tissue engineering [4].

Composition of hydrogel	Properties
<ul style="list-style-type: none"> <li>- Natural or their derivates</li> <li>- Synthetic</li> <li>- Combination of natural and synthetic</li> </ul>	<ol style="list-style-type: none"> <li>1. Injectability</li> <li>2. Degradability</li> <li>3. Mechanical strength</li> <li>4. Water content</li> <li>5. Water character</li> <li>6. Sterilizability</li> <li>7. Addition of cell/ drug</li> <li>8. Easy handling</li> <li>9. Close or open pores</li> <li>10. Shape/volume ratio</li> <li>11. Chemical modification</li> </ol>

Several treatments can be applied in order to take care of a tissue or organ failure. For example, the damaged tissue can be repaired, replaced or regenerate. The easiest treatment, in case of injured organs, is to use extracorporeal system, where a polymeric passive membrane acts as an exchange device with blood. Also, a great attention is given to *in-vivo* tissue regeneration, which means incorporating cells directly in the hydrogel and implanting this bio-hybrid system in the host after a proper growth *in vitro* [1]. In the Table 1.5 are reported the advantages and disadvantages of in the used of hydrogel in tissue engineering.

**Table 1.5:** List of advantages and disadvantages in the use of hydrogel in tissue engineering.

<b>Advantages</b>	<b>Disadvantages</b>
<ul style="list-style-type: none"><li>✓ Usually biocompatible</li><li>✓ High amount of water which can protect cells and drugs</li><li>✓ Good transport to and from cells</li><li>✓ Could be modified with receptor peptide ligands to improve cell adhesion</li><li>✓ Can be projected to be injected in vivo in liquid form and react at body temperature to form the network</li></ul>	<ul style="list-style-type: none"><li>- Mechanically weak</li><li>- Difficult to handle</li><li>- Difficult to sterilize</li><li>- Difficult to incorporate drugs and cells into a hydrogel</li></ul>

## 1.2 Aim of the study

The purpose of my thesis work is to synthesize a photocurable hydrogel. Polycaprolactone (PCL) and polyethylene-glycol (PEG) were chosen as the starting materials for the realization of a double-network structure.

However, these polymers need to be modified since, otherwise, they are not suitable for photopolymerization.

In order to reach my goal, I spent three months in Sweden, at KTH Royal Institute of Technology, where I functionalized the biocompatible oligomers precursors. The functionalization relied on the esterification reaction of PCL and PEG with methacryloyl chloride in the presence of triethylamine. The effectiveness of the methacrylation was investigated by means of FTIR-ATR, H-NMR and DSC analysis. Moreover, nanographene oxide from cellulose *via* microwave carbonization process was firstly synthesized and then functionalized with methacryloyl chloride.

With regard to the preparation of the hydrogels, the main work, carried out in Turin, consists on the generation of the network *via* free radical photopolymerization in the presence of bis(acyl)phosphane oxide (BAPO) as a photoinitiator. Many formulations were prepared and different studies were conducted on the crosslinked network such as gel fraction content, swelling degree, attenuated total reflectance Fourier transformed infrared spectroscopy (ATR-FTIR) measurements, and dynamic mechanical thermal analysis (DMTA).



## 2 Materials

This chapter is focused on the materials used in this work. First the hydrogel precursors polycaprolactone (PCL) and polyethylene glycol (PEG) are investigated, with a particular interest for their main physio-chemical properties. Then, the functionalization methods used for the chemical modification of both PCL and PEG are illustrated in detail, describing the experimental protocol that has been followed.

In the second part of the chapter, nanographene oxide (nGO) synthesis and functionalization are discussed, focusing on five different routes of methacrylation.

To conclude, the last sections are devoted to the preparation of the photocurable hydrogels. Different formulations were prepared varying both the weight percentage of the methacrylated precursors and their molecular weight. The photopolymerization process was also illustrated in detail.

### 2.1 Hydrogel precursors

Polycaprolactone (PCL-diol, 2,000 and 14,000 g/mol molecular weights) and polyethylene glycole (PEG, 3,000, 4,000 and 6,000 g/mol) were purchased from Sigma Aldrich and used as hydrogels precursors.

PCL is a semi-crystalline hydrophobic polyester commonly obtained *via* a ring-opening polymerization of  $\epsilon$ -caprolactone in the presence of stannous octanoate. It has a glass transition temperature (T<sub>g</sub>) of -60 °C, a melting temperature (T<sub>m</sub>) that can vary in the range from 58 °C to 65°C and a tensile strength of 0,4 GPa. It is approved by the Food and Drug Administration (FDA, USA) for biomedical application both in drug delivery for the realization of medical devices and in tissue engineering as bone graft substitute. As regards *in-vivo* application, it is subjected to hydrolysis due to the presence of aliphatic ester linkages along its main chain and then is expelled by renal secretion or incorporated in tricarboxylic acid cycle. However, it is not bio-based and shows low degradation rate [11].

PEG, instead, is one of the most common synthetic polymers used for the synthesis of hydrogels, especially in cartilage tissue engineering. It doesn't provoke any immune response, it is hydrophilic, bio-based and can easily degrade in biological environment. IEG is a non-ionic homopolymer of ethylene oxide (EtO). It is synthesized by reacting EtO with water in the presence of a catalyst and under high-pressure conditions. It has a glass transition temperature of almost -65 °C and a melting temperature that ranges from 61 °C to 65 °C. It is characterized by the presence of hydroxyl ending chains able to form hydrogen bonds, thus making PEG soluble in water and in the majority of organic solvents [12].

#### 2.1.1 Oligomers functionalization

However, as already introduced in Chapter 1, both PCL and PEG need to be functionalized, since, otherwise, they cannot be used to generate a chemical network *via* photopolymerization. Accordingly, the idea was to perform an end-capping process to

substitute the hydroxyl ending groups of both PCL-diol and PEG with methacrylate ones. Initially, polycaprolactone diacrylate was prepared, but after a closer look to the potential applications of the hydrogels in the biomedical field, it was decided to proceed with a methacrylation process. Actually, the methacrylates groups are less reactive than the acrylate one, but they take advantages in term of lower toxicity.

Besides modifying the synthesis, also other process parameters were optimized. As regards the functionalization of PCLDMA, it was decided to change the solvent from benzene to toluene because, even if the dispersion process is slower, toluene is less harmful. Furthermore, the reaction temperature was varied from 80°C to 60°C to reduce the amount of side reactions.

PCLDMA oligomers were synthesized with different molecular weights; respectively 2,000 g/mol and 14,000 g/mol.

#### 2.1.1.1 Polycaprolactone diacrylation

PCL (2,000 g/mol) was firstly dissolved in benzene while magnetically stirring. Then triethylamine (TEA, Sigma Aldrich) and acryloyl chloride dehydrated (Sigma Aldrich) were added to the solution.

The reaction was carried out for 3 h at 80°C under stirring condition into a round bottle flask of 250ml. Triethylamine hydrochloride was filtrated away as by-product using a 0.45µm pore-size filter. PCLDA was then left to precipitate in n-Hexane and the powder thus obtained was subsequently dried in a vacuum oven at 25°C for 24 h. The synthesis is schematically illustrated in Figure 2.1.

The following Table 2.1 reports the chemicals used for PCL diacrylation.

According to a previous work found in literature, a total conversion of PCL-diol cannot be reached, but if PCL-diol and acryloyl chloride are mixed in a 1:3 mole-ratio, it is possible to obtain conversions degrees up to 97.1%. Initially, the increase of acryloyl chloride amount seemed to lead to higher conversion rates, but exceeding the 1:3 mole ratio, a decrease in the conversion was observed, maybe caused by side reactions [13].

**Table 2.1:** Chemicals used for PCL diacrylation.

<b>Materials</b>	<b>Amount</b>
PCL-diol (Mw=2000)	4 g (2 mmol)
TEA	0,84 ml (6 mmol)
Acryloyl chloride	0,58 ml (6 mmol)
Benzene	40 ml

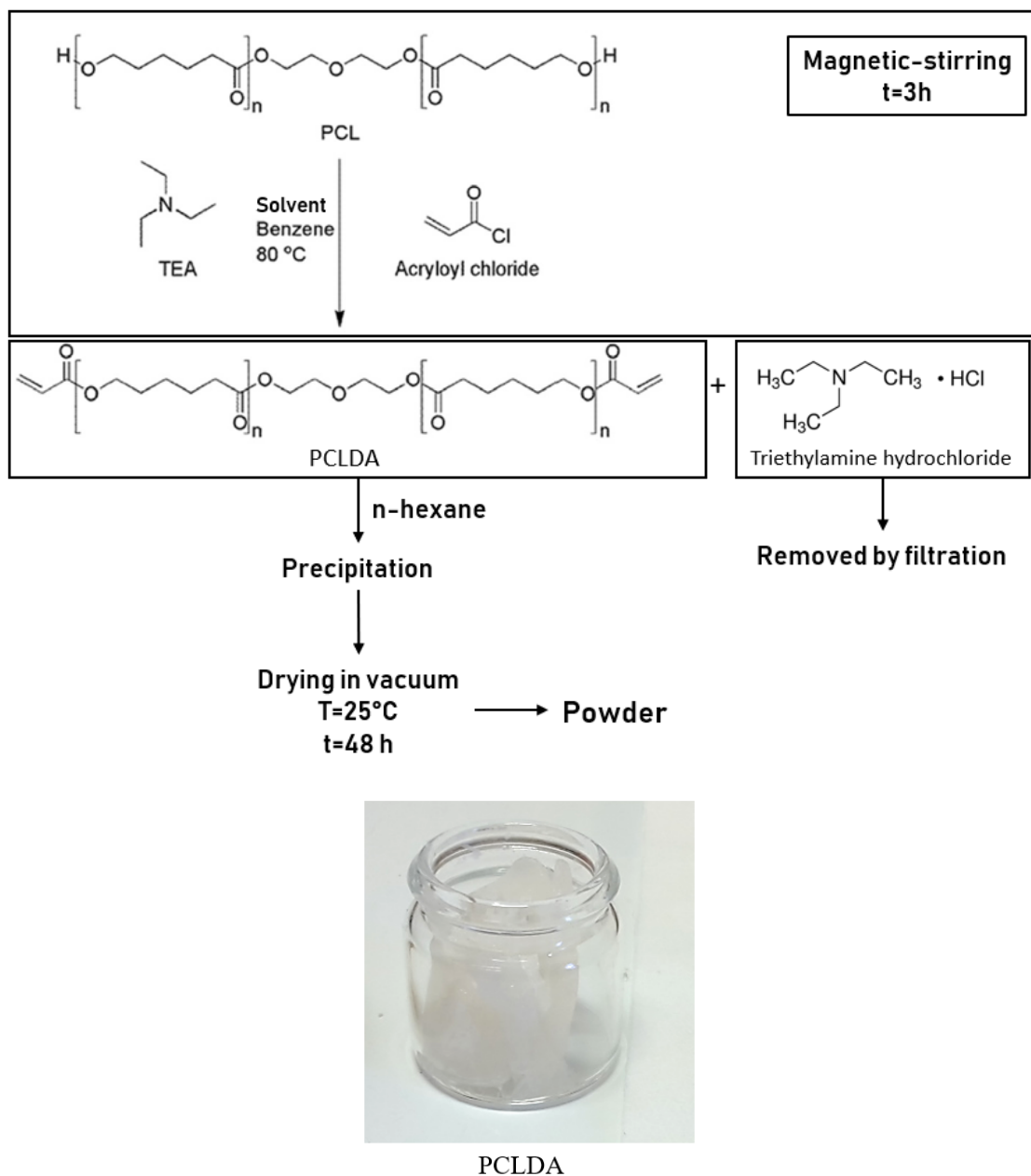


**Figure 2.1:** Schematic representation of PCLDA synthesis procedure and PCLDA final product.

#### 2.1.1.2 Polycaprolactone dimethacrylation

As previously discussed, two PCL differing only in molecular weights (2,000 and 14,000 g/mol) were used.

According to the experimental protocol, PCL-diol (2,000 g/mol) was dispersed in 250 ml of toluene by means of magnetic stirring till the solution became homogeneous. Methacryloyl chloride (Sigma Aldrich) and triethylamine (Sigma Aldrich) were then added respectively as second reagent and catalyst. The PCL-diol (2,000 g/mol)/methacryloyl chloride/triethylamine molar ratio was 1:3:3.

The solution was magnetically stirred; the reaction continued for 3 h at 60°C and triethylamine hydrochloride was filtrated away as a by-product using a 0.45  $\mu\text{m}$  pore-size filter (Figure 2.2).

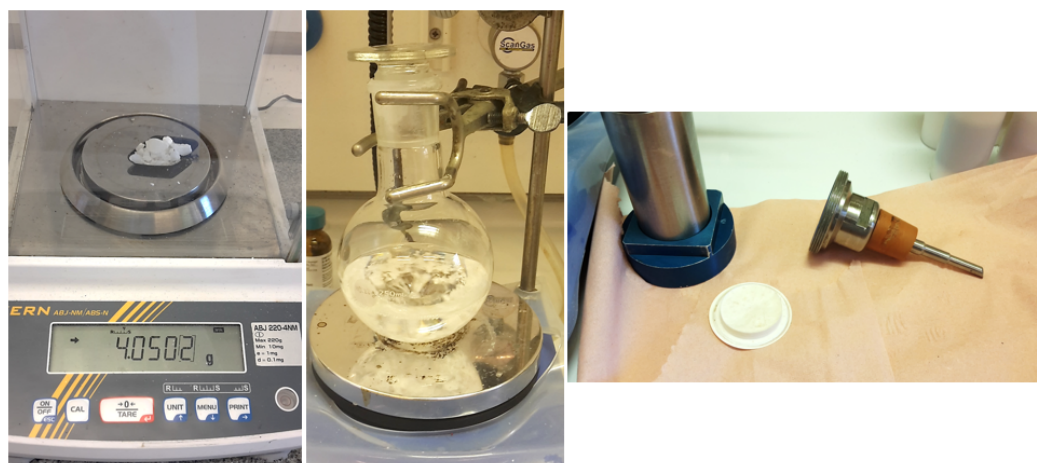


**Figure 2.2:** Experimental set-up of PCL dimethacrylation: PCL-diol weighted with a precision balance, dissolution in toluene, triethylamine salt stacked in the filter.

Then PCLDMA was then left to precipitate in n-Hexane and the white powder thus obtained was dried in a vacuum oven at 25°C for 48 h.

The scheme of the process is represented in Figure 2.3.

The same protocol was followed for the methacrylation of PCL (14,000 g/mol). In this second reaction the PCL-diol (14,000 g/mol)/methacryloyl chloride/triethylamine molar ratio was varied to 1:2.3:2.3.

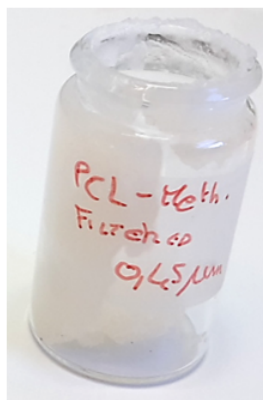
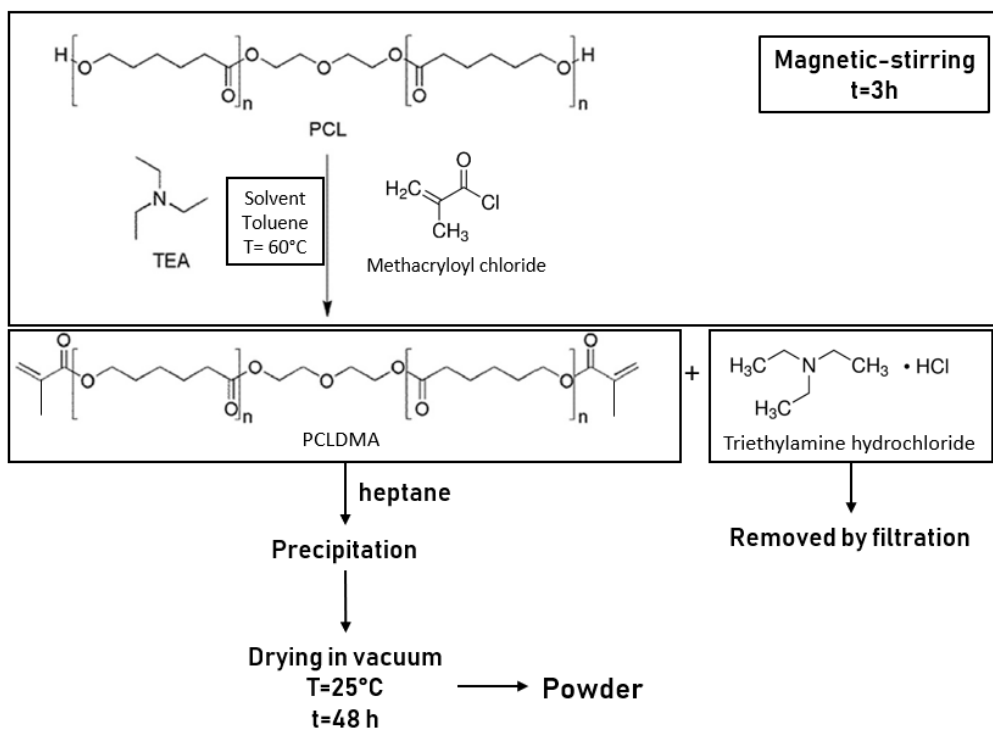
In the following Table 2.2 and 2.3 the chemicals used for the methacrylation of both PCL 2,000 and PCL 14,000 are given.

**Table 2.2:** Chemicals used for PCL 2k dimethacrylation.

Materials	Amount
PCL-diol (Mw2000)	6 g (6 mmol)
TEA	2.51 ml (18 mmol)
Methacryloyl chloride	1.76 ml (18 mmol)
Toluene	121.2 ml
n-Hexane	

**Table 2.3:** Chemicals used for PCL 14k dimethacrylation.

Materials	Amount
PCL (Mw=14,000)	8 g (0.57 mmol)
Toluene	80 ml (10.25 wt%)
Triethylamine	0.18 ml (1.29 mmol)
Methacryloyl chloride	0.13 ml (1.29 mmol)
n-Heptane	



PCLDMA

**Figure 2.3:** Schematic representation of PCLDMA synthesis procedure and PCLDMA final product.

### 2.1.1.3 Polyethylene glycol dimethacrylation

The dimethacrylation process was performed on PEG with three different molecular weights (3,000; 4,000 and 6,000 g/mol).

First attempts have been made to dissolve PEG in toluene, but they proved to be unsatisfactory because the dispersion was incomplete. To overcome this problem, it was decided to change toluene with dichloromethane. Triethylamine and methacryloyl chloride were then added dropwise to the dichloromethane solution while continuously stirring and the reaction was carried out under nitrogen atmosphere for the whole night.

As previously described for the methacrylation of PCL, trimethylamine hydrochloride salt was removed by filtration. PEGDMA was subsequently precipitated, immersing it in ice-cold

diethyl ether for three times. The product was dialyzed for three days, freeze-dried and then put in a vacuum oven at RT for other two days [14].

The main steps of the experimental protocol are shown in Figure 2.4, whereas Table 2.4, 2.5 and 2.6 report the chemicals used for the methacrylation of PEG (2,000; 4,000 and 6,000).

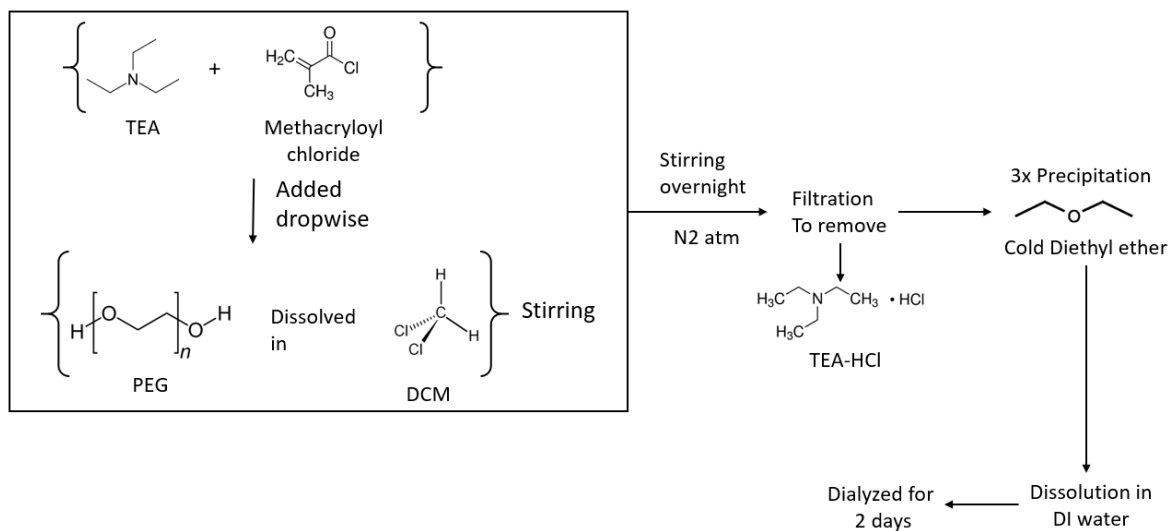


**Figure 2.4:** From the left: reaction under nitrogen atmosphere; filtration performed to remove triethylamine salt, precipitation in ice-cold diethyl ether, final product after freeze-drying process.

**Table 2.4:** Chemicals used for PEG 3k dimethacrylation.

Material	Amount
PEG (M <sub>w</sub> =3,000)	9 g (3 mmol)
Toluene	150 ml
Methacryloyl chloride	1.17 ml (12 mmol)
Triethylamine	1.67 ml (12 mmol)
Diethyl ether	

**Table 2.5:** Chemicals used for PEG 4k dimethacrylation.

Material	Amount
PEG (Mw=4,000)	9 g (2,25 mmol)
DCM	68 ml
TEA	1.25 ml (9 mmol)
Methacryloyl chloride	0.88 ml (9 mmol)
Diethyl ether	

**Table 2.6:** Chemicals used for PEG 6k dimethacrylation.

Material	Amount
PEG (Mw=6,000)	12.008 g (2 mmol)
DCM	66 ml
Methacryloyl chloride	1.12 ml (8 mmol)
Triethylamine	0.78 ml (8 mmol)
Diethyl ether	

## 2.2 Nanographene oxide synthesis and functionalization

Nanographene oxide was obtained directly from cellulose *via* a green microwave assisted carbonization process, which optimizes a well-established synthetic method reported in the scientific literature [15]. First, 2g of  $\alpha$ -cellulose were immersed in 20 mL of 0.1 g/mL H<sub>2</sub>SO<sub>4</sub> water solution. The solution was then heated using a flexiWAVE microwave device (Milestone Inc.) setting the temperature to increase up to 220°C in 20 minutes and to keep the isothermal conditions for 2 hours under a nitrogen flux.

Later, the solution was filtrated and the black carbon spheres thus obtained were first washed in deionized water and then left drying in a vacuum oven for 12 hours at room temperature. The carbon spheres were subsequently oxidised in a 70% HNO<sub>3</sub> solution (1:100 w/w), which was sonicated for 50 minutes at 45 °C and then heated up to 90 °C while magnetically stirring for 50 minutes to complete the oxidation process.

Finally, the nGO spheres were separated from the water acidic medium by evaporation in vacuum conditions, freeze-dried and then kept for seven days in a vacuum oven at T=25°C.

The following Figure 2.5 illustrates the steps of the procedure followed for the synthesis of nGO.



**Figure 2.5:** Experimental procedure followed for the synthesis of nGO.

As regards the functionalization process, the nGO nanoparticles were modified by means of methacrylation to make them covalently cross-linkable to the hydrogel network. Five different routes of methacrylation will be presented below.

### 1) First route

Nanographene oxide was dispersed in dimethyl sulfoxide by means of ultrasonication for 10 minutes. Triethylamine (TEA) was gradually added to the mixture while magnetically stirring for 30 minutes. Afterwards, the solution was cooled using an ice-cold bath and methacryloyl chloride was added dropwise. The temperature was then raised to 45°C and the stirring proceeded for 24 h (Figure 2.6).

According to literature [16], the following steps should be washing and precipitation of the products, but our suspension was too stable. Therefore, we did not succeed in precipitating MA-nGO, neither by adding a centrifugation step.

The chemicals used are reported in Table 2.7.

**Table 2.7:** Chemicals used for the synthesis of nGO following the first route.

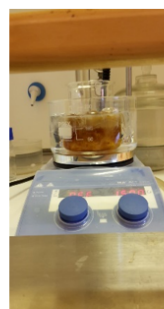
Materials	Amount
nGO	0,38 g
DMSO	152 ml
Triethylamine	3.65 ml
Methacryloyl chloride	2.58 ml
Isopropanol	76 ml



nGO dispersion  
in DMSO



TEA addition



Methacryloyl  
chloride addition  
at 0°C



Suspension too stable  
to be separated

**Figure 2.6:** First synthesis route of MA-nGO.

## 2) Second route

Nanographene oxide was dispersed in ethanol. Methacryloyl chloride was added dropwise as a second reagent, while TEA was no longer used as catalyst, since nGO is found to be highly reactive itself (Figure 2.7). After two hours of magnetic stirring, the solution was heated up to 120 °C and distilled water was added to get rid of both the solvent and the hydrochloric acid produced in the reaction.

Finally, the suspension was freeze-dried for two days.

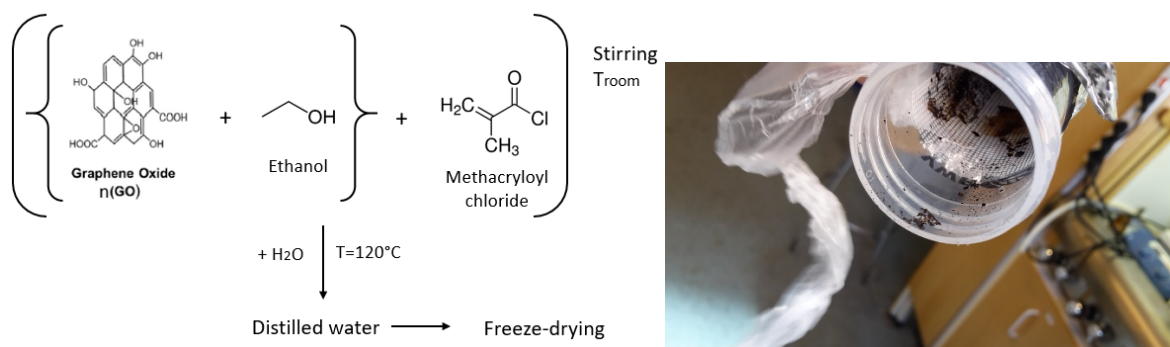


**Figure 2.7:** Second synthesis route of MA-nGO.

## 3) Third route

Nanographene oxide was immersed in anhydrous dimethylformamide (DMF, Sigma Aldrich) and left in an ultrasonication bath for 10 min.

TEA was added in excess and methacryloyl chloride was poured dropwise using a syringe while vigorous stirring under nitrogen flux at 0°C to avoid the possible severe reaction of Methacryloyl chloride and DMF at higher temperature (Figure 2.8 and 2.9). The system was then gradually warmed up to room temperature in stirring condition for 24 h. MA-nGOs were subsequently transferred into dialysis bag and left there for three days to remove residue small molecules. The purified product was finally put in the vacuum oven at  $T_{\text{room}}$  [17].

The chemicals used are reported in Table 2.8.

**Table 2.8:** Chemicals used for the synthesis of nGO following the third route.

Materials	Amount
nGO	500 mg
DMF	75 ml
TEA	0,5 ml
Methacryloyl chloride	40 $\mu$ L (0,41 mmol)

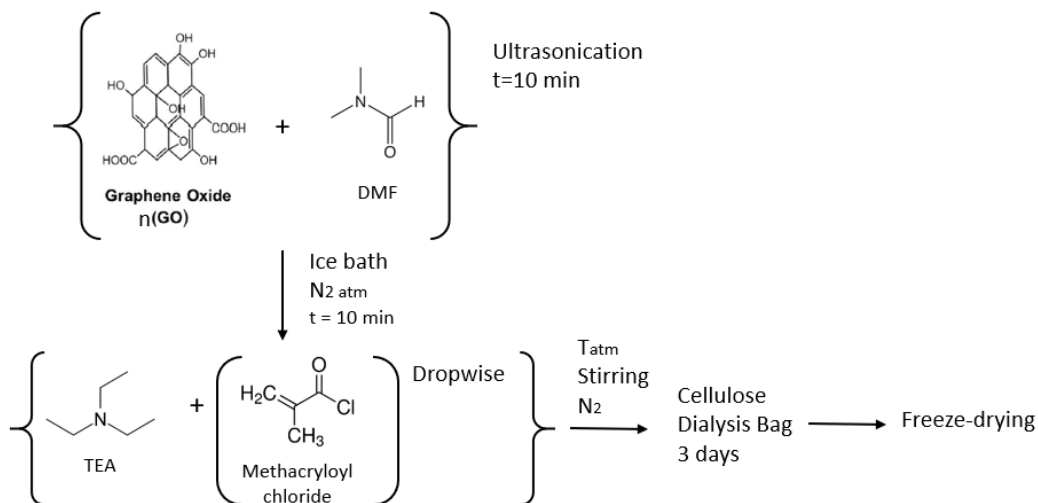


**Figure 2.8:** Schematic illustration of the third route procedure.



**Figure 2.9:** From left batch with nGO and reagents, cellulose dialysis bag and MA-nGO after dialysis.

#### 4) Fourth route

Nanographene oxide spheres were dispersed in ethanol and ultrasonicated for 10 minutes. Methacryloyl chloride was injected slowly, while magnetically stirring for 18 hours at room temperature. Then, distilled water is added, heating up the solution to 80°C under vacuum conditions while stirring, in order to evaporate both ethanol and HCl (Figure 2.10 and 2.11)

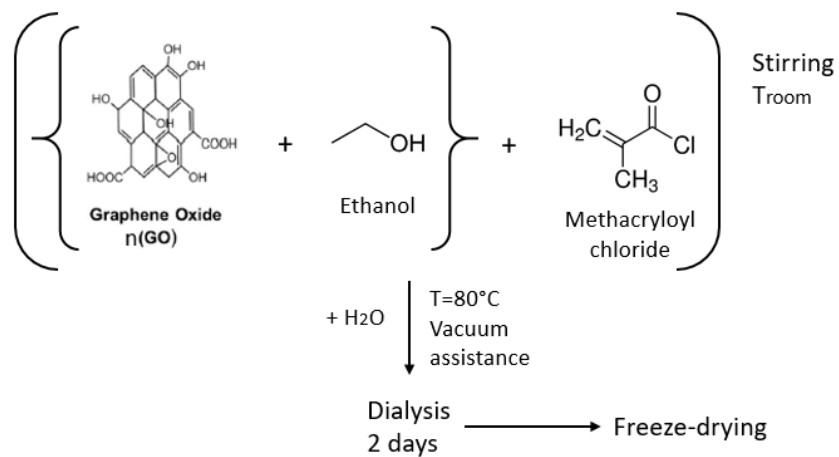


**Figure 2.10:** Schematic illustration of the fourth route procedure.



**Figure 2.11:** From the left: vacuum system, dialysis, final product.

### 5) Fifth route

The fifth route is similar to the fourth one, except for the dialysis that was skipped (Figure 2.12).

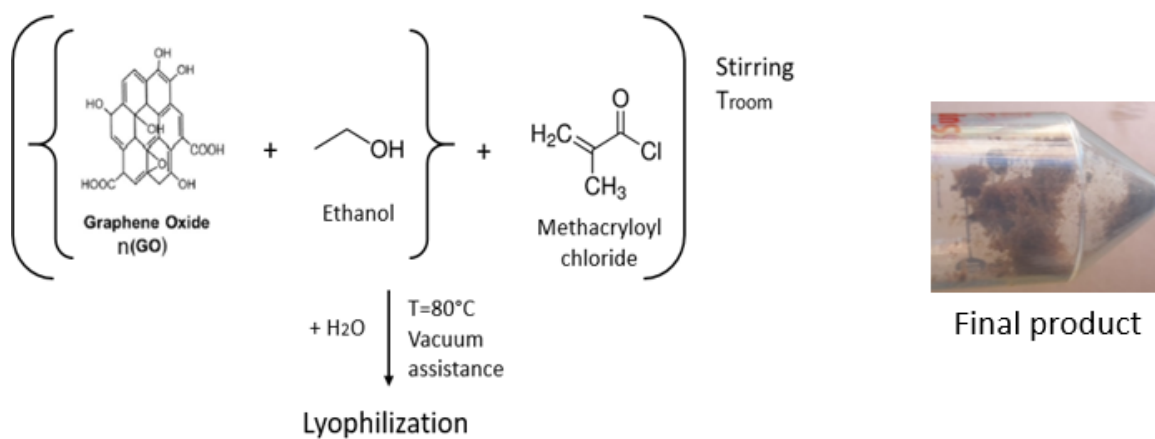


**Figure 2.12:** Schematic illustration of the fifth route procedure.

### 2.3 Hydrogel preparation

The hydrogels three-dimensional network was obtained by radical photopolymerization. Bis(2,4,6-trimethylbenzoyl)-phenylphosphineoxide (BAPO; commercialized by BASF under the trade name IRGACURE 819) was used as photoinitiator (PhI) to set off the chain-growth polymerization on the methacrylic double bonds of both PCLDMA and PEGDMA.

BAPO is a Norrish type I PhI, which generates radicals via  $\alpha$ -cleavage mechanism when irradiated under UV light. The following Figure 2.13 shows the photochemical cleavage pathway of BAPO into two free radical intermediates: phosphinoyl and acyl radicals. (N.B.: the phosphinoyl radical is about 1000 times more reactive than the acyl radicals through an efficient  $\alpha$ -cleavage).

In this type of reaction, the carbonyl group accepts a photon and is excited to a photochemical triplet state through spin crossing. As a result, two radical fragments are obtained by photocleavage.

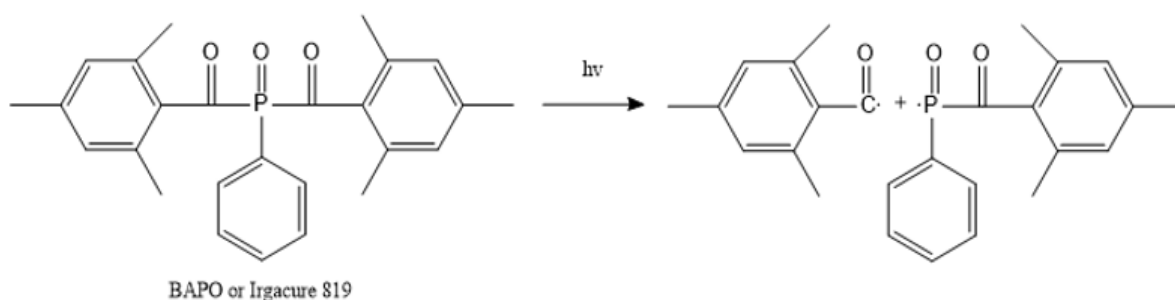


**Figure 2.13:** BAPO photobleaching mechanism under UV irradiation.

Considering the experimental set-up, PCLDMA and PEGDMA were first dispersed in various solvents:

- acetone
- water-acetone mixture (PCL is not soluble)
- ethanol
- propylene carbonate

Firstly, dissolution tests have been done to evaluate the oligomers solubility in each solvent. In order to achieve homogeneous solutions, the polymers concentrations were set at 15% wt. in acetone, acetone-water and ethanol, while at 20% wt. in propylene carbonate (PC).

The following Table 2.9 reports the formulations being prepared by varying: 1) the solvent, 2) the molecular weight of PCLDMA and PEGDMA and 3) the oligomers weight ratio.

**Table 2.9:** Solution prepared with different molecular weights, weight ratios and solvents.

1 <sup>st</sup> Oligomer	Solvent	2 <sup>nd</sup> Oligomer	Solvent	Weight ratio
PCLDMA 2k	Acetone (85% wt.)	PEGDMA 3k PEGDMA 4k	Acetone (85% wt.)	30:70 50:50 70:30
PCLDMA 2k	Acetone (85% wt.)	PEGDMA 3k PEGDMA 6k	Water (85% wt.)	30:70 50:50 70:30
PCLDMA 2k	Ethanol (85%wt)	PEGDMA 3k PEGDMA 4k	Ethanol (85%wt)	30:70 50:50 70:30
PCLDMA 2k	PC (80%wt)	PEGDMA 3k PEGDMA 4k PEGDMA 6k	PC (80%wt)	30:30 50:50 70:30
PCLDMA 14k	PC (85%wt)	PEGDMA 3k	PC (80%wt)	30:70

BAPO (2 phr) was then added to each solution while stirring for 3 minutes. The solution was then poured into polydimethylsiloxan (PDMS) molds and irradiated for 7 min under Nitrogen flux using a Dymax ECE 5000-UV lamp (15 J/cm<sup>2</sup>).

The experimental protocol is illustrated in Figure 2.14.

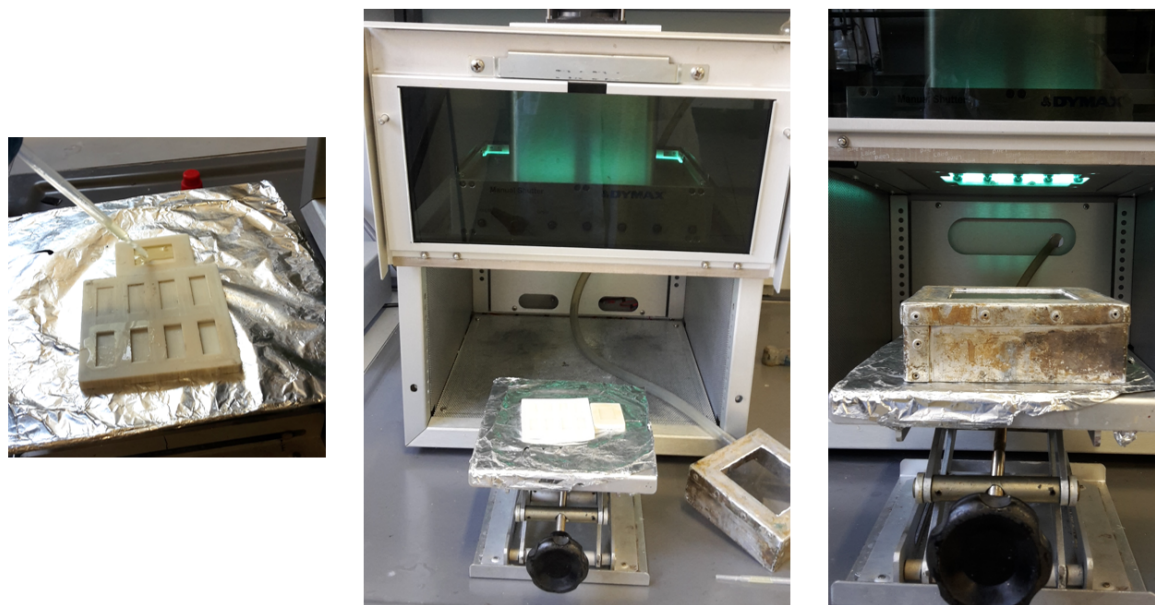


**Figure 2.14:** Experimental protocol followed for the preparation of the photocurable hydrogels.

Experimental evidences showed that using acetone, acetone-water and ethanol as solvents, the network formation wasn't achieved due to their fast evaporation (Figure 2.15).



**Figure 2.15:** Examples of photocuring failures induced by the evaporation of the solvent.

In order to evaluate the cross-linking capacity of each oligomer, also some formulation containing just PCLDMA or PEGDMA were prepared.

Experimental evidences led to conclude that the network-structure cannot be obtained using PEGDMA (3,000/4,000/6,000), probably because of both low amounts of reactive groups and high molecular weights. Contrary, PCLDMA oligomers are able to generate mechanically stable cross-links by themselves.

Accordingly, it was decided to prepare hydrogels combining the synthesized PCLDMAs with a commercial PEGDMA (purchased from Sigma Aldrich) with a lower molecular weight (750 g/mol).

In the following Table 2.10 are listed all the formulations prepared with the commercial PEGDMA.

**Table 2.10:** Formulation prepared with PEGDMA 750.

1 <sup>st</sup> Oligomer	2 <sup>nd</sup> Oligomer	Solvent	Oligomers ratio
PCLDMA 2k	PEGDMA 750	PC (70%wt)	30:70
			50:50
			70:30
PCLDMA 14k	PEGDMA 750	PC (70%wt)	30:70
			50:50
			70:50
	PEGDMA 750	PC (70%wt)	
	PEGDMA 750	Solvent free	

The hydrogels thus obtained are shown in Figure. 2.16. As can be clearly observed, in the case of PCLDMA 14k-PEGDMA 750 [70:30] the network wasn't formed, probably because a higher percentage of PCLDMA implies too rigidity in the chain motion and lower number of functional groups.

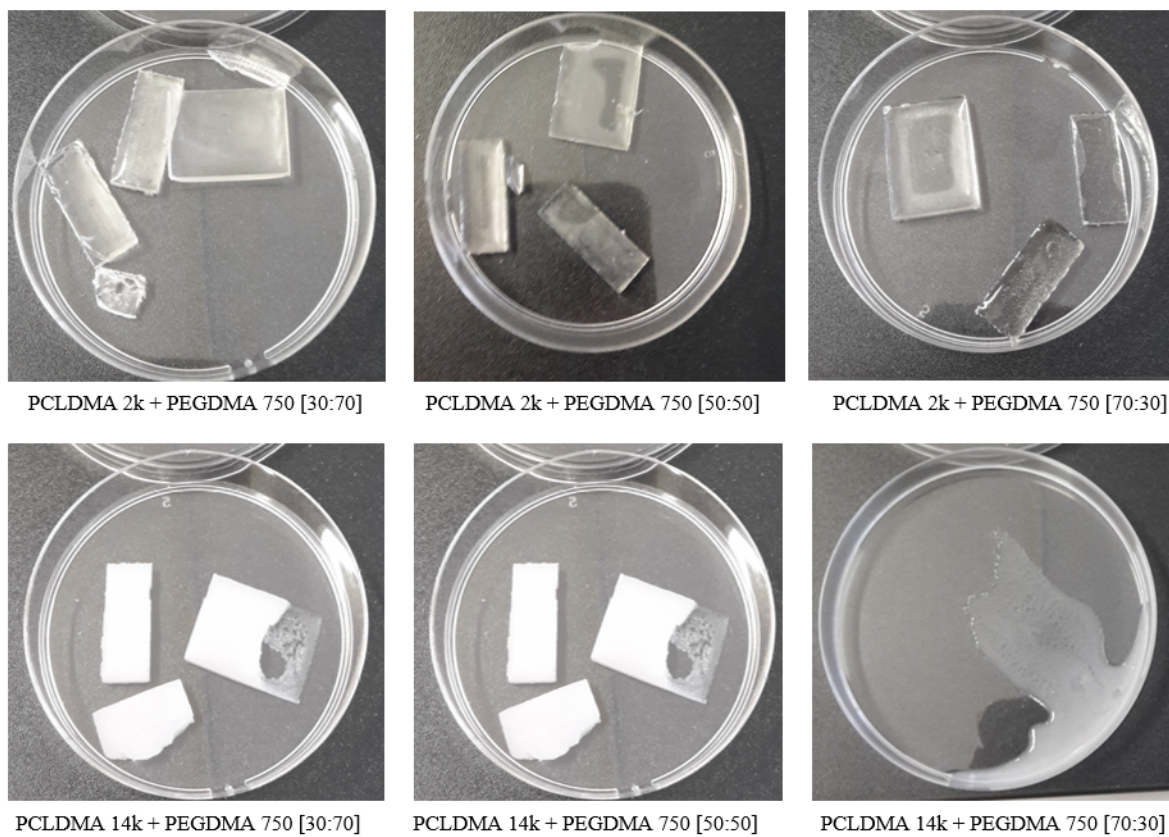


**Figure 2.16:** Hydrogels prepared via photocrosslinking.



### 3 Methods

In this chapter, different characterization techniques used to investigate both the methacrylated oligomers and the photocurable hydrogels are discussed, first giving a brief overview on their working principles and then illustrating the experimental protocols followed to make the measurements.

The effectiveness of methacrylation of both PCL and PEG was evaluated by means of proton nuclear magnetic resonance ( $^1\text{H-NMR}$ ), attenuated total reflectance - fourier transform infrared (ATR-FTIR) spectroscopy, differential scanning calorimetry (DSC) and thermogravimetric analysis (TGA). The molecular weights of the oligomers, both virgin and functionalized, were analysed using size exclusion chromatography (SEC), while MA-nGO was investigated by Zeta potential ( $\zeta$ ) measurements.

The last sections are devoted to the photocurable hydrogels, discussing the characterization techniques used to study both their swelling and dynamo-mechanic behaviours.

After that, all the instruments used to characterize both the materials and the hydrogel network will be described in both theoretical and practical view

#### 3.1 Proton nuclear magnetic resonance ( $^1\text{H-NMR}$ )

Proton Nuclear Magnetic Resonance ( $^1\text{H-NMR}$ ) is a non-destructive spectroscopic technique typically used to determine the molecular structure of a sample. The working principle of  $^1\text{H-NMR}$  comes from electro-magnetic physical principles.

Each nucleus has a proper spin, some are neutral and others are charged. The latter are able to create a magnetic moment ( $\mu$ ) proportional to the spin. In absence of magnetic fields ( $B_0$ ) nuclear spins are randomly oriented, while, when a field is applied, two spin states exist:  $\alpha$  ( $+1/2$ ) and  $\beta$  ( $-1/2$ ). The first state has lower energy and tends to align parallel to the external magnetic field, while the second has higher energy and tends to align with an antiparallel configuration. The following Figure 3.1 shows the energy difference between the two spin states.

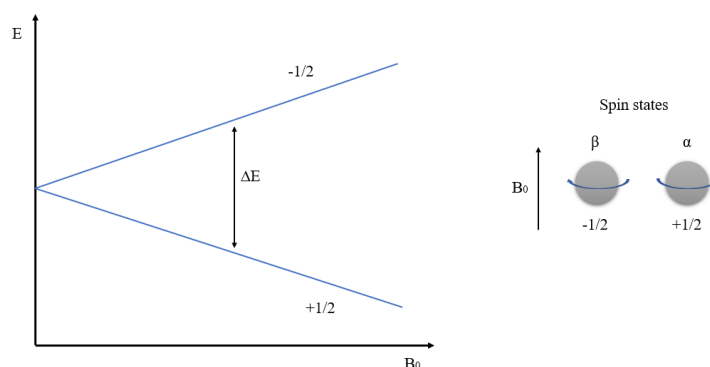


**Figure 3.1:** Correlation between the spin states and the magnetic field.

As illustrated, the energy difference ( $\Delta E$ ) between these two states tends to zero when the external field is equal to zero, whereas diverges as the magnetic field increases.

For H-NMR measurements  $\Delta E$ , commonly given in terms of frequency ( $\nu$ ), varies from 20 to 900 MHz, the typical radio frequencies, depending on the nucleus that has to be investigated.

The following formula (equation 3.1) expresses the direct correlation between nucleus momentum and frequency:

$$\nu = \frac{\mu B_0}{hI} \quad (3.1)$$

where  $\nu$  is the frequency [Hz],  $h$  is the Planck's constant ( $h=6.626 \cdot 10^{-34}$  [J\*s]) and  $I$  is the spin (+1/2 or -1/2). Hydrogen nucleus ( $^1\text{H}$ ) has  $\mu=2.7927$ .

Generally speaking, all nuclei feel the influence of three different magnetic fields generated by the Earth, NMR and other nuclei. Only the last two fields are taken into account for H-NMR measurements, specially the one generated by other nuclei. This is the reason why protons  $^1\text{H}$  are non-equivalent in many compounds, since protons within a compound create diverse magnetic fields thus giving different signal in H-NMR spectra.

As regard the magnetic field of H-NMR, radio frequency radiations are sent into the specimen through a coil. The emission of the absorbed radiations is controlled by means of a second coil, which then transmits the information to a computer. The emitted energy, in the radio frequency region, produces an NMR signal. This signal is reported in a graph where on the horizontal axis are given the chemical shifts  $\delta$  (measured in ppm), which are calculated using a proton of tetramethylsilane ( $\text{CH}_3$ )<sub>4</sub>Si, set at 0.00 ppm [18], as a reference. In the Figure 3.2 are shown the H-NMR apparatus, the samples tube and a scheme of the process.

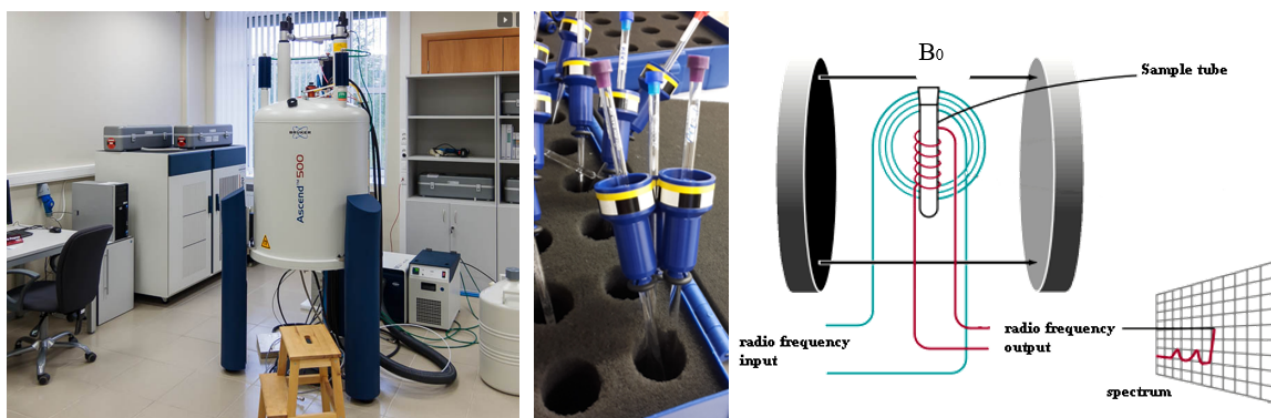


**Figure 3.2:** H-NMR apparatus [19], sample tubes required for this analysis and scheme of the process [20].

In this work, H-NMR was used to characterise both functionalized and virgin oligomers.

The measurements were performed by means of Avance 400 (400.13 MHz - Bruker, USA) spectrometer at room temperature. The samples were dissolved in Deuteriochloroform

(CDCl<sub>3</sub>) since deuterium hydrogen isotope is invisible in the spectrum. The H-NMR glass tubes were filled with about 10 mg/mL of solution.

### 3.2 Attenuated Total Reflectance - Fourier transform infrared (ATR-FTIR) spectroscopy

The Attenuated Total Reflection Fourier Transform IR Spectroscopy (ATR-FTIR) is a typical spectroscopic technique used for both qualitative and quantitative characterization of materials. Unlike the traditional and well-established Fourier Transform Infrared Spectroscopy (FTIR), ATR allows to reduce some problems, i.e. the preparation of the sample and the spectral reproducibility.

According to its working principle schematically presented in Figure 3.3, the sample is first positioned onto an optical dense crystal marked by high refractive index. Then, an IR beam is sent to the crystal surface with a certain angle. As a result of internal reflection, an evanescent wave is generated and directed towards the sample surface penetrating it from 0.5 up to 5  $\mu\text{m}$ . The detector measures the variations occurring in the IR beam due to the alteration of the evanescent wave, induced by the infrared energy-absorptions of the sample. These variations are uniquely dependent on the type of material because the absorption regions are related its chemical structure. Therefore, the recorded spectra, which are considered as the fingerprints of the chemical species, are evaluated to identify the composition of the sample.

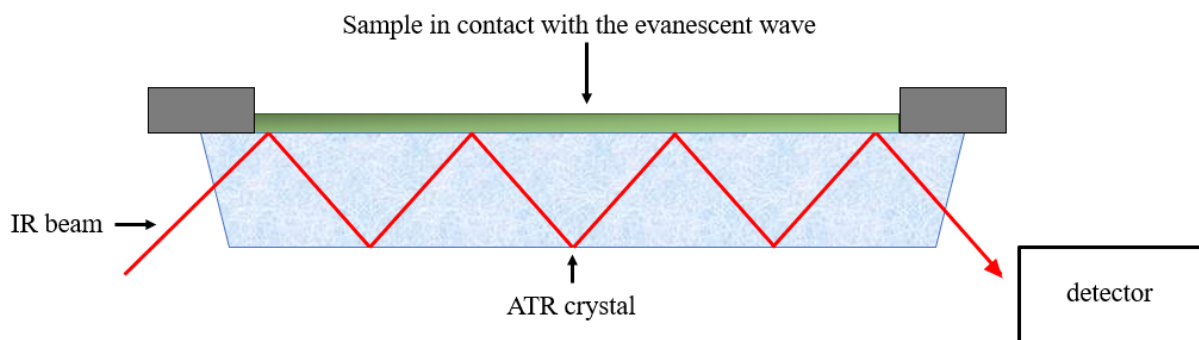


**Figure 3.3:** Schematic representation of ATR-FTIR working principle.

In this work, ATR-FTIR was used to evaluate the purity of both the oligomers and the nGO as well as the success of the functionalization. The tests were performed using a Perkin-Elmer Spectrum 2000 (16 scans, resolution 2  $\text{cm}^{-1}$ ).

The instrumental ATR-FTIR apparatus used for the characterization of the oligomers is shown in Figure 3.4.



**Figure 3.4:** ATR-FTIR instrumental apparatus.

With regard to the investigations of the hydrogels, the analyses were carried out using a Nicolet iS50 FT-IR Spectrometer (16 scans, resolution  $4\text{ cm}^{-1}$ ) with ATR accessory (Thermo Scientific, Madison WI). The spectra were recorded in transmission mode and evaluated using OMNIC software.

### *3.3 Differential scanning calorimetry (DSC)*

Differential scanning calorimetry (DSC) is a thermo-analytical analysis widely used to evaluate the response of materials to temperature. The tests are performed in a measurement chamber that detects the heat flow variations arising between the sample and a reference crucible, whose heat capacity is set constant over the whole process. According to the thermal behaviour of materials, specimens undergo physical transitions (e.g. glass transition, crystallization, melting and others) corresponding to thermal fluctuations. In order to detect such fluctuations, during the whole test both the sample and the reference are kept at the same temperature that is set to increase linearly over time.

The physical transitions are recorded and reported in a thermogram, showing heat flow variations on y-axis and temperature on x-axis, which is investigated to evaluate enthalpies of transitions.

A schematic representation of a DSC measurement chamber is shown in Figure 3.5. The crucibles can be made of aluminum, copper, gold, alumina or platinum according to the material that has to be analysed. Usually, the crucibles lids present holes in the middle, thus allowing the penetration of a controlled atmosphere during the test.

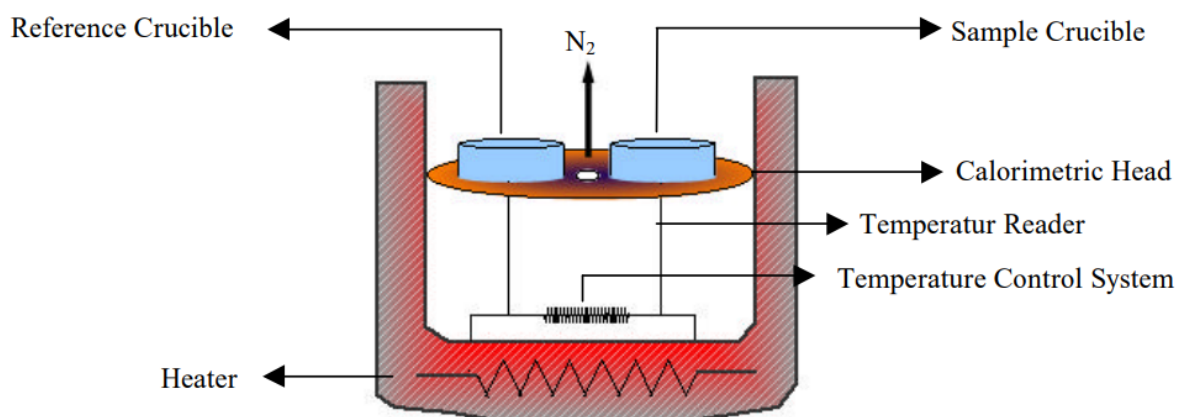


**Figure 3.5:** Scheme of a DSC measurement chamber [21].

DSC was used in this work to evaluate the thermal transition of the functionalized oligomers comparing them to the virgin samples. The measurements were carried out at a heating rate of 10 °C/min with a DSC Mettler Toledo DSC 820 using 100 $\mu$ L aluminium crucibles. This analysis was also performed on the final hydrogels (PCLDMA 2k + PEGDMA 750 and PCLDMA 14k + PEGDMA 750 with weight ratio of 50:50), in order to investigate the presence of crystalline domains.

The DSC apparatus used for the characterization of the oligomers is shown in Figure 3.6.

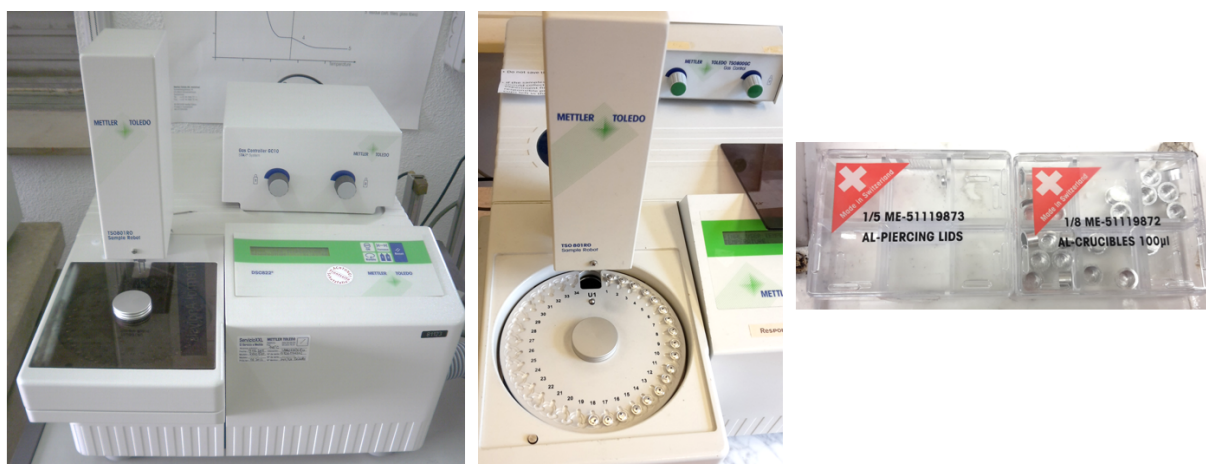


**Figure 3.6:** DSC Mettler Toledo 820 and crucibles used in DSC analysis.

### 3.4 Size-exclusion chromatography (SEC)

Size-exclusion chromatography (SEC) is a chromatography technique used to separate molecules or macromolecules immersed in a solvent, known as mobile phase, according to their size/molecular weight. The samples solutions are forced through a column where a micro-porous matrix, which has to be inert, physically and chemically stable, acts as the

filtration medium (Figure 3.7). Smaller molecules can enter the matrix pores, thus having an average residence time that is higher than the one measured for bigger molecules. Therefore, particles with same size are supposed to exit together. The times of elution are reported as peaks into the chromatogram.

It is important to notice that the molecules volume estimated by this technique doesn't correspond to the real analyte volume, but it gives an indication of its hydration volume.

SEC measurements allow to estimate both the number average molecular weight ( $M_n$ ) (3.2) and the weight average molecular weight ( $M_w$ ) (3.3):

$$\bar{M}_n = \sum n_i M_i \quad (3.2)$$

$$\bar{M}_w = \sum w_i M_i \quad (3.3)$$

where  $n_i$  is the number fraction:  $n_i = \frac{N_i}{\sum N_i}$ , ( $N_i$  is the number of molecules  $i$ ), and  $w_i$  is weight fraction:  $w_i = \frac{W_i}{\sum W_i}$ , ( $W_i$  is the weight of molecules  $i$ ) [22].

Usually, the SEC system is coupled with viscometers, light scattering and concentration detectors in order to have an indication of intrinsic viscosity, molecular weight and macromolecules conformation.

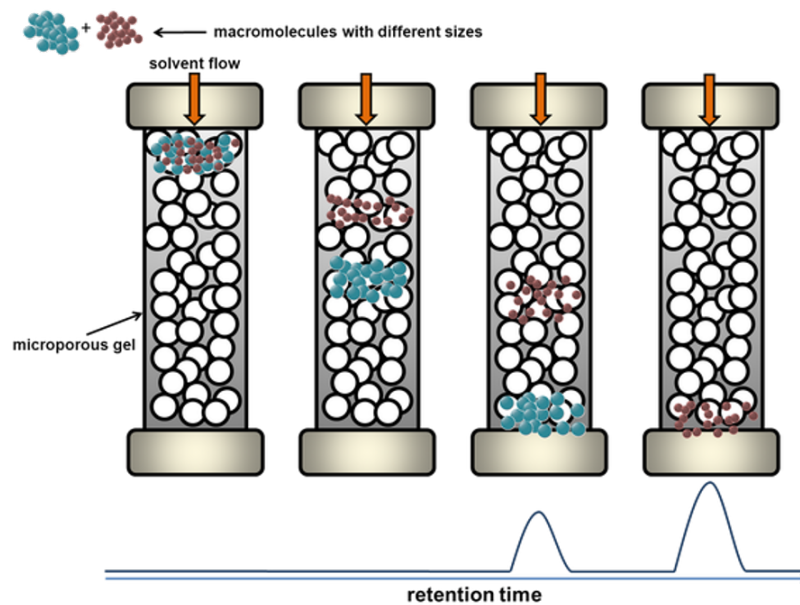


**Figure 3.7:** GPC column principle of work [23].

SEC was used in this study to obtain an estimation of the molecular weight of PCL diols and PCLDMA.

The measurements were carried out using a Malvern apparatus coupled with Viscotek viscometer, RI detector, light scattering and temperature-controlled system (Fig. 3.8) Before the tests, the samples were opportunely dissolved in Tetrahydrofuran (THF) solvent in a concentration of 4 mg/mL for PCL and PCLDMA 2k; 2mg/mL for PCL and PCLDMA 14k.

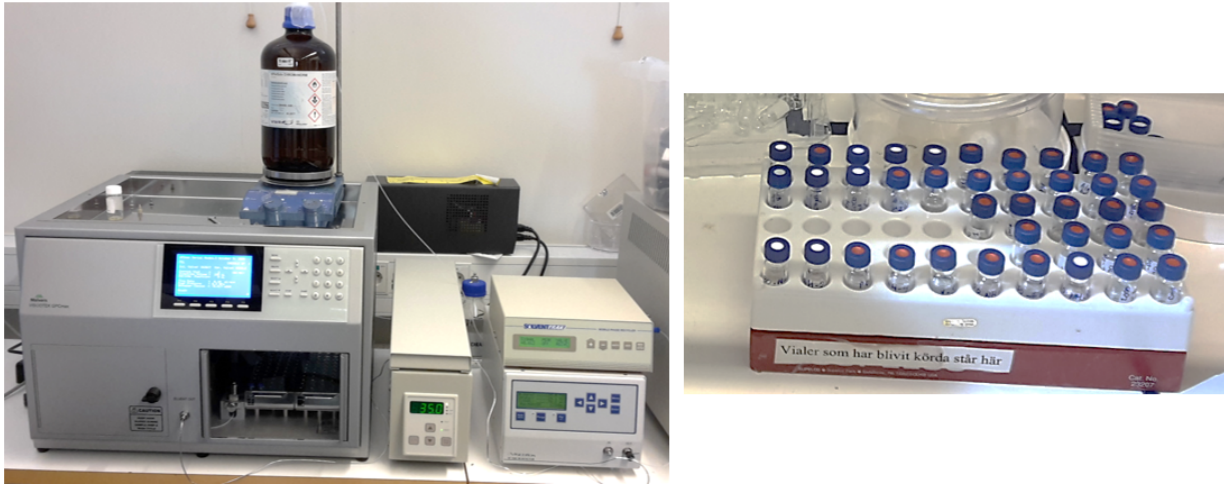


**Figure 3.8:** SEC apparatus and sample tubes used in this technique.

### 3.5 Thermogravimetric analysis (TGA)

Thermogravimetric analysis (TGA) is a technique used to investigate materials weight losses upon heating, which can occur as a result of different physical processes induced by temperature such as oxidation, degradation and decomposition. With regard to the experimental set-up (Figure 3.9) the measurement is carried out in a measurement chamber. The sample is inserted within a crucible that is positioned onto a precision micro-balance. Common crucible types are made of alumina, quartz, graphite, glass, platinum or stainless steel. The heating rate is precisely controlled during the whole experiment as well as the atmosphere. In the following Figure 3.9, is represented a scheme of the TGA chamber.

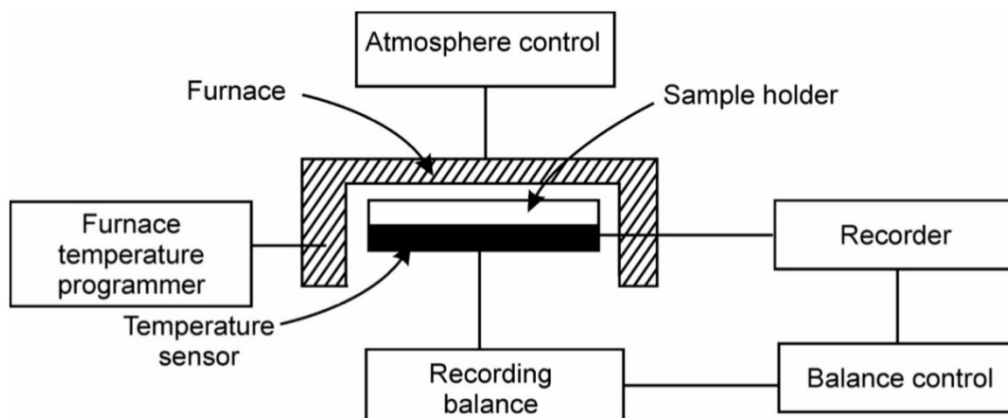


**Figure 3.9:** Schematic representation of TGA measurement chamber [24].

TGA was used in this study to investigate the thermal stability of nGO as compared to that of MAnGO. The samples were placed in alumina crucibles (70  $\mu$ L) that are used without lids. The tests were run up to 800  $^{\circ}$ C under Nitrogen flux, using a TGA Mettler Toledo (USA) and the results were analysed using STARe software. (Figure 3.10).



**Figure 3.10:** TGA apparatus and alumina crucible.

### 3.6 Zetasizer potential analyzer

Zetasizer potential analyser is an accurate method used to evaluate the stability of a suspension. It measures the electrostatic attraction or repulsion arising between the particles. Flocculation and precipitation occur when the electric repulsion is lower than the Van der Waals attractive force. Generally, particles in aqueous media have an electrostatic surface charge that is partially neutralized by the counter ions layer (Fig. 3.11). When particles are subjected to an electric field, they move together with the second layer. Zeta potential ( $\zeta$ ) is the measure of the difference between the electric potential of the particles and the potential of the liquid environment.

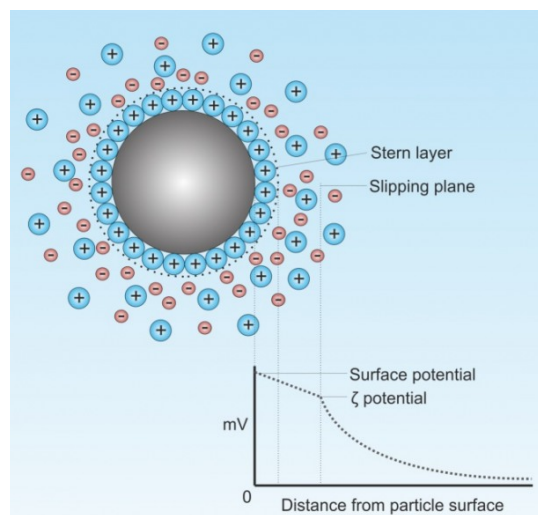


**Figure 3.11:**  $\zeta$ -potential [25].

This instrument measures  $\zeta$ -potential by monitoring the speed of particles that are subjected to an electrical field. Their velocity is indeed, linearly related to the potential.

Considering the experimental set-up, the sample holder is a folded capillary cell provided by two electrodes (Figure 3.12) and the speed of the particles is monitored by means of a laser beam.

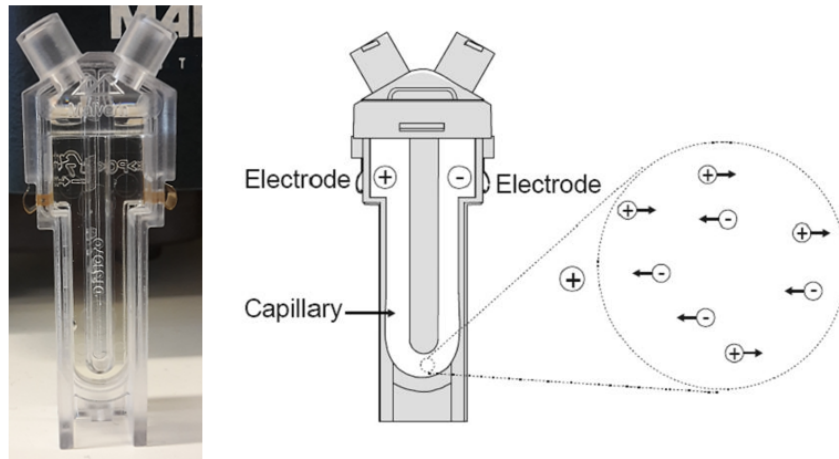


**Figure 3.12:** Sample holder [26].

The greater is the  $\zeta$ -potential, the greater is the stability of the suspension, since a higher charged volume will repel strongly others particles.

Zetasizer potential analyser was used in this work to characterize MAnGO as compared to nGO.

The instrument used to record the data is a Zetasizer Malvern (Figure 3.13); the particles size range that can be analysed goes from 0.3 nm to 10  $\mu$ m. The measure performed on the nanoparticles was carried out in the dynamic light scattering configuration at 20°C in water. Three samples were prepared for each measurement in a concentration of 0.1 mg/mL.



**Figure 3.13:** Z potential instrument [27].

### 3.7 Swelling degree

The swelling degree was measured to evaluate the amount of water that can be absorbed by the synthesized hydrogels. The samples are first dried in vacuum oven for 24 h, under mild vacuum conditions. Then, the specimens are weighted ( $W_d$ ) and immerse into deionized water.

The degree of water absorption (10) is calculated after 5, 10, 20, 30, 60, 90 minutes and then again after 1,2,4 days by measuring the weight of the hydrogels ( $W_w$ ). The degree of swelling can be calculated using the following formula (equation 3.4):

$$\text{Swelling degree} = \frac{W_w - W_d}{W_d} \times 100\% \quad (3.4)$$

Furthermore, also the water content of the hydrogels can be easily calculated using the data recorded during the measurements of swelling (equation 3.5):

$$\text{Equilibrium water content} = \frac{W_w - W_d}{W_w} \times 100\% \quad (3.5)$$

### 3.8 Dynamic mechanical thermal analysis (DMTA)

Dynamic mechanical thermal analysis (DMTA) is a technique commonly used to study materials behaviours, i.e. stiffness (storage and loss moduli) and damping ( $\tan\delta$ ), as a function of temperature, stress, time and frequency. In this technique a sinusoidal and cyclic deformation is applied to a sample with a known geometry and setting a specific frequency, and the material changes are evaluated as the temperature varies.

To successfully understand DMTA, it is necessary to investigate the viscoelasticity phenomenon. Viscoelastic materials, unlike elastic one, cannot be described using Hook's law and therefore the stress and strain signals are not in phase. Actually, the strain signal is divided into two components: one in phase with the strain and the other out of phase by 90 degrees. The first one gives an indication of how the tested material behaves like an ideal solid while the second indicates how it behaves like an ideal fluid. Taking into account these principles, DMTA measures the sample response to the sinusoidal deformation in terms of storage modulus, which is the indication of the in-phase response, and loss modulus, indicating instead the out of phase response. Also the ratio between the moduli is reported under the name of damping or  $\tan\delta$  (Figure 3.14) and gives an indication of how good the material is at absorbing energy.

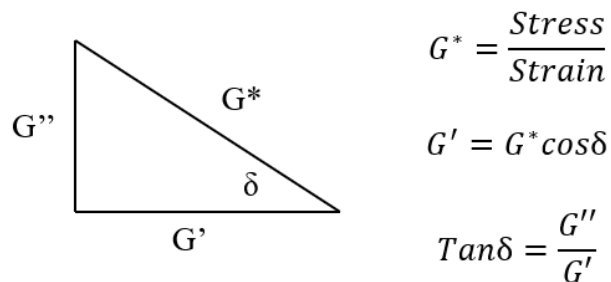


**Figure 3.14:** Complex modulus.

Furthermore, DMTA is considered the most sensitive technique for the measure of glass transition temperatures ( $T_g$ ), since the  $T_g$  is highlighted in both the storage modulus graph in correspondence to a drastic drop of magnitude, and in the peak of the  $\text{tan} \delta$  curve.

This characterization analysis was used in this work to measure the  $T_g$  of the synthesized hydrogels. The measurements were carried out using a Tritec 2000 DMA (Triton Technology Ltd, U.K.) machine, with heating rate of  $3^\circ\text{C}/\text{min}$  and frequency of 1 Hz. The temperature was set to increase from  $-120^\circ\text{C}$  to  $60^\circ\text{C}$ .

The following Table 3.1 reports the geometrical parameters of the samples that have been tested.

**Table 3.1:** Geometrical parameters of the samples used for DTMA.

Samples	Length [mm]	Width [mm]	Thickness [mm]
PCLDMA 2k + PEGDMA [50:50]	11.25	7.05	1.62
PCLDMA 2k + PEGDMA [30:70]	10.79	7.11	1.54
PCLDMA 2k + PEGDMA [70:30]	10.00	6.03	1.28
PCLDMA 14k + PEGDMA [50:50]	10.00	7.00	1.63
PCLDMA 14k + PEGDMA [30:70]	10.50	7,01	1.55



## 4 Results and discussion

The results of the characterization analysis previously investigated in Chapter 3, are presented and discussed within this chapter.

In the first sections, the results coming from the measurements made on both oligomers and nGO are presented to confirm the effectiveness of their methacrylation. SEC data are then evaluated to investigate the different molecular weight of the functionalized PCL oligomers and the results of the thermogravimetric analysis are shown to compare the five different synthesis procedures followed for the methacrylation of the nGOs.

The last part of the chapter is devoted to the discussion of the results coming from the characterization of the photocurable hydrogels. First, ATR-FTIR and H-NMR spectra are discussed in detail to confirm the effectiveness of crosslinking. Then, the thermomechanical properties and swelling behaviours of the different hydrogels are investigated.

### 4.1 Evaluation of functionalization of PCL and PEG

#### 4.1.1 Characterization of the oligomers by means of ATR-FTIR

The attenuated total reflectance - fourier transform infrared spectroscopy was used to evaluate the chemical structure of the modified oligomers, as compared to the one of the starting materials.

##### 4.1.1.1 PCL diacrylation and dimethacrylation

As we can see from the Figures 4.1, 4.2 and 4.3 the recorded spectra of the PCL-diol oligomers are very similar, just differing for the -OH broad peaks at around  $3500\text{ cm}^{-1}$ , which has a lower intensity in the case of PCL-diol 14k. This is due to the longer carbon chains that make the ending groups difficult to be detected. All of the spectra show the typical peaks of C-H bond at  $2950$  and  $2865\text{ cm}^{-1}$ , C=O vibration at  $1723\text{ cm}^{-1}$  and C-O-C vibration at around  $1165\text{ cm}^{-1}$ .

PCL diacrylation was confirmed both by the presence of C=C bending peak at  $820\text{ cm}^{-1}$  and by the disappearance of the OH vibrational peak at around  $3500\text{ cm}^{-1}$ .

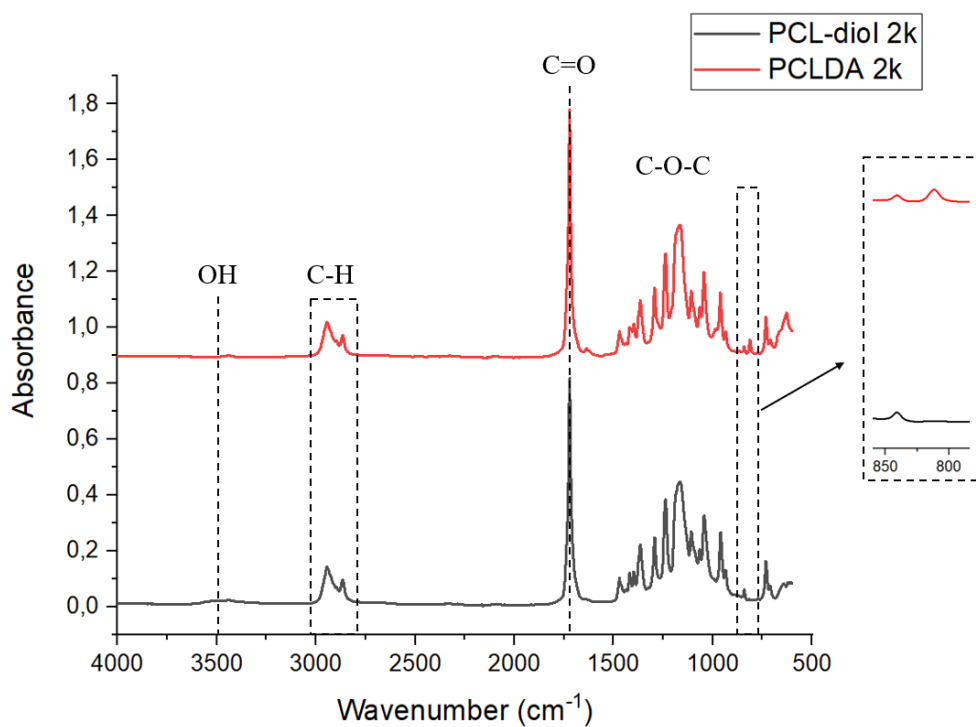


**Figure 4.1:** ATR-FTIR spectra of PCL-diol and PCLDA 2k.

The methacrylation of all of PCL, both 2k and 4k, was confirmed by the appearance at 1630  $\text{cm}^{-1}$  of the C=C stretching peak in both the spectra of the methacrylated samples (Figures 4.2 and 4.3).

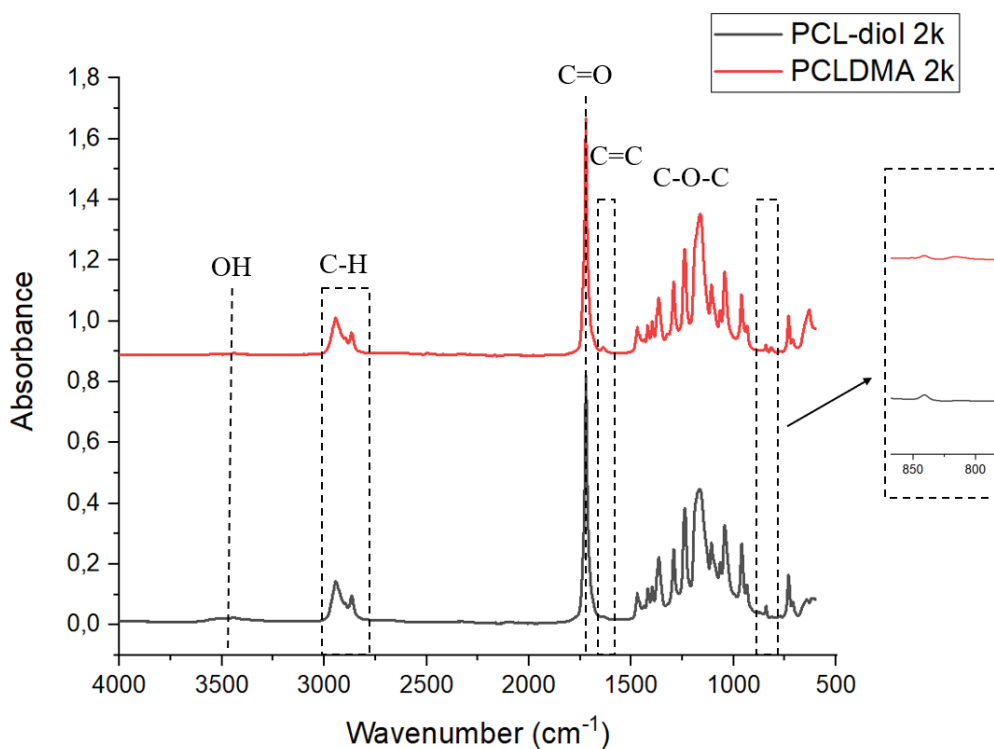


**Figure 4.2:** ATR-FTIR spectra of PCL-diol and PCLDMA 2k.

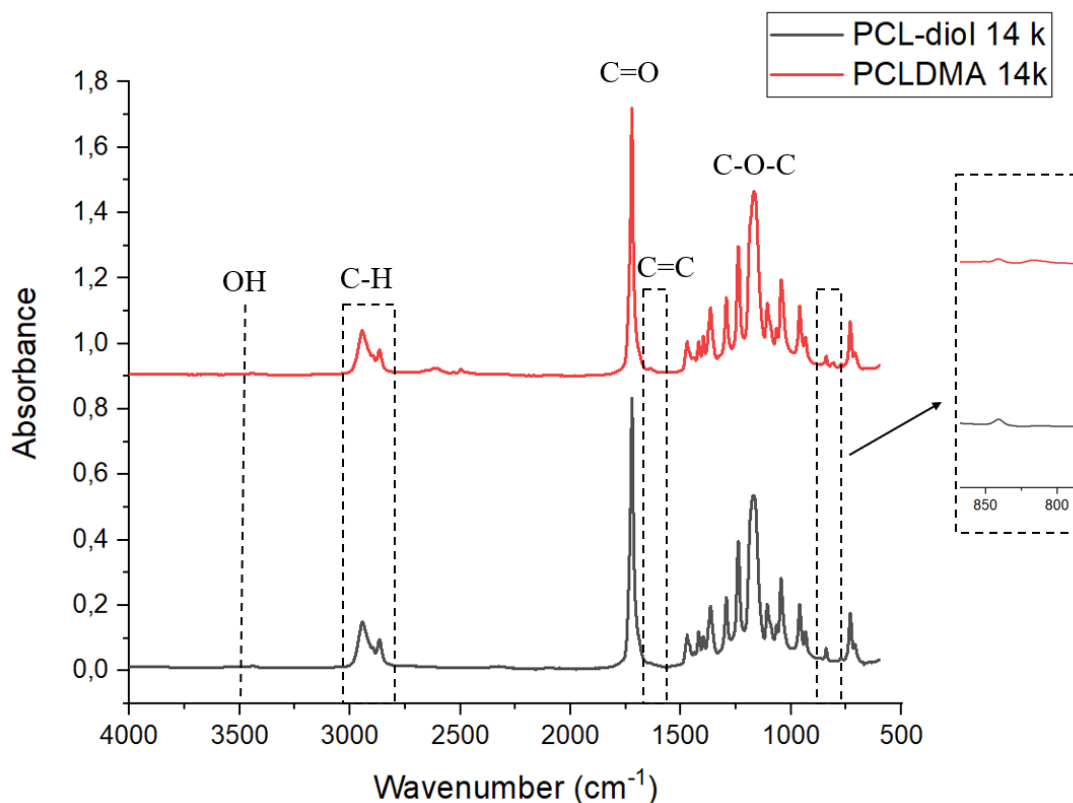


**Figure 4.3:** ATR-FTIR spectra of PCL-diol 14k and PCLDMA14k.

#### 4.1.1.2 PEG dimethacrylation

The following Figure 4.4 shows the spectra of PEG 3k both before and after the functionalization.

The spectra display the typical peak of  $-\text{CH}_2-$  stretching at  $2870\text{ cm}^{-1}$  and the asymmetric C-O-C stretching peaks at  $1102$  and  $1241\text{ cm}^{-1}$ . However, the peak at  $3470\text{ cm}^{-1}$  corresponding to the  $-\text{OH}$  vibration did not disappear. The unexpected presence of this peak can be probably ascribed to an insufficient amount of methacryloyl acid used in the synthesis. Nevertheless, the appearance of three new peaks respectively at  $1700$ ,  $1640$  and  $1323\text{ cm}^{-1}$ , corresponding respectively to  $-\text{COO}-$ ,  $\text{C}=\text{C}$  and  $-\text{CH}_3$  groups vibration [28], can be clearly observed.

Overall can be concluded that the functionalization of PEG 3k has led to a partial degree of methacrylation [29].

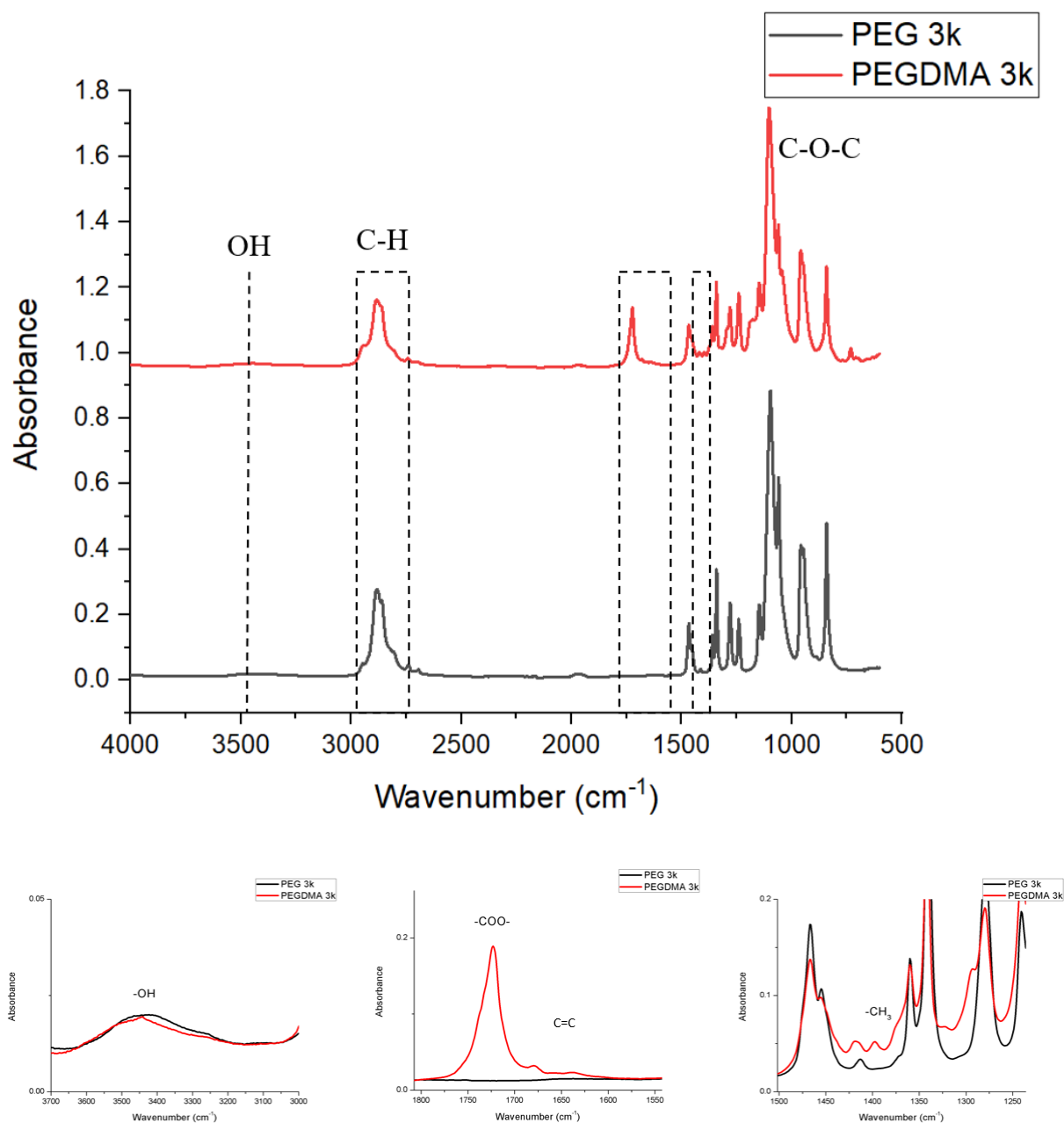


**Figure 4.4:** ATR-FTIR spectra of PEG and PEGDMA 3k.

The spectra of PEG and PEGDMA 4k (Figure 4.5) shows absorption bands at 1715, 1640, 1325 cm<sup>-1</sup> related to -COO-, C=C and -CH<sub>3</sub> characteristic vibrations. Furthermore, unlike the previous spectra, the disappearance of the hydroxyl broad peak can be easily observed at around 2461 cm<sup>-1</sup>, thus confirming the effectiveness of methacrylation.

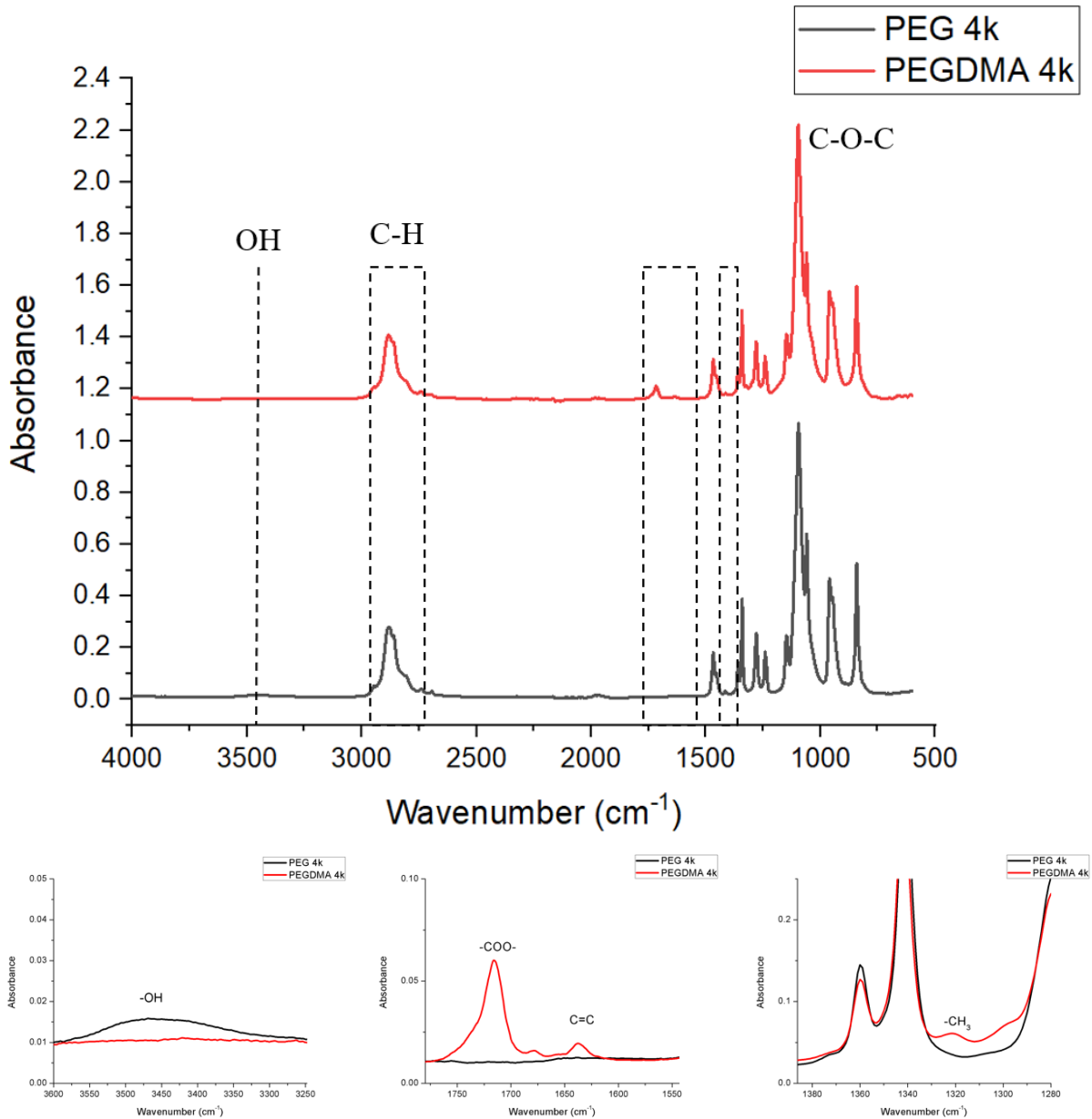


**Figure 4.5:** ATR-FTIR spectra of PEG 4k and PEGDMA 4k.

The following figure 4.6 reports the comparison between the spectra of PEG and PEGDMA 6k. Likewise the previous spectra shown in Figure 4.5, both the disappearance of the broad -OH peak and the appearance of the -COO-, C=C and -CH<sub>3</sub> peaks can be clearly detected respectively at 3470, 1728, 1648 and 1323 cm<sup>-1</sup>, confirming one more time the effectiveness of methacrylation.

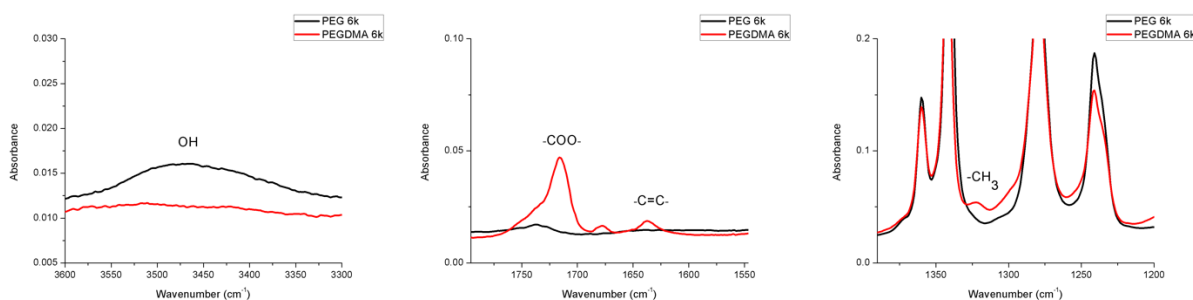
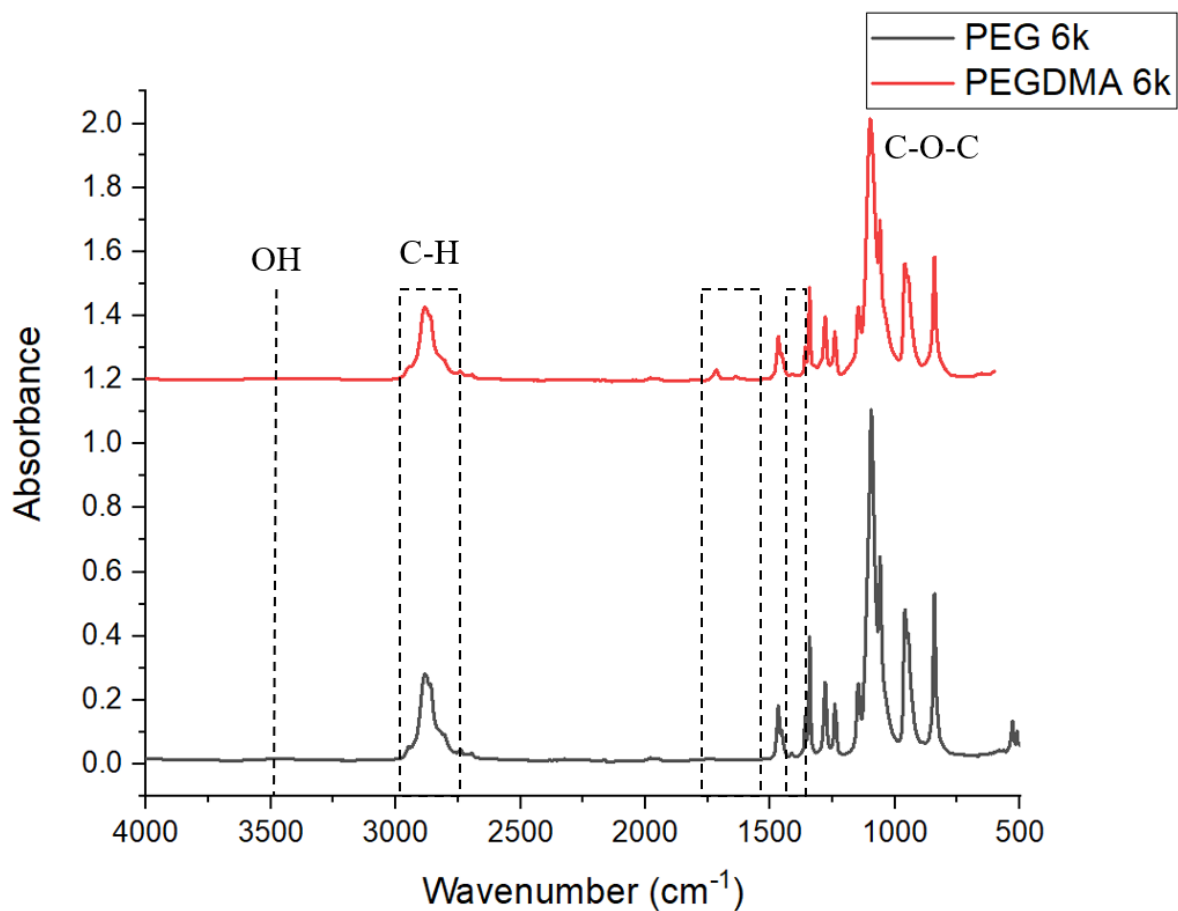


**Figure 4.6:** ATR-FTIR spectra of PEG and PEGDMA 6k.

Overall, those evidences indicate that the methacrylation was successfully carried out, thus confirming the synthetic protocol that has been followed.

#### 4.1.2 H-NMR

Proton nuclear magnetic resonance was used to investigate the effectiveness of methacrylation. Moreover, H-NMR data were also used to calculate approximately their molecular weights of the oligomers.

In the Figure 4.7 is reported the PCL-diol 2k H-NMR spectrum, where every peak is uniquely identified.

In order to calculate the molecular weight of the oligomer,  $\delta_i$  peak-area was taken as a reference. Assuming that the integral of  $i$ -peak corresponds to the signal of 4 hydrogens

located in i-position (equation 4.1),  $M_w$  was estimated using the following equations 4.2 and 4.3:

$$\delta_i = 1 = 4H \rightarrow 1H = 0,25 \quad (4.1)$$

$$\delta_d = 8,06 \sim 8 \rightarrow 32H \rightarrow 16C_d \rightarrow 16 \text{ repeating units} \rightarrow 16 * 114 = 1824 \frac{g}{mol} \quad (4.2)$$

$$M_{w\_PCL\_2k} = 1824 + 104 + (2 * 115) = \mathbf{2158} \frac{g}{mol} \quad (4.3)$$

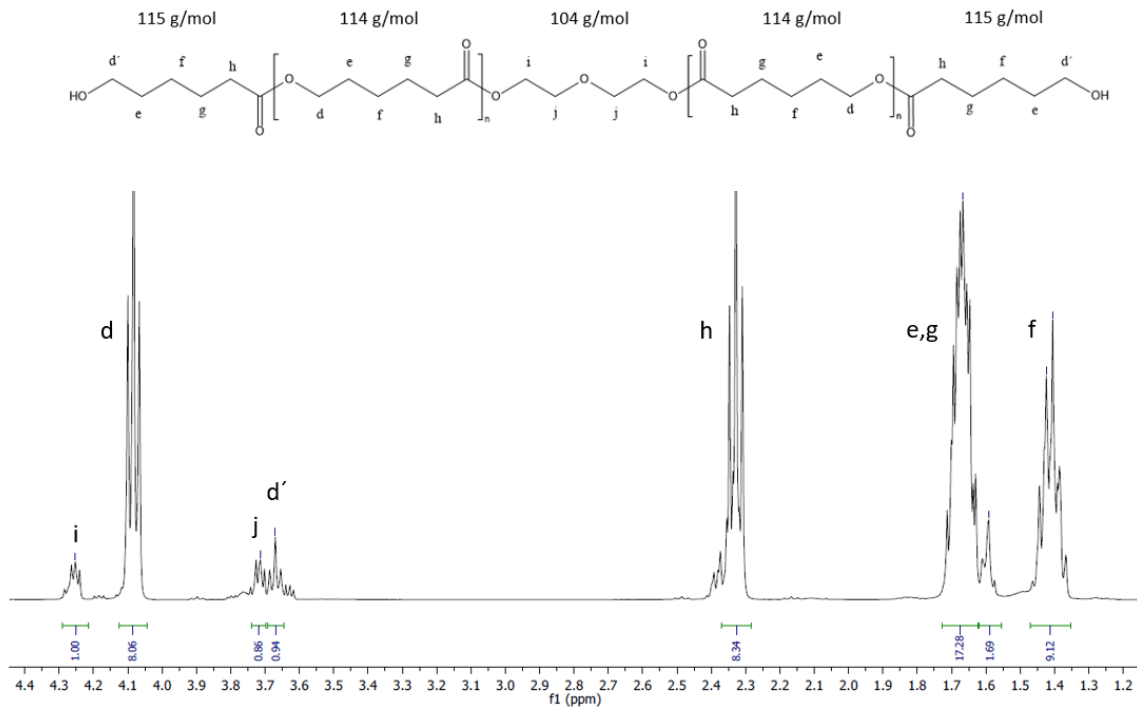


**Figure 4.7:** H-NMR spectrum of PCL-diol 2k

The spectrum of PCLDMA 2k is shown in Figure 4.8. The methacrylic group appeared in  $\delta$  6.11, 5.56 and 1.95. Molecular weight was calculated using Equation 4.4, 4.5 and 4.6, by means of the same procedure as before:

$$\delta_i = 2,39 \sim 2 = 4H \rightarrow 1H = 0,5 \quad (4.4)$$

$$\delta_d = 26,32 \sim 26 \rightarrow 52H \rightarrow 26C_d \rightarrow 26 \text{ repeating units} \rightarrow 26 * 114 = 2964 \frac{g}{mol} \quad (4.5)$$

$$M_{w\_PCLDMA\_2k} = 2964 + 104 + (2 * 159) = \mathbf{3386} \frac{g}{mol} \quad (4.6)$$

This value, which is higher than expected, can be explained by the occurrence of side reactions involving triethylamine that developed in the functionalization reaction. This hypothesis is also demonstrated by the presence of some unexpected peaks at  $\delta$  3.13 and  $\delta$  3.11.

Furthermore, the percentage of conversion was calculated as the ratio of the peaks (Equation 4.7):

$$\delta_a : \delta_b : \delta_c : \delta_i : \delta_j = 1 : 1 : 3 : 2 : 2 \quad (4.7)$$

This ratio corresponds to a total conversion.

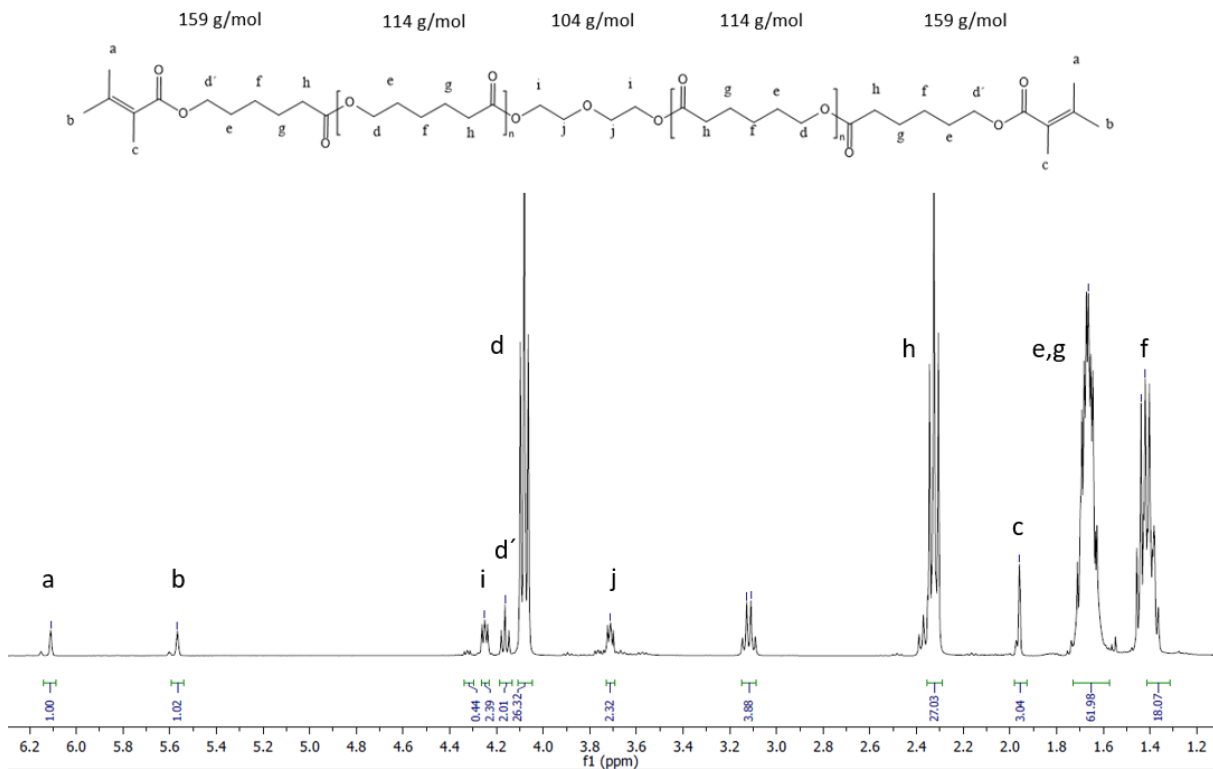


**Figure 4.8:** H-NMR spectrum of PCLDMA 2k.

The PCL-diol 14k graph is shown in Figure 4.9. The molecular weight was estimated as before, (Equations 4.8, 4.9 and 4.10):

$$\delta_i = 1 = 4H \rightarrow 1H = 0,25 \quad (4.8)$$

$$\delta_a = 31,92 \sim 32 \rightarrow 128H \rightarrow 64C_a \rightarrow 64 \text{ repeating units} \rightarrow 64 * 114 = 9216 \frac{g}{mol} \quad (4.9)$$

$$M_{w\_PCL\_14k} = 9216 + 104 + (2 * 115) = \mathbf{9550} \frac{g}{mol} \quad (4.10)$$

Unexpectedly, the measured molecular weight was well below 14000. This low value can be due to batch aging and potential degradation.

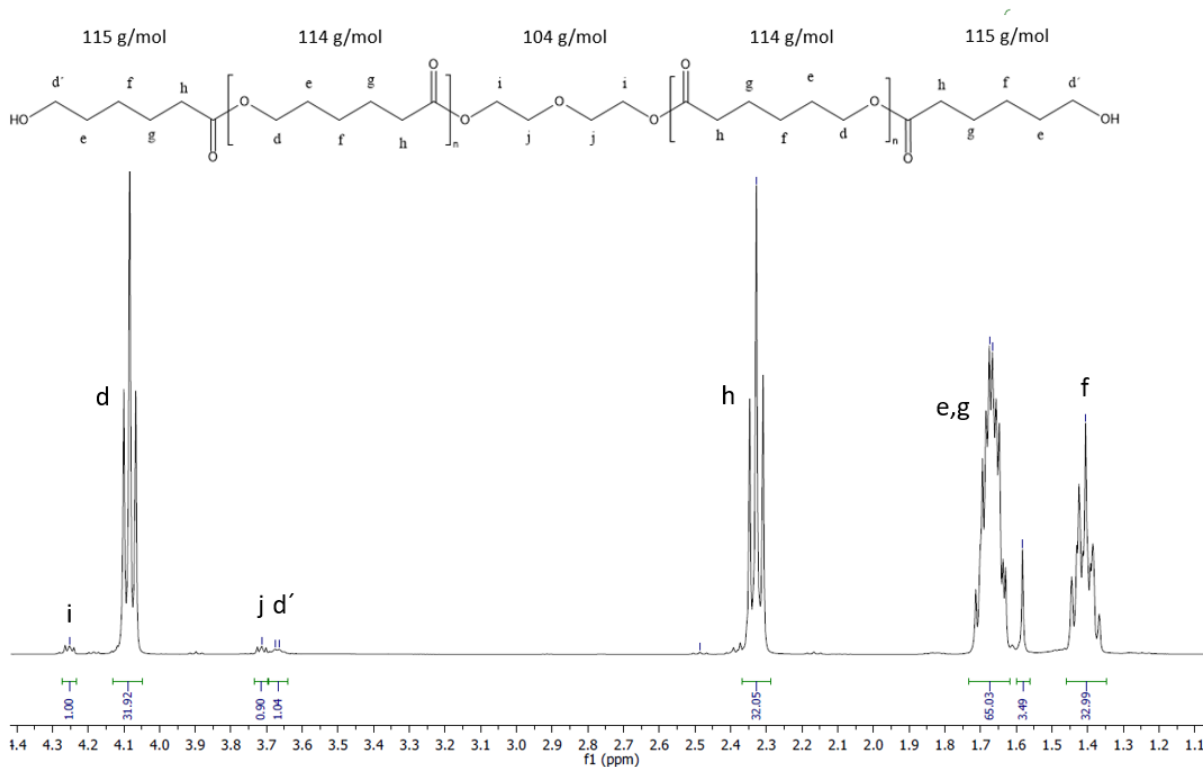


**Figure 4.9:** H-NMR spectrum of PCL-diol 14k.

The H-NMR spectrum of PCL-DMA 14k graph is shown in Figure 4.10. As previously discussed for PCL-diol 2k, also the PCL-diol 14 shows an increase of molecular weight after the methacrylation. However, the  $M_w$ , obtained by means of Equation 4.11, 4.12 and 4.13, resulted lower than expected probably due to the occurrence of side reaction involving triethylamine. As before, the presence of peaks at  $\delta$  3.13 and  $\delta$  3.11 prove the validity of this assumption.

$$\delta_i = 5.89 \sim 6 = 4H \rightarrow 1H = 1.5 \quad (4.11)$$

$$\delta_d = 205.4 \sim 205 \rightarrow 136.67H \rightarrow 68C_d \rightarrow 68 \text{ repeating units} \rightarrow 68 * 11 = 9840 \frac{g}{mol} \quad (4.12)$$

$$M_{w\_PCLDMA\_14k} = 9840 + 104 + (2 * 159) = \mathbf{10262} \frac{g}{mol} \quad (4.12)$$

The percentage of conversion was calculated as the ratio of the peaks' integrals (Equation 4.13):

$$\delta_a : \delta_b : \delta_c : \delta_i : \delta_j = 1 : 1 : 3 : 6 : 6 \quad (4.13)$$

This result corresponds to 33% of conversion. We can also notice that there are others new peaks in the graph, which can be attribute to side reaction products.

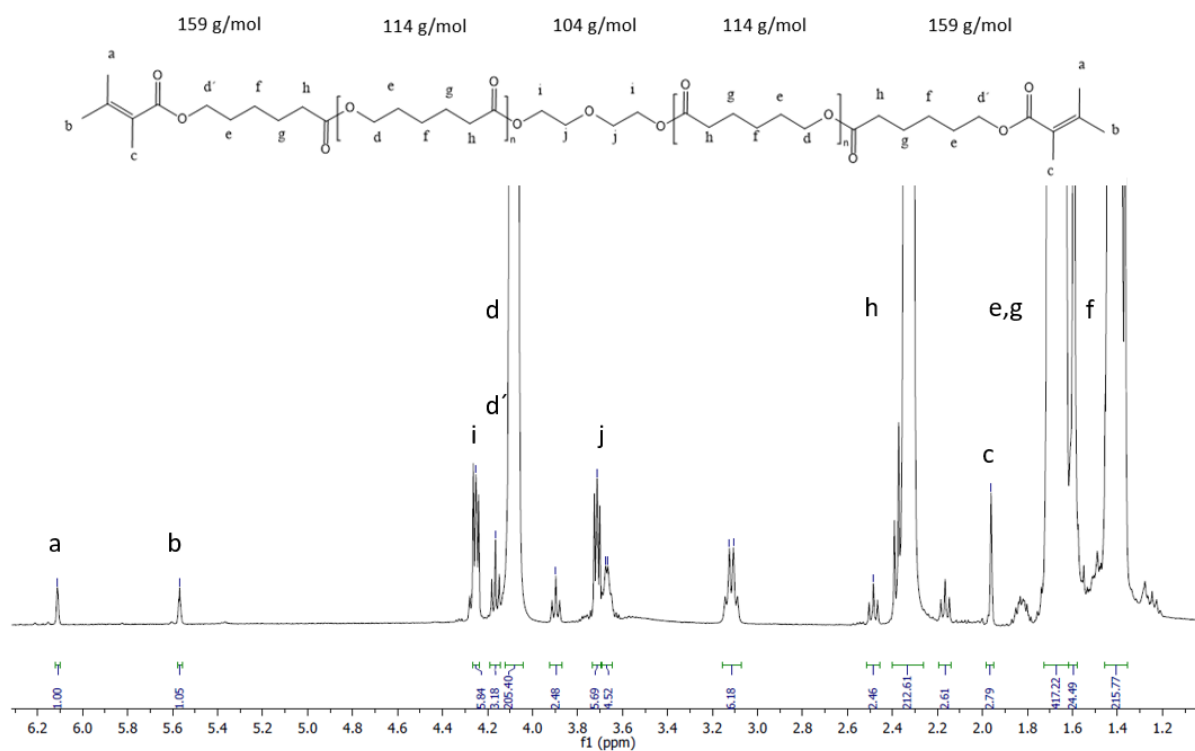


**Figure 4.10:** H-NMR spectrum of PCLDMA 14k.

PEG and PEGDMA 3k, 4k and 6k spectra are reported respectively in the Figures 4.11, 4.12 and 4.13. In all of the graphs the methacrylation is confirmed by the presence of peaks in  $\delta$  6.15, 5.59 and 1.97 ppm range.

Differently from the discussion on PCL and PCLDMA, both the calculation of the molecular weights of PEG and PEGDMA and the total conversion were difficult to be determined. This issue arises from the structure of PEG itself, which makes the determination of a peak reference very complicated. Accordingly, the spectra of PEG and PEGDMA are evaluated just for comparative analysis.

With regard to the spectrum of PEG, it can be noticed the presence of an impurity at  $\delta=1.79$  in both the original material and in the functionalized one.

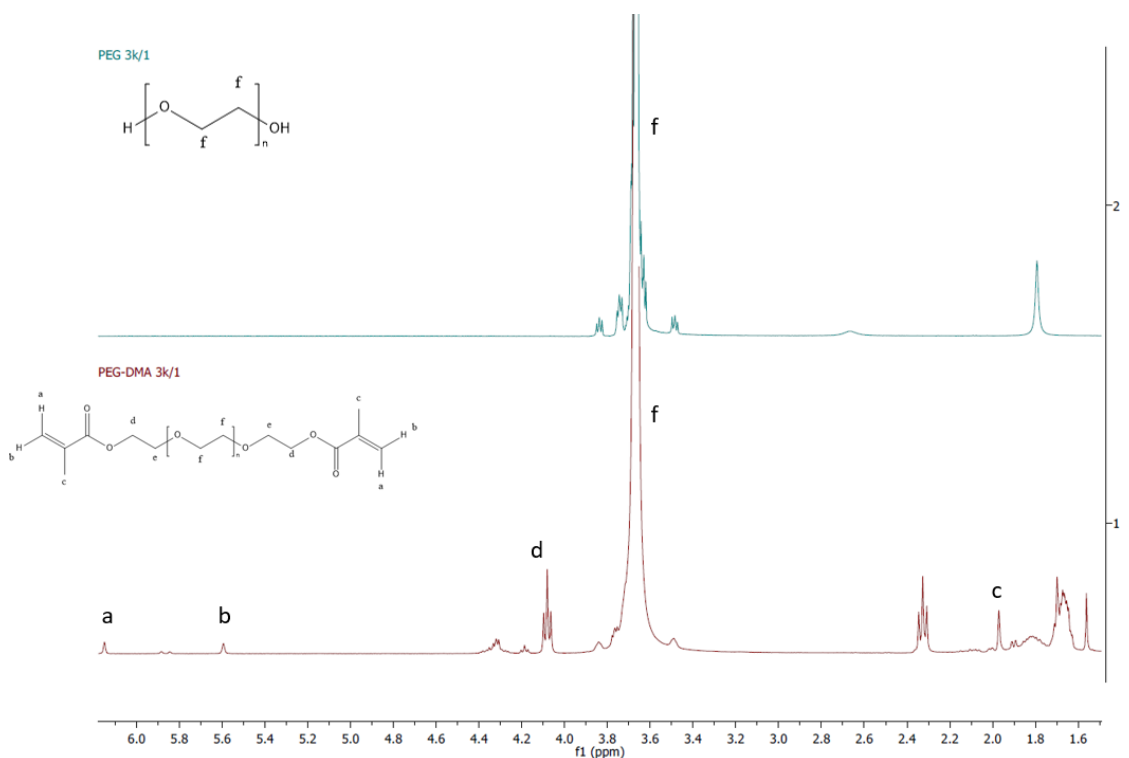


**Figure 4.11:** H-NMR spectra of PEG and PEGDMA 3k.

In both the Figure 4.12 and 4.13, the spectra of PEGDMA 4k and 6k show three characteristic peaks at  $\delta=3.13$ , 3.11 and 1.44 which can be attributed to an excess of triethylamine, ascribable either to an incorrect filtration or to an insufficient washing with diethyl ether.

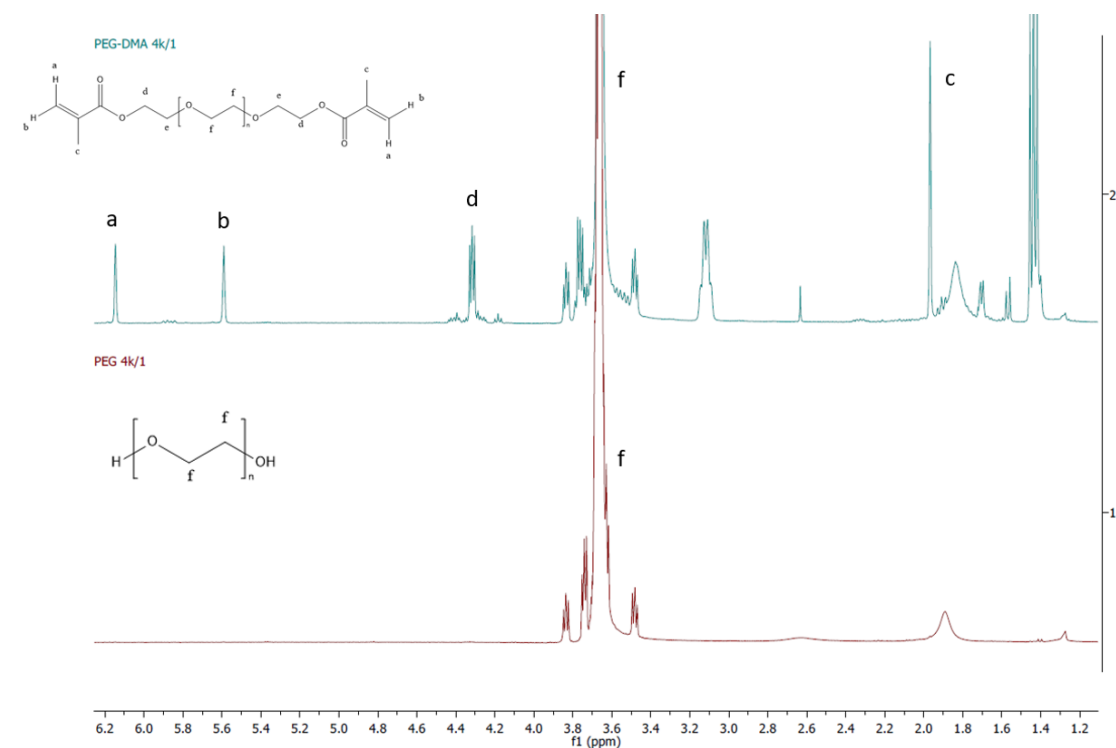


**Figure 4.12:** H-NMR spectra of PEG and PEGDMA 4k.

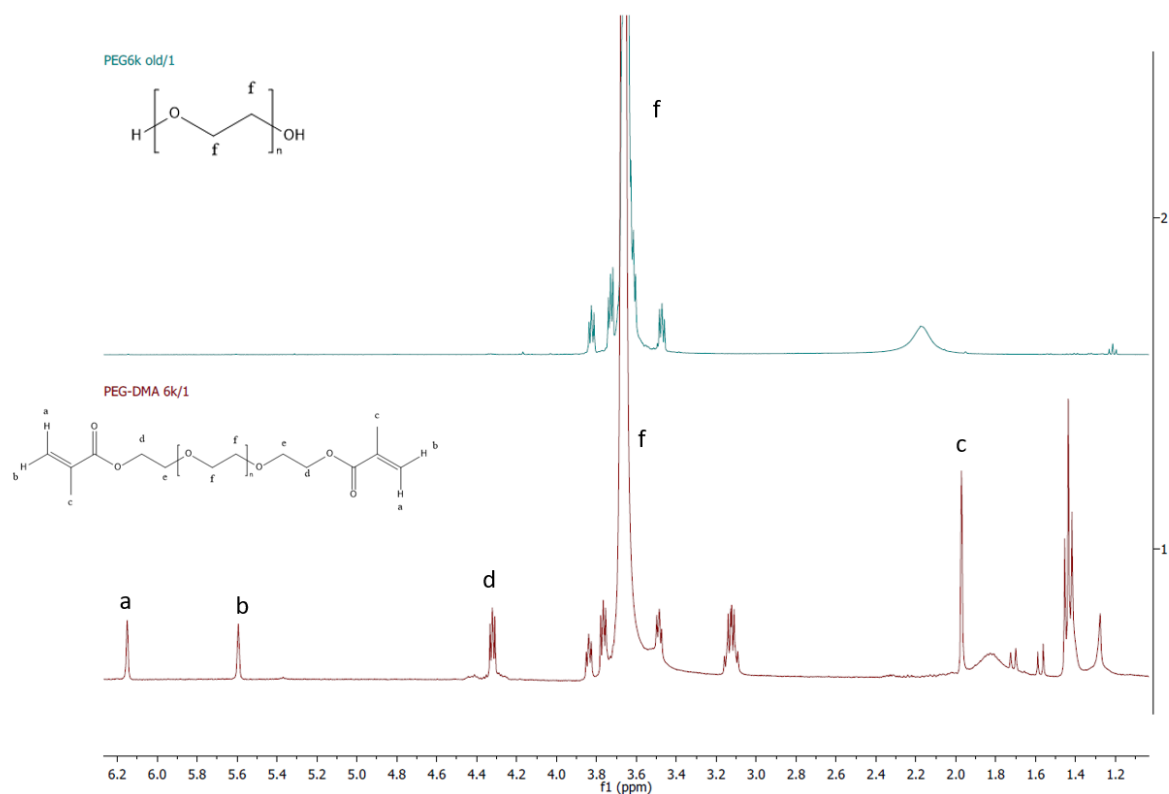


**Figure 4.13:** H-NMR spectra of PEG and PEGDMA 6k.

#### 4.1.3 Comparison between the thermal behaviours of both virgin and functionalized oligomers by means of DSC

Differential scanning calorimetry was used to investigate the variations in the thermal transitions of oligomers as a result of the functionalization. Moreover, it was also used to estimate the crystallinity percentage of the oligomers [30].

PCL-diol, PCLDA and PCLDMA thermograms are reported in Figure 4.14, while Figure 4.15 displays the DSC curves of PCL-diol and PCLDMA 14k.

As expected, the melting temperature ( $T_m$ ) and the enthalpy of fusion decrease as a result of the incorporation of acrylate and methacrylate moieties along the main chains of the oligomers.

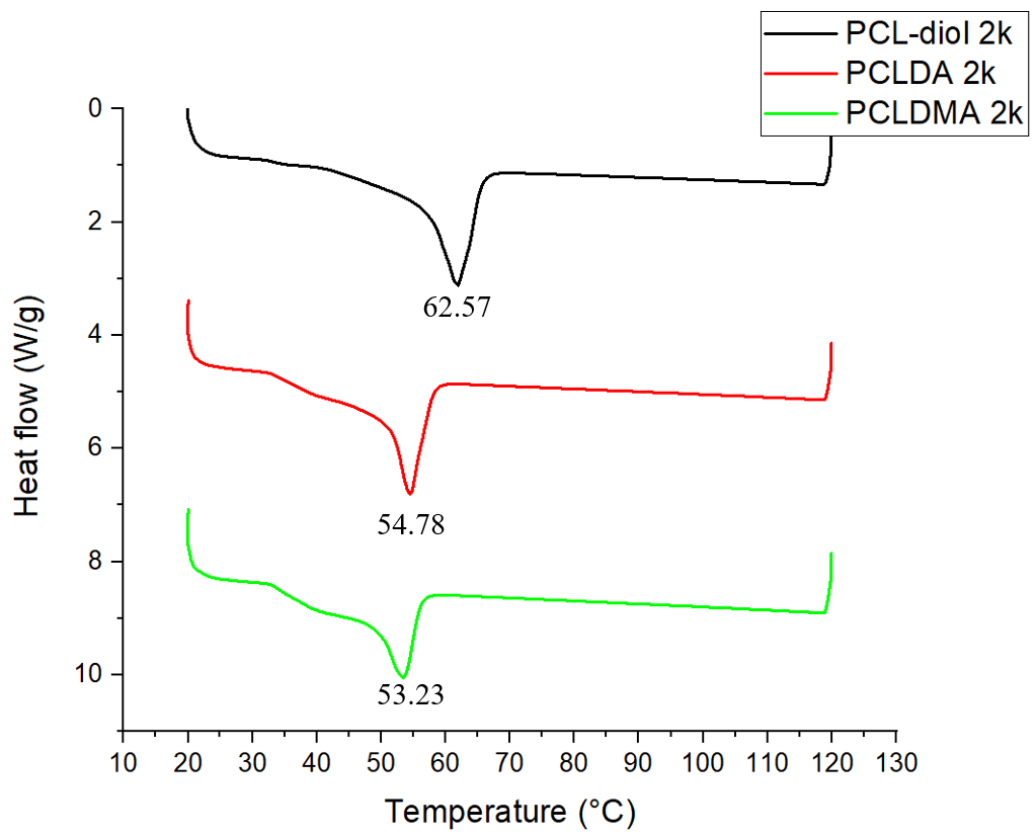


**Figure 4.14:** DSC thermograms of PCL-diol, PCLDA and PCLDMA.

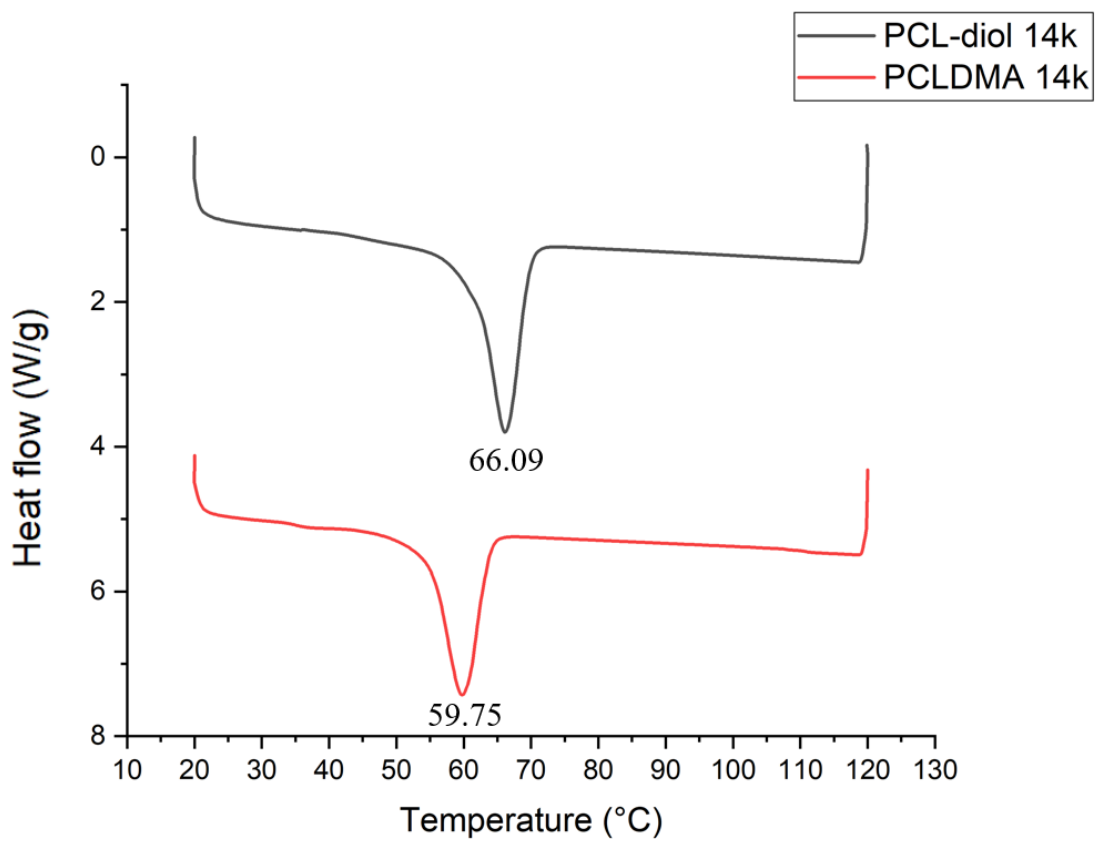


**Figure 4.15:** DSC thermograms of PCL-diol and PCLDMA 14k.

The following Table 4.1 reports all the data recorded for PCL-diol, PCLDA and PCLDMA, including melting transition temperatures, enthalpies of fusion and degrees of crystallinity, which was calculated as the ratio of the experimental enthalpy of fusion and the theoretical enthalpy of fusion of PCL 100% crystalline ( $\Delta H_{ref}=135.44$  J/mol) [31].

With regard to the crystallization of the oligomers, longer chains have low mobility and therefore they reach lower degrees of crystallinity with respect to the shorter ones.

**Table 4.1:** DSC data.

Material	$T_m$ (°C)	$\Delta H_m$ (J/g)	Crystallinity (%)
PCL-diol 2k	62.57	96.38	71.16
PCLDA 2k	54.78	66.36	49.00
PCLDMA 2k	53.23	56.89	41.01
PCL-diol 14k	66.09	85.34	63.01
PCLDMA 14k	59.75	76.46	56.45

The DSC curves of PEG and PEGDMA both 3k and 8k are shown in Figure 4.16 and Figure 4.17. In the thermograms of both PEGDMA 3k and PEGDMA 6k, the enthalpy of fusion peak shift to lower temperatures, as compared to the PEG ones. This behaviour can be ascribed to presence of the methacrylate groups in the functionalized oligomers.

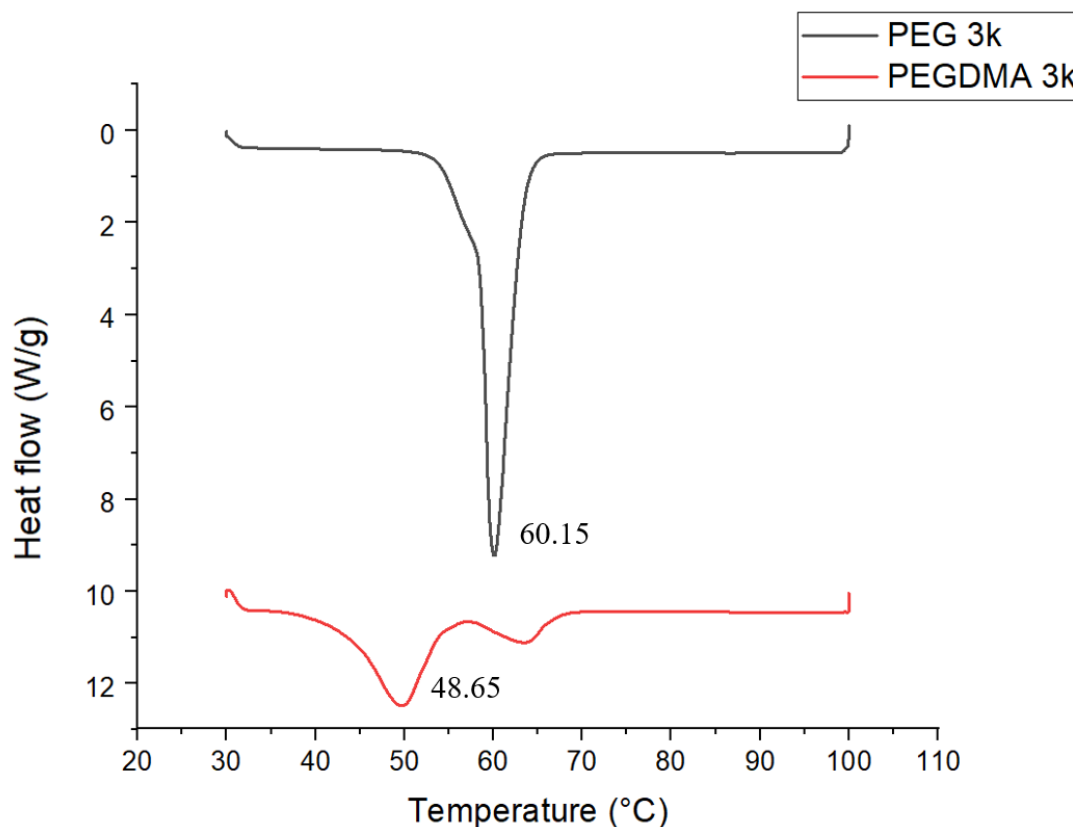


**Figure 4.16:** DSC thermograms of PEG and PEGDMA 3k.

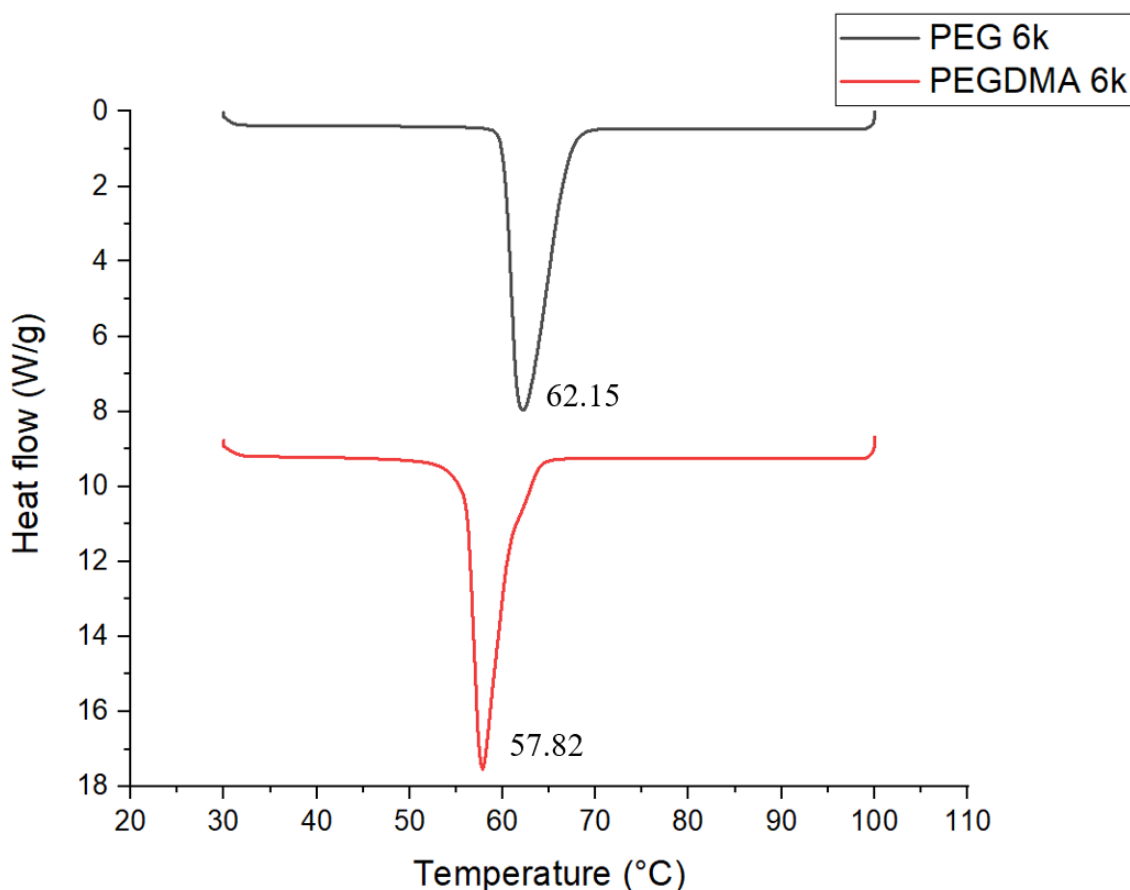


**Figure 4.17:** DSC thermograms of PEG and PEGDMA 6k.

Table 4.1 reports all the data recorded for PEG and PEGDMA, including melting transition temperatures and enthalpies of fusion.

**Table 4.2:** DSC data

Material	$T_m$ (°C)	$\Delta H_m$ (J/g)
PEG 3k	60.15	202.16
PEGDMA 3k	48.65	88.27
PEG 6k	62.15	228.33
PEGDMA 6k	57.82	180.29

#### 4.1.4 Evaluation of the oligomers' molecular weights

The molecular weights of both PCL and PCLDMA oligomers are evaluated by means of size exclusion chromatography (SEC) measurements.

The following Figure 4.18 displays four SEC comparative curves. The graphs on the left show the volume, known as retention volume, at which the solute elute from the column, while the graphs on the right give an estimation of the molecular weights. It is important to notice that this instrument is able to measure only the hydrodynamic volume that strongly depends on the affinity between sample and solvent. Therefore, is not accurate but can be quite precise, so it is only useful for comparative purpose.

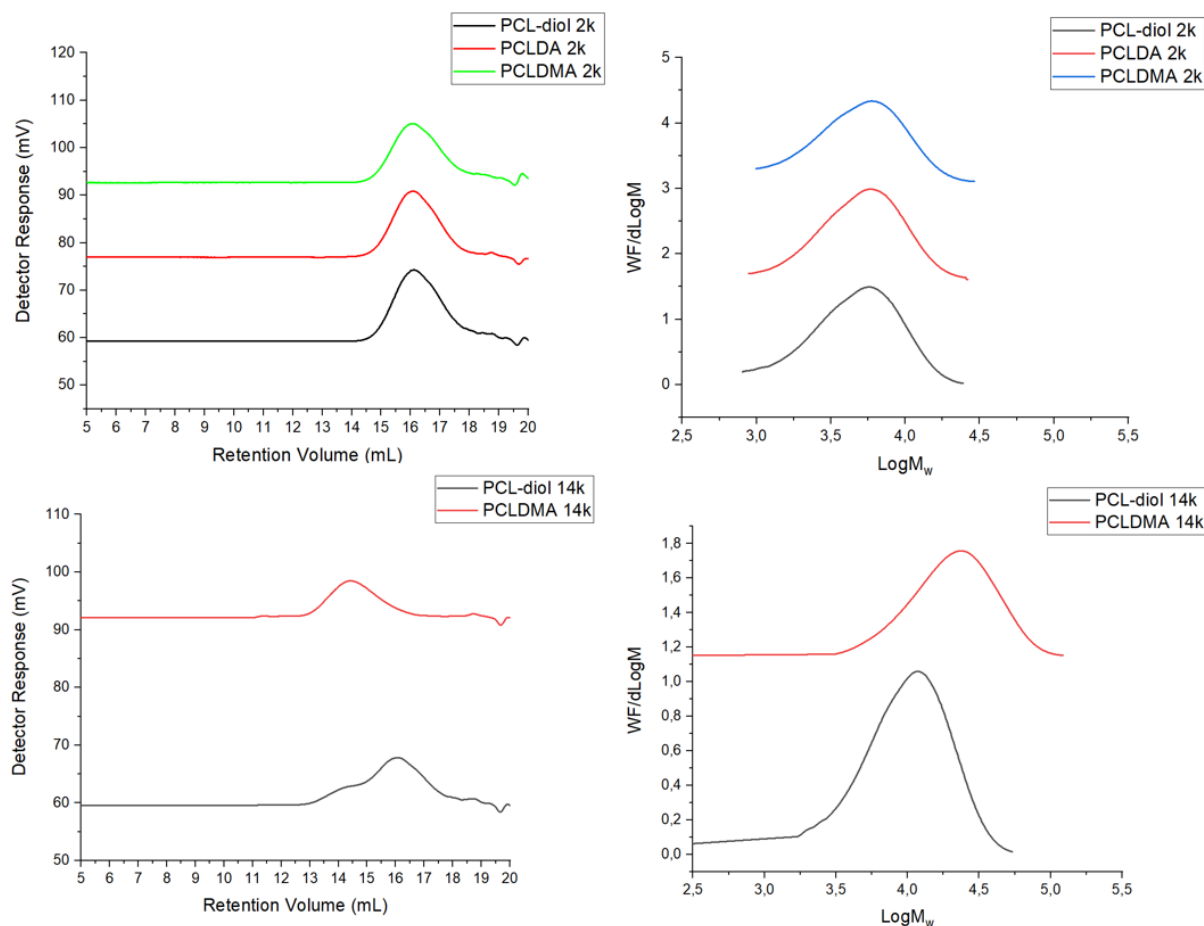


**Figure 4.18:** SEC plots of PCL-diol 2k, PCLDA 2k, PCLDMA 2k, PCL-diol 14k and PCLDMA 14k.

The number average molecular weight ( $M_n$ ), the weight average molecular weight ( $M_w$ ), the retention volume and the polydispersity index (PDI or  $\mathcal{D}$ ), which is the ratio of  $M_n$  and  $M_w$  and denotes the distribution of a single molecular mass in a batch, are given in Table 4.3.

PDIs close to one indicate that in each sample there are chains with approximately the same length. Moreover, PDI values around 1.5 are compatible with the free radical polymerization mechanism, which was followed to synthesize the oligomers. As regards the retention volume, the values given in the table increase as the length of the chains increases. After the methacrylation, the volume of PCLDMA 2k is nearly the same as PCL-diol 2k one, while the PCLDMA 14k volume increases of about 5% with respect to the PCL-diol 14k.

**Table 4.3:** Highlights results from SEC graphs.

Material	Pick RV (mL)	$M_n$ (Da)	$M_w$ (Da)	PDI ( $\mathcal{D}$ )= $M_w/M_n$
<b>PCL-diol 2k</b>	16.017	3,952	6,259	1.584
<b>PCLDA 2k</b>	16.017	4,141	6,337	1.53
<b>PCLDMA 2k</b>	16.067	3,969	6,073	1.53

<b>PCL-diol 14k</b>	14.267	18,342	2,823	1.518
<b>PCLDMA 14k</b>	14.233	18,735	29,004	1.548

## 4.2 Methacrylation of nanographene oxide evaluation

### 4.2.1 Confirmation of nGO methacrylation by means of ATR-FTIR spectroscopy

ATR-FTIR was also used to investigate the chemical structure of nanographene oxide as compared to the one of methacrylated nanographene,

The Figure 4.19 shows the comparison between three batches of untreated nGO and one batch of nGO that underwent a dialysis process. The last sample was prepared in order to evaluate the effect of water in the nGO spheres.

The OH broad, C=O and C=C peaks can be detected at  $3400\text{ cm}^{-1}$ ,  $1700\text{ cm}^{-1}$  and  $1550\text{ cm}^{-1}$  respectively. However, in the case of the nGOs subjected to dialysis, two more peaks are clearly visible at  $2929\text{ cm}^{-1}$  and  $2851\text{ cm}^{-1}$ , corresponding to the C-H stretch vibrations of methylene group. The presence of these peaks can be explained by assuming the reduction of nanographene oxide to nanographene caused by water molecules.

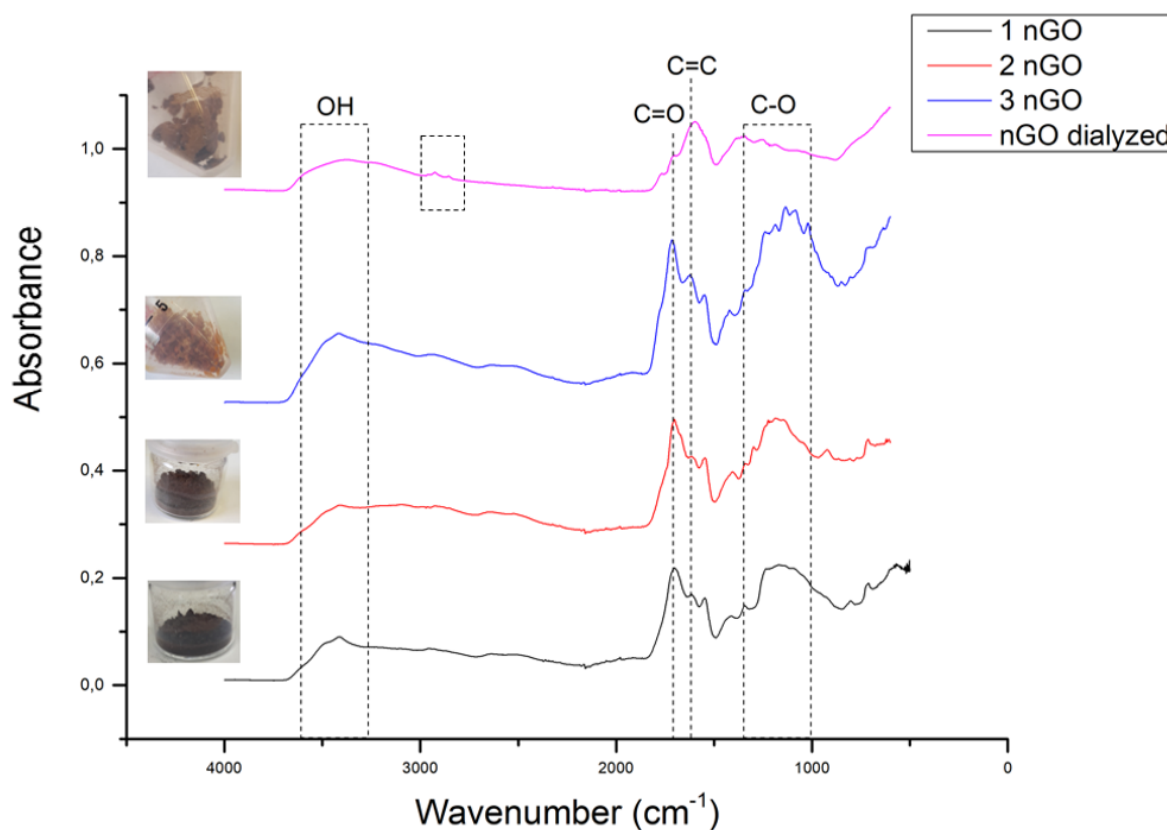


**Figure 4.19:** ATR-FTIR spectra of nGO spheres.

In Figure 4.20, a comparison between the spectra of nGO and MA-nGO obtained following three different routes is given. The spectrum illustrated with the black line refers to the MA-

nGO heated at 120 °C, the red curve refers to the MA-nGO first heated at 80°C in vacuum assistance and then dialyzed, while the violet one refers to the MA-nGO heated at 80°C and then lyophilized.

As a result of methacrylation, the OH peak intensity decreases always, except for the MA-nGO that were dialyzed. Moreover, two defined peaks at 2970  $\text{cm}^{-1}$  ascribable to the CH stretch in C-CH<sub>3</sub> compound, can be clearly seen in the cases of both the MA-nGO heated at 120 °C and MA-nGO only lyophilized. These can be considered as a confirmation of the methacrylation process.

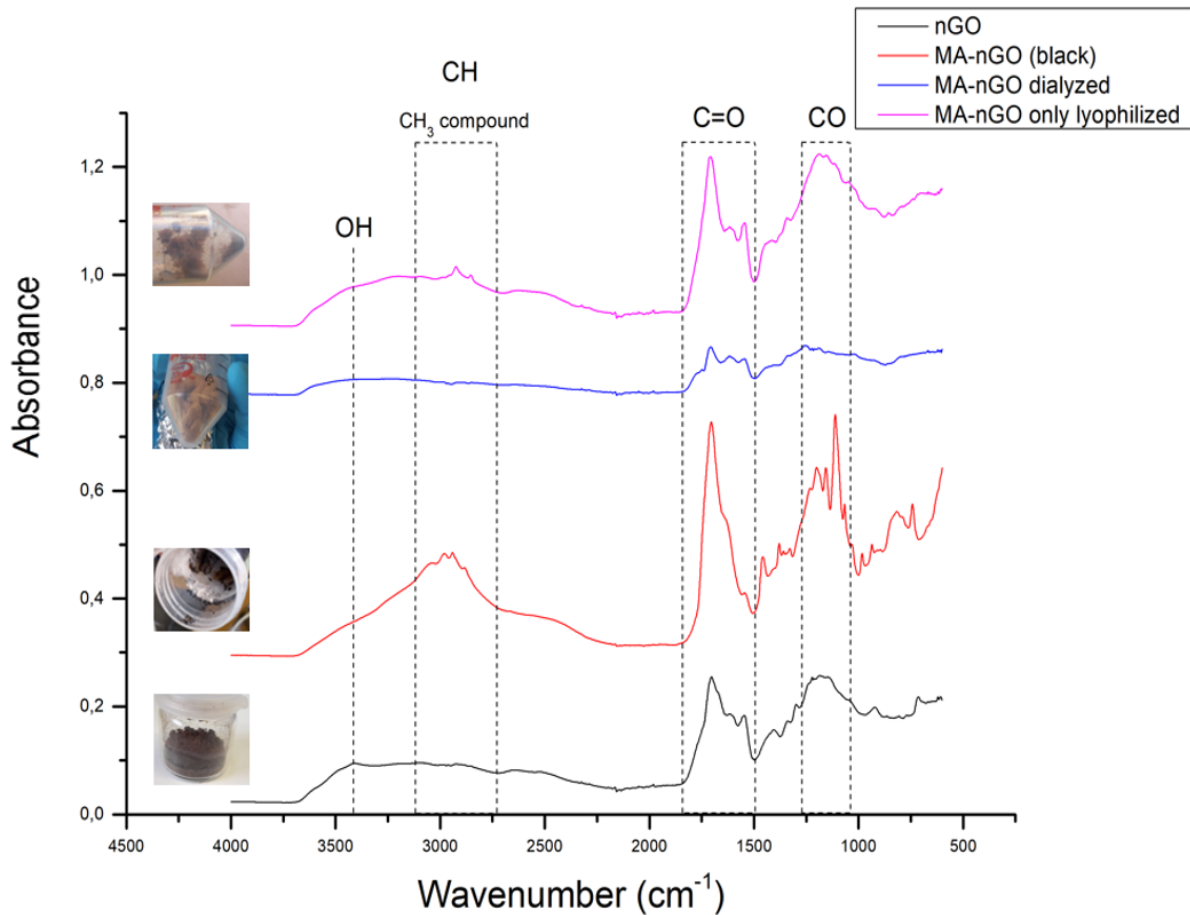


**Figure 4.20:** FTIR spectra comparison of MA-nGO spheres.

#### 4.2.2 Thermal behaviours of nGO and MA-nGO

The thermogravimetric analysis was performed to compare the different methacrylation synthesis of nGO.

According to TGA results reported in the Figure 4.21, MA-nGO starts to degrade at 100°C, Therefore, it can be stated that the MA-nGOs heated at 120°C, have already degraded. All the others MA-nGO nanospheres shows an enhanced thermal stability with respect to the starting nGO, except for the dialyzed MA-nGO, whose thermogram doesn't show residues at 675°C.

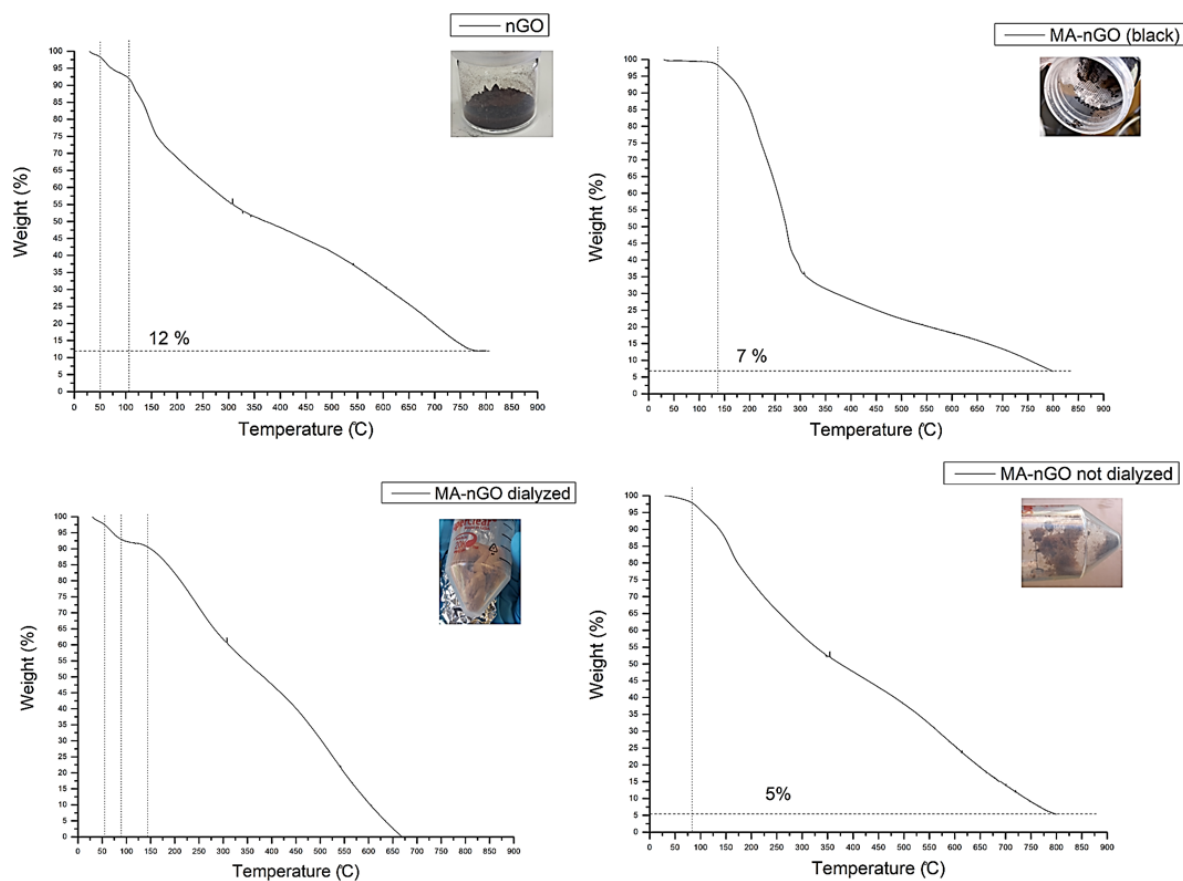


**Figure 4.21:** TGA thermograms of nGO, MA-nGO black, MA-nGO dialyzed and MA-nGO not dialyzed.

#### 4.2.3 Evaluation of the nGO and MAnGO stability in water

$\zeta$ -potential analyses were performed to investigate the stability of the nanospheres in water solutions.

As can be seen in Table 4.4, the methacrylation entails a lack of stability. Overall, the nanoparticles heated at 120°C, are less stable in water than the others.

**Table 4.4:** nGO and MAnGO data.

Material	$\zeta$ -potential (mV)	Standard deviation
nGO	-61.67	9.57
MA-nGO black	-40.16	3.37
MA-nGO dialyzed	-49.26	1.73
MA-nGO not dialyzed	-41.73	4.36

### 4.3 Hydrogels characterization

As previously described in Chapter 2, the photocurable hydrogels were obtained starting from PCLDMA 2k, 14 k and the commercial PEGDMA 750. The last oligomer was chosen

because the desired cross-linking reaction between polycaprolactone dimethacrylate and high molecular weight polyethylene glycol dimethacrylate didn't occur.

#### 4.3.1 Spectroscopic characterization

Attenuated total reflectance- Fourier infrared spectroscopy was used to evaluate the effectiveness of the cross-linking reaction. In order to emphasize the peaks of interest, the spectra were evaluated from 2250 to 500  $\text{cm}^{-1}$ . Each formulation was tested three times: one spectrum was recorded before UV-irradiation and two spectra after 7 min of irradiation (top and bottom surfaces of the sample).

The spectra of PCLDMA 2k + PEGDMA 750 are shown in Figures 4.22, 4.23 and 4.24.

In all of the spectra the disappearance of the peaks at 810 and 1320  $\text{cm}^{-1}$ , corresponding to the C=C-H and -CH<sub>3</sub> respectively, confirms the success of cross-linking. Both the spectra of PCLDMA 2k + PEGDMA 750 [30:70] and [50:50] show the complete disappearance of the C=C peak at 1640 as a consequence of the cross-linking reaction, thus potentially indicating the achievement of a total conversion.

Furthermore, giving a closer look at the spectra reported in Figure 2.22, the disappearance of the peak of C-O-C asymmetric stretching at 1298  $\text{cm}^{-1}$ , could be ascribed to the network formation that is supposed to hinder such vibration. Also, the C=O peak of the hydrogel spectra shifted to 1728  $\text{cm}^{-1}$  as compared to the one of the liquid formulation at 1716  $\text{cm}^{-1}$ , thus indicating a change in the chemical environment in the proximity of C=O bond.

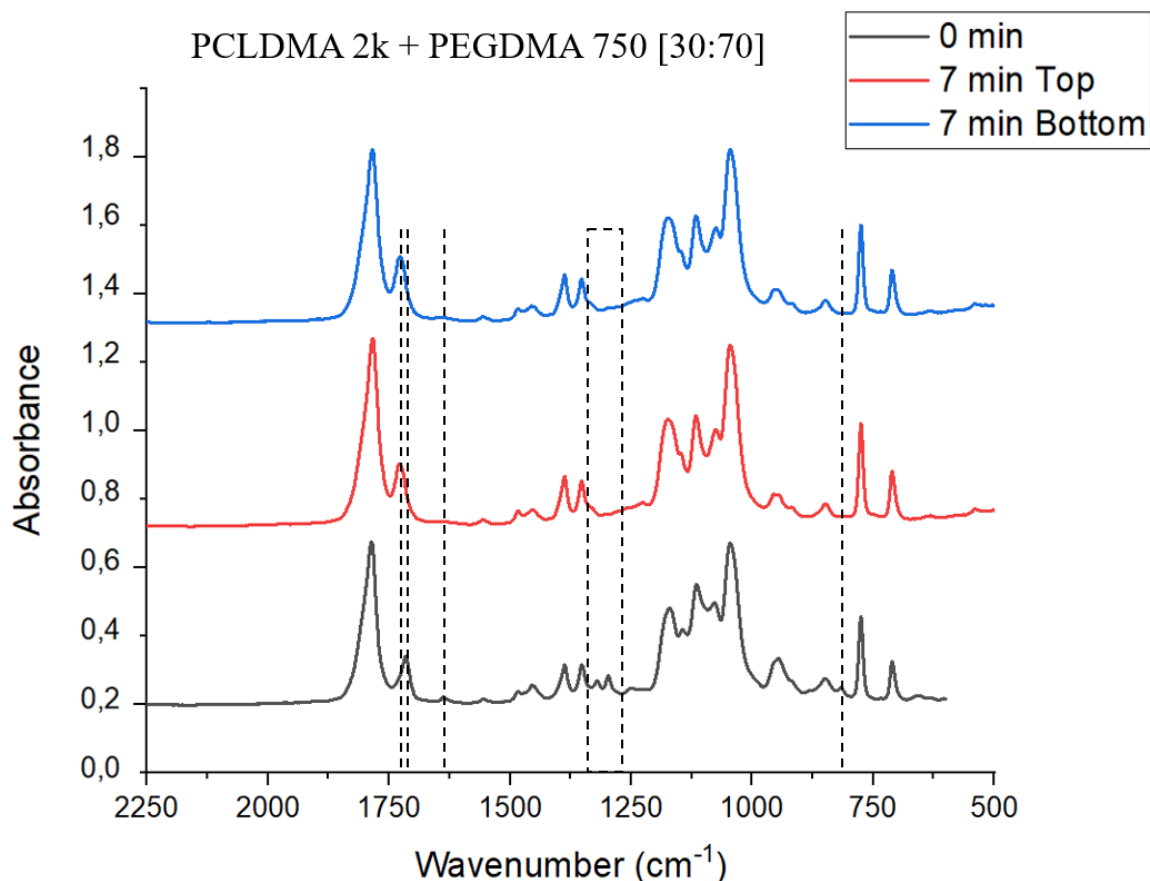


**Figure 4.22:** ATR-FTIR spectra of the PCLDMA 2k + PEGDMA 750 [30:70] formulation before and after the UV-irradiation.

Either in the Figure 4.23 or 4.24, the C=O peak shift is not significant.

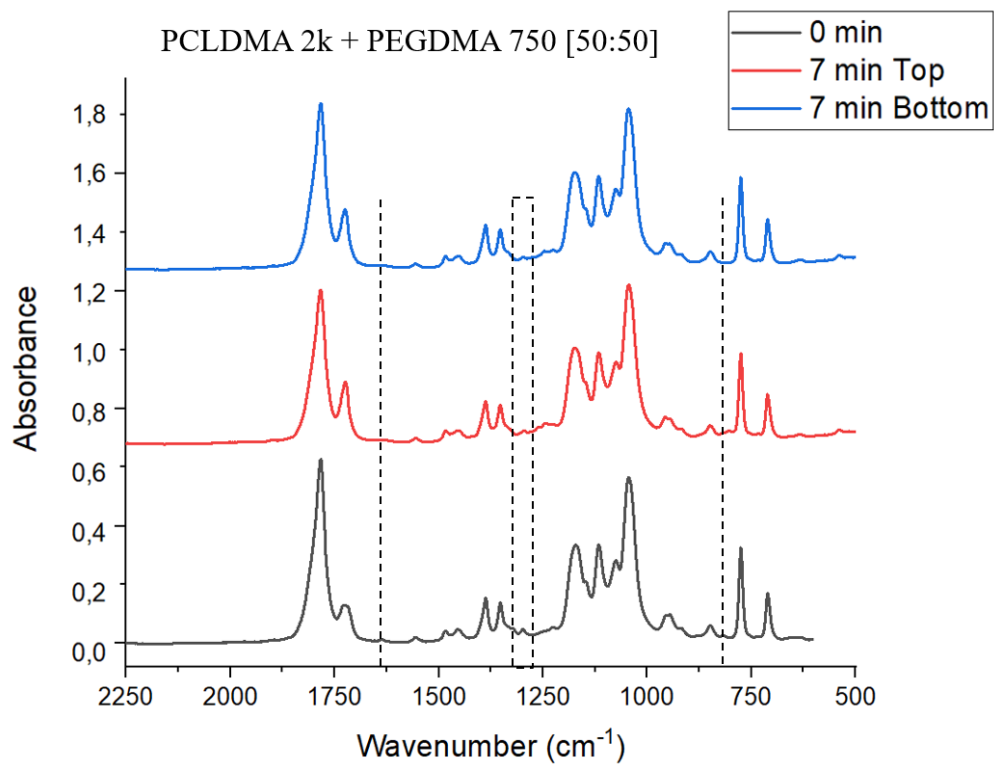


**Figure 4.23:** ATR-FTIR spectra of the PCLDMA 2k + PEGDMA 750 [50:50] formulation before and after the UV-irradiation.

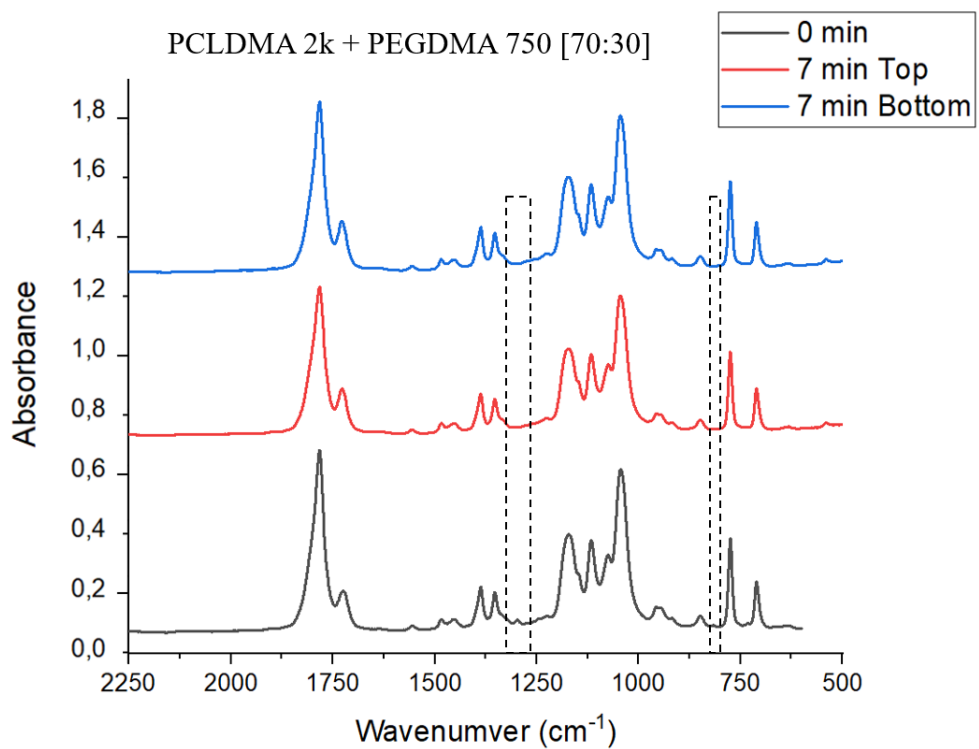


**Figure 4.24:** ATR-FTIR spectra of the PCLDMA 2k + PEGDMA 750 [70:30] formulation before and after the UV-irradiation.

The spectra of PCLDMA 14k + PEGDMA 750 (both 30:70 and 50:50) hydrogels are presented in the following Figures 4.25 and 4.26. In order to evaluate the results more accurately, the spectra are reported from 1950 to 600  $\text{cm}^{-1}$ .

In both the Figures, it can be observed the disappearance of the C=C-H bond at 820  $\text{cm}^{-1}$  in the spectra of the cured formulation, thus confirming the effectiveness of crosslinking.

Looking at Figure 4.25, the peaks at 1294 and 1242  $\text{cm}^{-1}$  clearly disappear, while when the PCLDMA molecular weight is lower those peaks only decrease in intensity, as shown in the previous figures. Another difference concerning the different molecular weights of PCLDMA is that a higher  $M_w$  provokes the right shift of the C=O bond from 1788 to 1780  $\text{cm}^{-1}$  and the sharply decrease of the area of peak at 1720  $\text{cm}^{-1}$  after the UV irradiation. Moreover, the peak at 732  $\text{cm}^{-1}$ , corresponding to alkene bending, disappears after UV irradiation.

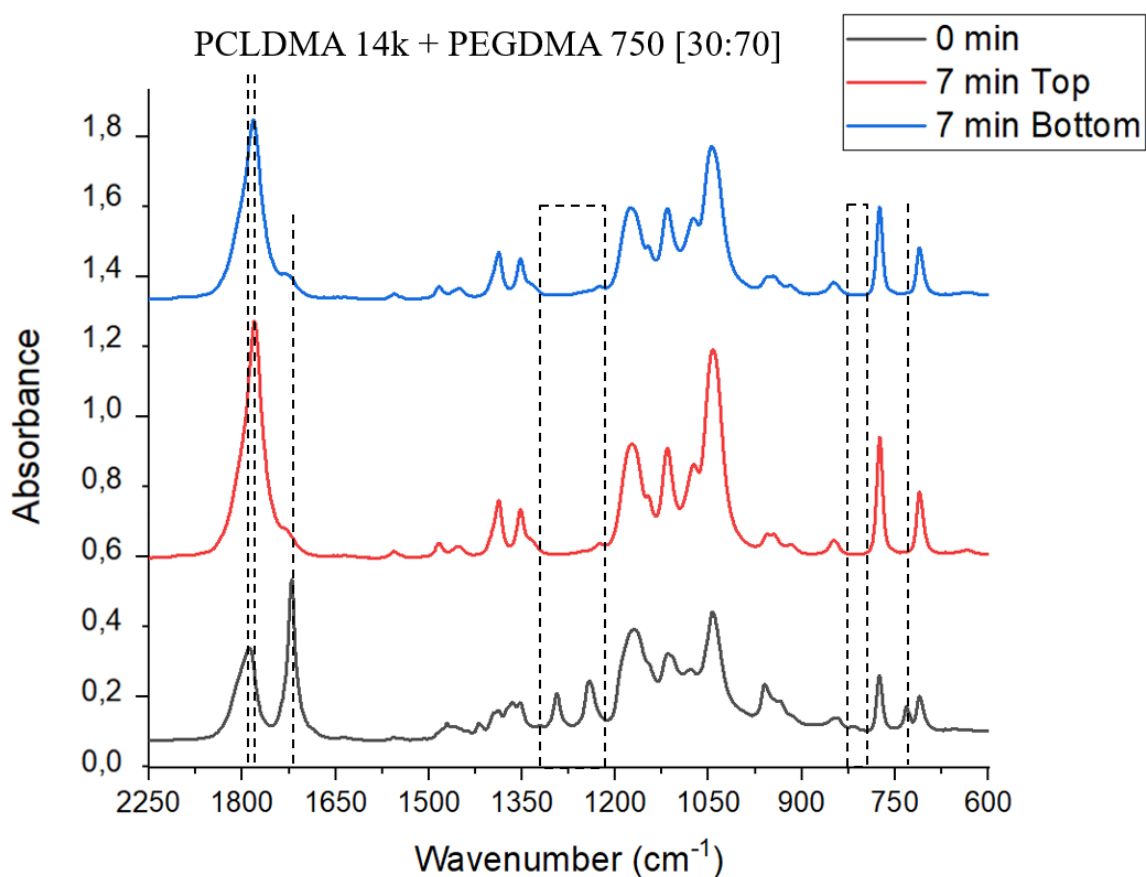


**Figure 4.25:** ATR-FTIR spectra of the PCLDMA 14k + PEGDMA 750 [30:70] formulation before and after the UV-irradiation.

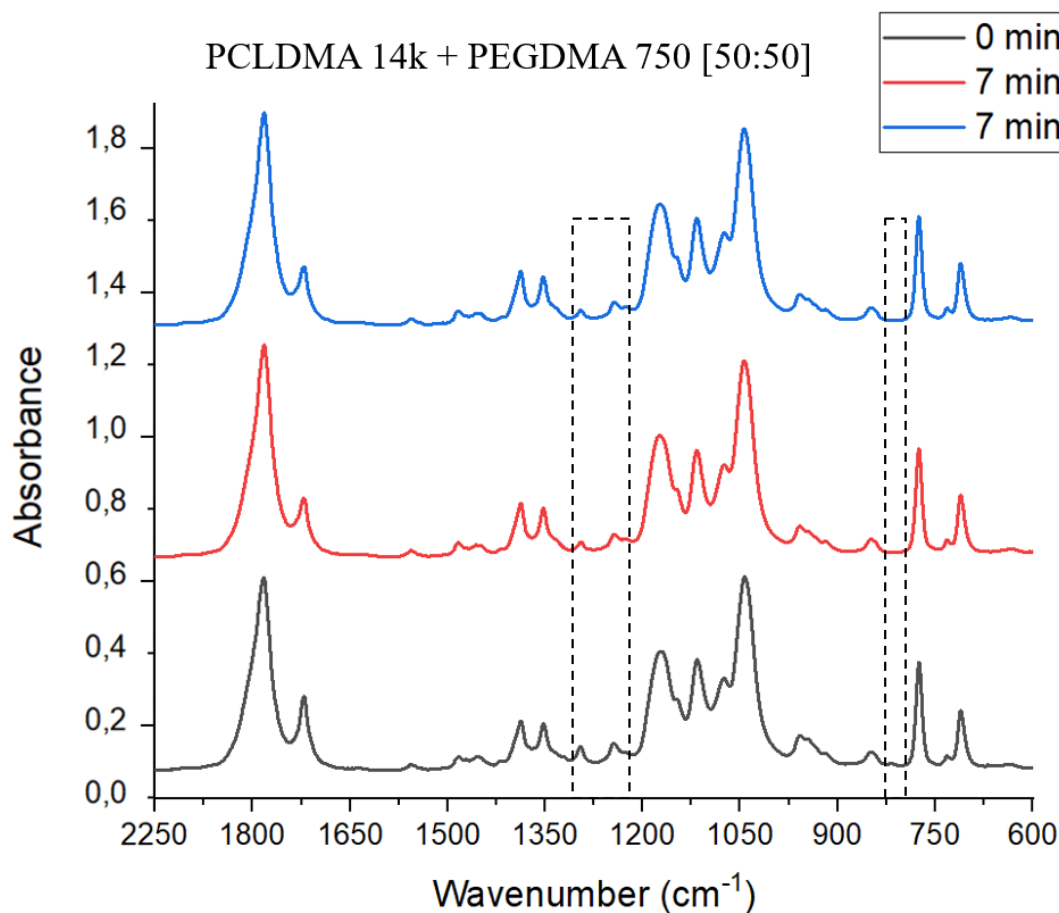


**Figure 4.26:** ATR-FTIR spectra of the PCLDMA 14k + PEGDMA 750 [50:50] formulation before and after the UV-irradiation.

#### 4.3.2 DMTA

Dynamic mechanic thermal analysis was used to evaluate the thermomechanical behaviour of the hydrogels. The measurements were carried out between -100 and 60 °C.

The Figure 4.27 illustrates the thermomechanical behaviour of the following samples: 1) PCLDMA 2k + PEGDMA 750 (50:50) and 2) PCLDMA 14k + PEGDMA 750 (50:50).

As can be seen, the storage modulus ( $G'$ ) decreases by about two order of magnitude from  $10^9$  to almost  $10^7$  Pa. Two distinct flexes of  $G'$  are also clearly visible, thus indicating the presence of two glass transition temperatures. This evidence means that during the cross-linking reaction occurs a partial phase separation. The first  $T_g$  belongs to the PCLDMA domains while the second one can be attributed to the PEGDMA ones. Lower molecular weights of PCLDMA entail a higher cross-linking density and, as a consequence, also a stiffening of the structure, which leads to a higher glass transition temperature with respect to PCLDMA 14k.

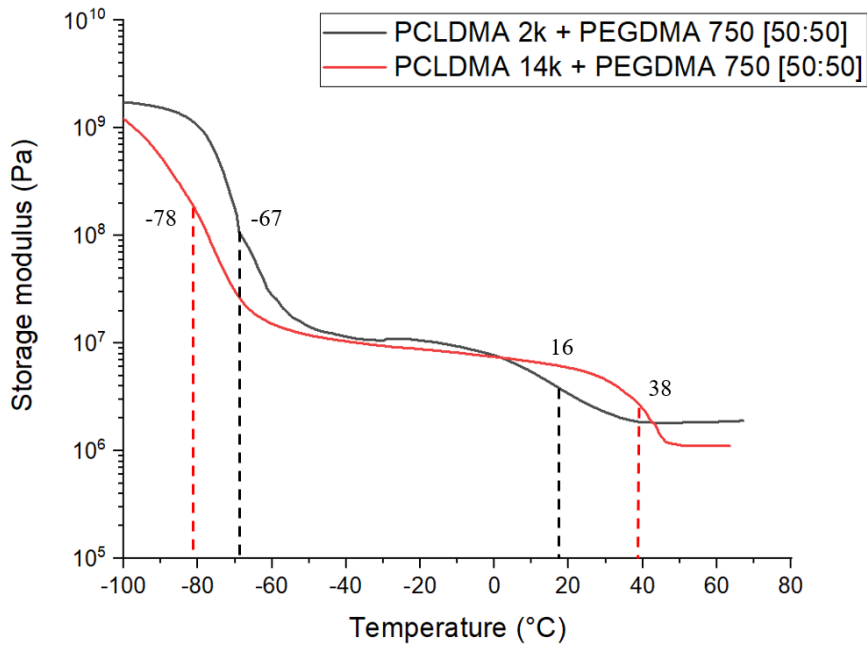


**Figure 4.27:** Thermomechanical behaviour of the PCLDMA 2k + PEGDMA 750 (50:50) and PCLDMA 14k + PEGDMA 750 (50:50) hydrogels.

### 4.3.3 DSC

The DSC analysis was performed to compare the PCLDMA 2k + PEGDMA 750 and PCLDMA 14k + PEGDMA 750 both [50:50] weight ratio. As it can be observed in the graph, in the first hydrogel the chains length is not enough to create crystalline domain, while in the second sample it is clearly visible the melting peak of PCLDMA 14k at 38°C.

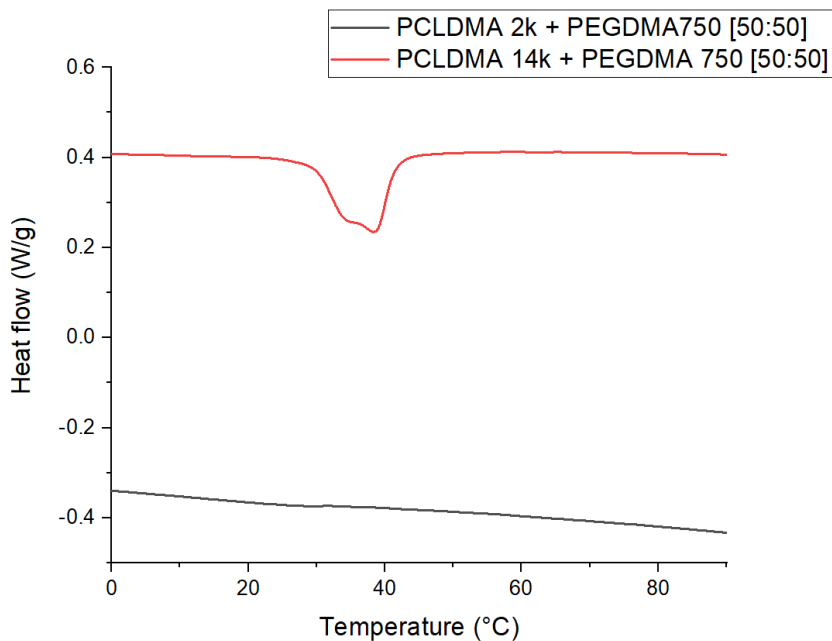


**Figure 4.28:** DSC graph comparison between PCLDMA 2k + PEGDMA 750 and PCLDMA 14k + PEGDMA 750

#### 4.3.4 Swelling behaviour

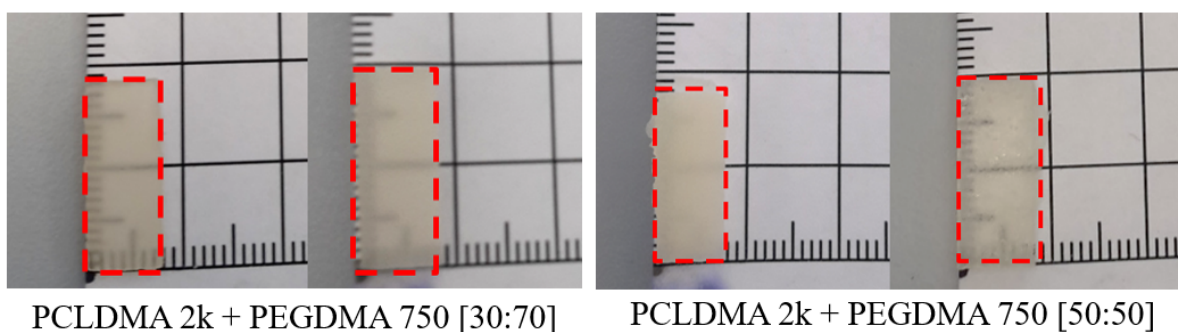
The equilibrium water content and the swelling degree were calculated by means of measuring the weight of both the dried and the wetted hydrogel. The results are reported in the Table 4.5.

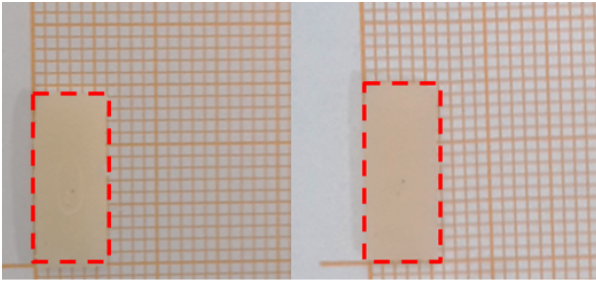
The swelling degree decreases enhancing the PCLDMA content as expected for hydrophobic domain. Moreover, higher molecular weight of PCLDMA leads to an enhancement of the swelling degree. This can be explained considering a lower cross-linking density in the hydrogel formed with longer chains. The same trend can be seen also in the equilibrium water content.

**Table 4.5:** Equilibrium water content and swelling degree.

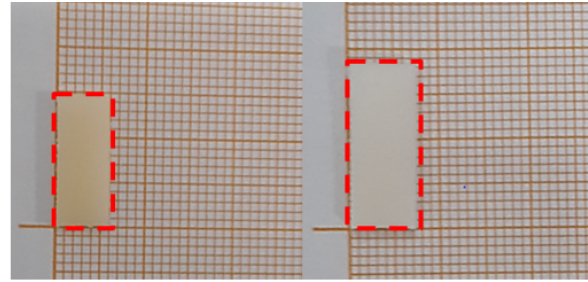
Hydrogel	Equilibrium water content	Swelling degree
PCLDMA 2k + PEGDMA [30:70]	34.08%	51.7%
PCLDMA 2k + PEGDMA [50:50]	28.98%	40.87%
PCLDMA 2k + PEGDMA [70:30]	5.15%	5.4%
PCLDMA 14k + PEGDMA [30:70]	44.96%	81.7%
PCLDMA 14k + PEGDMA [50:50]	36.54%	57.59%
PEGDMA 750	68.36%	216.13%

Some hydrogels pictures taken before and after the swelling measurement are reported in Figure 4.29.

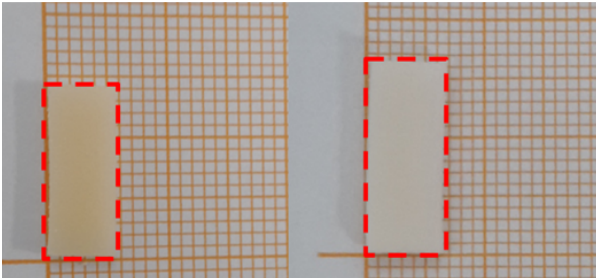




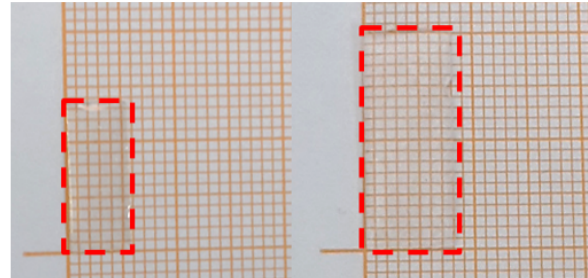
PCLDMA 2k + PEGDMA 750 [70:30]



PCLDMA 14k + PEGDMA 750 [30:70]



PCLDMA 14k + PEGDMA 750 [50:50]



PEGDMA 750

**Figure 4.29:** Pictures taken on the samples before and after the swelling measurement.

## 5 Conclusion and future works

In this study, the synthesis of photocurable hydrogels made of polycaprolactone (PCL) and polyethylene glycol (PEG) was investigated and discussed in detail.

First, the biocompatible oligomers were synthesized with different molecular weights and functionalized by substituting the hydroxyl ending groups with methacrylates ones *via* an esterification reaction to make them suitable for a photo-polymerization process. The effectiveness of the methacrylation was confirmed by means of ATR-FTIR, H-NMR and DSC measurements.

Then, bio-based carbon nanospheres of graphene oxide were also obtained directly from cellulose *via* a microwave assisted process. Five different functionalization procedures have been investigated by means of ATR-FTIR, TGA and Zeta-potential analysis.

In conclusion, several photocurable formulations were successfully prepared varying both the weight percentages of the oligomers and their molecular weights. The typical three-dimensional hydrogels network was obtained *via* a free radical photopolymerization reaction, using bis(acyl)phosphane oxide (BAPO) as the photoinitiator. The thermomechanical properties and the swelling behaviour of the photocured hydrogels were investigated by means of DTMA and swelling measurements.

In the future, both the biocompatibility and the incorporation of MAnGOs within the hydrogel structure will be investigated, since, the covalently attachment of MAnGOs within the network is supposed to assign biofunctionality to the hydrogel enhancing the cells adhesion [32] and thus offering a new design strategy for hydrogel in tissue engineering field.



## References

- [1] Naziha Chirani, L'Hocine Yahia, Lukas Gritsch, Federico Leonardo Motta, Soumia Chirani and Silvia Faré, "History and Applications of Hydrogels," *Journal of Biomedical Sciences*, vol. 4, p. 2:13, 2015.
- [2] Ahmed, Enas M., "Hydrogel: Preparation, characterization, and applications: A review," *Journal of Advanced Research*, pp. 105-121, 2015.
- [3] Vasheghani-Farahani, Fariba Ganji and Ebrahim, "Hydrogels in Controlled Drug Delivery Systems," *Iranian Polymer Journal*, vol. 18, pp. 1-26, 2008.
- [4] Hoffman, Allan S., "Hydrogels for biomedical applications," in *Advanced Drug Delivery Reviews*, Seattle, ELSEVIER, 2002, pp. 3-12.
- [5] A.K. Bajpai, Sandeep K. Shukla, Smitha Bhanu, Sanjana Kankane, "Responsive polymers in controlled drug delivery," in *Progress in Polymer Science 33*, Jabalpur, ELSEVIER, 2008, p. 1088–1118.
- [6] Fariba Ganji, Samira Vasheghani-Farahani, and Ebrahim Vasheghani-Farahani, "Theoretical Description of Hydrogel Swelling: A Review," *Iranian Polymer Journal*, vol. 19, no. 5, pp. 375-398, 2010.
- [7] A. Berens, H. Hopfenberg, "Diffusion and relaxation in glassy polymer powders: 2. Separation of diffusion and relaxation parameters," Raleigh, ELSEVIER, 1978, pp. 489-496.
- [8] Muhammad Faheem Akhtar, Muhammad Hanif, Nazar Muhammad Ranjha, "Methods of synthesis of hydrogels . . . A review," *Saudi Pharmaceutical Journal*, vol. 24, p. 554–559, 2016.
- [9] P. Ferreira, J. F. J. Coelho, J. F. Almeida and M. H. Gil, "Photocrosslinkable Polymers for Biomedical Applications", INTECH Open Access Publisher, 2011.
- [10] Thakur Raghu Raj Singh, Garry Laverty, Ryan Donnelly, "HYDROGELS", CRC Press, 2018.
- [11] B.Saadab, U.W.Suterb, "Biodegradable Polymeric Materials," in *Encyclopedia of Materials: Science and Technology (Second Edition)*, ELSEVIER, 2001, pp. 551-555.
- [12] J.Brady, T.Dürig, P.I.Lee, J.-X.Li,
- [13] Yih-Lin Cheng, Freeman Chen, "Preparation and characterization of photocured poly ( $\epsilon$ -caprolactone) diacrylate/poly (ethylene glycol) diacrylate/chitosan for photopolymerization-type 3D printing tissue engineering scaffold application," *Materials Science and Engineering C*, vol. C 81, p. 66–73, 2017.
- [14] Cruise GM, Hegre OD, Scharp DS, Hubbell JA., "A Sensitivity Study of the Key Parameters in the Interfacial Photopolymerization of Poly(ethylene glycol) Diacrylate upon Porcine Islets," *John Wiley & Sons, Inc*, Vols. CCC 0006-3592, pp. 98/060655-11, 1998.

- [15] Nejla B. Erdal, Karin H. Adolfsson, Torbjörn Pettersson, and Minna Hakkarainen, “Green Strategy to Reduced Nanographene Oxide through Microwave Assisted Transformation of Cellulose,” *ACS Sustainable Chem.*, p. 1246–1255, 2017.
- [16] Sihang Liu, Mei Huang, “Preparation and Properties of Graphene Oxide Modified Nanocomposite Hydrogels,” in *Global Conference on Polymer and Composite Materials*, 2014.
- [17] Xifeng Liu, A. Lee Miller, Sungjo Park, Brian E. Waletzki, Andre Terzic, “Covalent crosslinking of graphene oxide and carbon nanotube into hydrogels enhances nerve cell responses,” *Journal of Materials Chemistry B*, vol. 4, pp. 6930--6941, 2016.
- [18] [Online]. “Nuclear Magnetic Resonance Spectroscopy,” [Online]. Available: <https://www2.chemistry.msu.edu/faculty/reusch/virttxtjml/spectrpy/nmr/nmr1.htm>. [Accessed 1 07 2018].
- [19] [Online]. Available: <http://cmr.spbu.ru/en/instruments/>. [Accessed 13 06 2018].
- [20] [Online]. Available: <https://myessozone.wordpress.com/2013/07/26/spektroskopi-nmr-nuclear-magnetic-resonance/>.
- [21] “Polymerization Technology – Laboratory Course Differential Scanning Calorimetry. Polyethylene Terephthalate synthesis.,” Catalyst screening, 2007.
- [22] Philipsen, Dr. Harry J.A, “Basic of GPC (SEC) separation including calibration options,” in *DSM*, Amsterdam, 2016.
- [23] [Online]. “Gel permeation chromatography (GPC),” [Online]. Available: <http://www.skz.de/en/research/technicalfacilities/pruefverfahren1/spektroskopie1/index.html>. [Accessed 11 04 2018].
- [24] [Online]. Available: <https://lalithvarun.blogspot.com/2013/02/what-is-thermogravimetric-analysis.html>. [Accessed 3 08 2018].
- [25] [Online]. “<https://www.coriolis-pharma.com/contract-analytical-services/zeta-potential/>,” [Online]. [Accessed 04 2018].
- [26] [Online]. Available: <http://departments.agri.huji.ac.il/zabam/zetasizer.html>. [Accessed 24 04 2018].
- [27] [Online]. Available: <https://www.atascientific.com.au/products/malvern-zetasizer-nano-zs/>. [Accessed 24 04 2018].
- [28] Paulo Jorge da Silva Bartolo, Ana Cristina Soares de Lemos, Antonio Mario Henriques Pereira, Artur Jorge Dos Santos Mateus, et al., “Vat polymerization technique for biotechnology and medicine,” in *High Value Manufacturing: Advanced Research in Virtual and Rapid Prototyping*, London, CRC Press, 2014, pp. 204-205.
- [29] Yinfeng He, Christopher J. Tuck, Elisabetta Prina, Sam Kilsby, Steven D. R. Christie, Stephen Edmondson, Richard J. M. Hague, Felicity R. A. J. Rose, Ricky D. Wildman, “A new photocrosslinkable polycaprolactone-based ink for three-dimensional inkjet printing,” *Journal of biomedical materials research part B*, vol. 105B, p. 1645–1657, 2017.

[30] HaeYong Kweon, Mi Kyong Yoo, In KyuPark , Ta Hee Kim, Hyun Chul Le, Hyun-Sook Lee, Jong-Suk Oh, Toshihiro Akaike, Chong-SuCho, “A novel degradable polycaprolactone networks for tissue engineering,” *Biomaterials*, vol. 24, p. 801–808, 2003.

[31] V.Crescenzi, G.Manzini, G.Calzolari, C.Borri, “Thermodynamics of fusion of poly- $\beta$ -propiolactone and poly- $\epsilon$ -caprolactone. comparative analysis of the melting of aliphatic polylactone and polyester chains,” *European Polymer Journal*, vol. 8, no. 3, pp. 449-463, 1972.

[32] Myungkyung Noh, Su-Hwan Kim, Jiyong Kim, Ju-Ro Lee, Gun-Jae Jeong, Jeong-Kee Yoon, Seokyung Kang, Suk Ho Bhang, Hee Hun Yoon, Jong-Chan Lee, Nathaniel S. Hwang and Byung-Soo Kim, “Graphene oxide reinforced hydrogels for osteogenic differentiation of human adipose-derived stem cells,” *Royal society of chemistry*, vol. 7, p. 20779–20788, 2017.



## Acknowledgements

First, I would like to thank my Relator Marco Sangermano for his enthusiasm, expertise, patience and for providing me the opportunity to work on this project.

I would like to extend my sincere gratitude to Minna Hakkarainen and Nejla Benyahia Erdal for their assistance and guidance during my work in KTH.

I would like to give my special thanks to my wonderful boyfriend Andrea Cosola for his personal support, his understanding, great patience and for pushing me farther than I thought I could go.

I would also like to thank my family and my best friends Greta Masserano, Giulia Santopolo and Davide Bignami for helping me survive all the stress from these years and not letting me give up.

Last of all, I would like to thank all my friends, especially Riccardo Novo, Andrea Novelli, Matteo Caprioli, Lorenzo Vigna, Ludovico Percivale, Alessandro Piglione and Luisa Baudino, who made me laugh and helped me directly or indirectly to complete my study.